







**ORIGINAL PAGE IS  
OF POOR QUALITY**

**PREFACE**

**This volume is the first of four which make up the Multisatellite Attitude Determination/Optical Aspect Bias Determination (MSAD/OABIAS) System Description and Operating Guide. The volumes are**

**Volume 1 - Introduction and Analysis**

**Volume 2 - System Description**

**Volume 3 - Operating Guide**

**Volume 4 - Program Listing and Sample Execution**

**This volume contains an introductory exposition of the MSAD/OABIAS System and describes the analytic basis for the OABIAS subsystem. This includes a detailed discussion of the recursive estimator algorithm, each of the 12 state vector elements, and the 8 observation models used.**

**Volume 2 describes the system flow and the components of the MSAD/OABIAS System. The table language description in this volume provides detailed information relating the operational displays on the IBM 2250 display device to specific COMMON areas and subroutines within the MSAD/OABIAS System.**

**Volume 3 contains a complete description of all MSAD/OABIAS NAMELIST control parameters, a description and sample of all printed output unique to OABIAS and of each IBM 2250 graphics display, an explanation of and user response for all error messages generated by the MSAD/OABIAS System, and a listing of the Job Control Language (JCL) required to operate the system.**

**Volume 4 contains the program listing with supplementary output and line printer plots of all IBM 2250 displays occurring during a sample execution of the program. This volume preserves, in source form, the MSAD/OABIAS System as it is presented in this document.**

**PRECEDING PAGE BLANK NOT FILMED**



**ORIGINAL PAGE IS  
OF POOR QUALITY**

**ABSTRACT**

This document describes the Multisatellite Attitude Determination/Optical Aspect Bias Determination (MSAD/OABIAS) System, designed to determine spin axis orientation and biases in the alignment or performance of optical or infrared horizon sensors and Sun sensors used for spacecraft attitude determination. MSAD/OABIAS uses any combination of eight observation models to process data from a single onboard horizon sensor and Sun sensor to determine simultaneously the two components of the attitude of the spacecraft, the initial phase of the Sun sensor, the spin rate, seven sensor biases, and the orbital in-track error associated with the spacecraft ephemeris information supplied to the system. In addition, the MSAD/OABIAS System provides a data simulator for system and performance testing, an independent deterministic attitude system for preprocessing and independent testing of biases determined, and a multipurpose data prediction and comparison system.

MSAD/OABIAS has extensive capabilities for an interactive graphics mode and makes use of the Graphics Executive Support System (GESS), formerly known as the Multisatellite Attitude Determination System (MSAD) services. MSAD/OABIAS is a multisatellite system capable of supporting, in its present form, the Small Scientific Satellite (S<sup>3</sup>), the Interplanetary Monitoring Platform (IMP), the Atmosphere Explorer (AE), and the Synchronous Meteorological Satellite (SMS) missions or any similar missions using optical or infrared horizon scanners and providing attitude data that can be read by the MSAD/OABIAS System.

**PRECEDING PAGE BLANK NOT FILMED**



# PRELIMINARY DRAFT

ORIGINAL PAGE IS  
OF POOR QUALITY

## TABLE OF CONTENTS

### VOLUME 1--INTRODUCTION AND ANALYSIS

<u>Section 1 - Introduction</u> .....	1-1
1.1 Motivation for Bias Determination .....	1-1
1.2 Historical Background .....	1-2
1.3 System Overview .....	1-4
1.3.1 OADRIV .....	1-6
1.3.2 ODAP .....	1-7
1.3.3 OASYS .....	1-7
1.3.4 OABIAS .....	1-8
1.3.5 PLOTOC .....	1-9
1.4 OABIAS Recursive Least-Squares Filter .....	1-9
1.4.1 Introduction .....	1-9
1.4.2 Observation Models .....	1-11
<u>Section 2 - Sensor Descriptions</u> .....	2-1
2.1 Sun Sensor .....	2-1
2.2 Horizon Detector .....	2-3
2.3 AE-C Wheel-Mounted Horizon Sensors .....	2-5
2.4 RAE-B Panoramic Attitude Sensor .....	2-6
<u>Section 3 - Analysis</u> .....	3-1
3.1 Introduction .....	3-1
3.2 OASYS--Deterministic Attitude Determination Subsystem .....	3-4
3.2.1 Input to Deterministic Process .....	3-4
3.2.2 Design Assumptions .....	3-5
3.2.3 Deterministic Logic .....	3-6
3.3 The Recursive Estimator Approach .....	3-16
3.3.1 Comparison Between Recursive Processing and Batch Processing Estimation Methods .....	3-16
3.3.2 The Basic Recursive Estimator Algorithm .....	3-19
3.3.3 Discussion of Weighting Factors .....	3-25
3.4 Implementation of the Recursive Estimator Algorithm in OABIAS .....	3-28
3.4.1 Principal Inputs .....	3-28
3.4.2 Observation Models .....	3-29
3.4.3 State Vector Elements .....	3-30

PRECEDING PAGE BLANK NOT FILMED

vii

PRELIMINARY DRAFT

# PRELIMINARY DRAFT

ORIGINAL PAGE IS  
OF POOR QUALITY

## TABLE OF CONTENTS (Cont'd)

### Section 3 (Cont'd)

3.4.4	Iterative Operation . . . . .	3-32
3.4.5	Single Observation Iteration . . . . .	3-34
3.5	Basic Geometry . . . . .	3-36
3.5.1	Coordinate Frame Flow Diagram . . . . .	3-36
3.5.2	Coordinate Frames GI' and GI . . . . .	3-38
3.5.3	Coordinate Frames SI and SC and State Vector Elements $x_3$ ( $\psi$ ) and $x_9$ ( $\omega$ ) . . . . .	3-40
3.5.4	Sun Sensor Geometry and State Vector Elements $x_8$ ( $\Delta\beta$ ) and $x_{10}$ ( $\epsilon$ ) . . . . .	3-43
3.5.5	Horizon Detector Geometry and State Vector Elements $x_4$ ( $\Delta\gamma$ ), $x_5$ ( $\phi_H^I$ ), $x_6$ ( $\phi_H^O$ ), and $x_{11}$ ( $\epsilon_H$ ) . . . . .	3-43
3.5.6	State Vector Element $x_7$ ( $\Delta\rho$ ) . . . . .	3-48
3.5.7	State Vector Element $x_{12}$ ( $\Delta t$ ) . . . . .	3-50
3.5.8	Transformation Matrix A and State Vector Elements $x_1$ ( $s_1$ ) and $x_2$ ( $s_2$ ) . . . . .	3-50
3.5.9	Transformation Matrices $B_I$ and $B_O$ . . . . .	3-53
3.6	Observation Models . . . . .	3-54
3.6.1	Model 1--Sun Angle Model . . . . .	3-55
3.6.2	Model 2--Sun Sighting Time Model . . . . .	3-58
3.6.3	Model 3--Nadir Vector Projection Model . . . . .	3-61
3.6.4	Model 4--Horizon Crossing Time Model . . . . .	3-66
3.6.5	Model 5--Sun to Earth-In and Sun to Earth-Out Dihedral Angle Model . . . . .	3-70
3.6.6	Model 6--Earth Width Model . . . . .	3-74
3.6.7	Model 7--Small Target Model . . . . .	3-77
3.6.8	Model 8--Sun to Earth Mid-Scan Dihedral Angle Model . . . . .	3-79
3.7	Computation of Central Body Angular Radius $\rho_c$ . . . . .	3-83
3.8	Computation of Horizon Crossing Vector $\hat{D}$ . . . . .	3-87
3.9	Weighting Factors of the Observation Models . . . . .	3-92
3.10	Summary of Section 3 . . . . .	3-97

### Appendix A - Model Observation Partial Derivatives

### Appendix B - Derivation of Recursive Processing Algorithm Used in OABIAS

# PRELIMINARY DRAFT

ORIGINAL PAGE IS  
OF POOR QUALITY

## TABLE OF CONTENTS (Cont'd)

### VOLUME 2--SYSTEM DESCRIPTION

<u>Section 4 - System Flow</u> . . . . .	4-1
4.1 Overview . . . . .	4-1
4.2 External Interfaces . . . . .	4-4
4.3 System Flow, Nongraphic Mode . . . . .	4-5
4.4 System Flow, Graphic Mode . . . . .	4-6
<u>Section 5 - Baseline Diagram and Subroutine Description</u> . . . . .	5-1
5.1 Baseline Diagram . . . . .	5-1
5.2 Subroutine Descriptions . . . . .	5-1
<u>Section 6 - COMMON Area Descriptions</u> . . . . .	6-1
<u>Appendix C - Description of GESS Tables</u>	

### VOLUME 3--OPERATING GUIDE

<u>Section 7 - Operating Guide</u> . . . . .	7-1
7.1 Introduction . . . . .	7-1
7.2 Resources . . . . .	7-1
7.3 Card Input . . . . .	7-1
7.3.1 NAMELIST CONTRL . . . . .	7-4
7.3.2 GESS Array Allocation Sizes . . . . .	7-5
7.3.3 GESS Display Status Flags . . . . .	7-5
7.3.4 NAMELIST MAIN . . . . .	7-6
7.3.5 NAMELIST LIST . . . . .	7-19
7.3.6 NAMELIST OPMANI . . . . .	7-31
7.3.7 NAMELIST BIASNL . . . . .	7-40
7.3.8 Description of a Sample NAMELIST . . . . .	7-49
7.4 OABIAS Data Set . . . . .	7-60
7.5 AE Data Set . . . . .	7-63
7.6 JPL Lunar and Solar Ephemeris File . . . . .	7-64
7.7 SUNRD Lunar and Solar Ephemeris File . . . . .	7-64
7.8 GTDS Spacecraft Ephemeris File . . . . .	7-65
7.9 DODS Spacecraft Ephemeris File . . . . .	7-65
7.10 Spacecraft Attitude Tape . . . . .	7-66

# PRELIMINARY DRAFT

ORIGINAL PAGE IS  
OF POOR QUALITY

## TABLE OF CONTENTS (Cont'd)

### Section 7 (Cont'd)

7.11	GESS Nonresident Tables .....	7-66
7.12	Printed Output .....	7-66
7.12.1	Printed Output From the GESS Executive .....	7-66
7.12.2	Printed Output From OADRIV .....	7-68
7.12.3	Printed Output From the ODAP Subsystem .....	7-68
7.12.4	Printed Output From the OASYS Subsystem .....	7-68
7.12.5	Printed Output From the OABIAS Subsystem .....	7-68
7.13	CalComp Plot Tape .....	7-93
7.14	GESS Displays .....	7-93
7.14.1	Display Status Flags and Key Assignments .....	7-93
7.14.2	Array Allocation Sizes .....	7-97
7.14.3	Main Control Display .....	7-97
7.14.4	Options for Copying AE Data Set .....	7-97
7.14.5	Simulation Options Display .....	7-97
7.14.6	NAMELIST LIST Display .....	7-102
7.14.7	Options for Reading Data .....	7-102
7.14.8	Reader Record Displays .....	7-102
7.14.9	Data Record Display .....	7-102
7.14.10	Data Selection Options for OASYS .....	7-103
7.14.11	NAMELIST OPMAN1 Display .....	7-112
7.14.12	OASYS Block Average Display .....	7-112
7.14.13	OASYS Plots of Single Frame Results .....	7-112
7.14.14	NAMELIST BIASNL Display .....	7-118
7.14.15	Final Results From OABIAS .....	7-118
7.14.16	Table of Errors From OABIAS .....	7-118
7.14.17	Table of Correlation Coefficients From OABIAS .....	7-126
7.14.18	State Component Plots From OABIAS .....	7-126
7.14.19	Plots of Uncertainties in State Components .....	7-126
7.14.20	Residual Plots From OABIAS .....	7-126
7.14.21	Options for Data Prediction .....	7-126
7.14.22	Plot of Predicted and Observed Rotation Angles .....	7-126
7.14.23	Plot of Predicted and Observed Earth Widths .....	7-134
7.14.24	Core Storage and Time Remaining Display .....	7-131
7.15	Control With Interactive Graphics .....	7-138
7.15.1	Programmed Function Keys .....	7-138
7.15.2	Asynchronous Calls .....	7-140
7.16	Error Messages .....	7-142
7.16.1	Messages Displayed in a Graphic Mode .....	7-142
7.16.2	Printed Message From the ODAP Subsystem .....	7-149

# PRELIMINARY DRAFT

## TABLE OF CONTENTS (Cont'd)

### Section 7 (Cont'd)

7.16.3	Printed Messages From the OASYS Subsystem . . . . .	7-155
7.16.4	Printed Error Message From OABIAS . . . . .	7-156
7.17	Job Control Language . . . . .	7-162

## VOLUME 4--PROGRAM LISTING AND SAMPLE EXECUTION

### Appendix D - Program Listing

### Appendix E - Sample Execution

ORIGINAL PAGE IS  
OF POOR QUALITY

# PRELIMINARY DRAFT

ORIGINAL PAGE IS  
OF POOR QUALITY

## LIST OF ILLUSTRATIONS

### Figure

1-1	MSAD/OABIAS Functional Subsystems . . . . .	1-5
2-1	Sun Sensing Geometry. . . . .	2-2
2-2	Horizon Detection Geometry . . . . .	2-4
2-3	RAE-B PAS Geometry . . . . .	2-7
3-1	Coordinate Frame Flow . . . . .	3-37
3-2	Criteria for Rotation of Frame GI . . . . .	3-41
3-3	Geometry of Frames GI, SI, and SC . . . . .	3-42
3-4	Sun Sensor Geometry at Sun Sighting. . . . .	3-44
3-5	Horizon Detector Geometry at Central-Body-In Crossing . . . . .	3-46 3-46
3-6	Generation of Earth Radius Bias $\Delta\rho$ by Sensor Triggering Level Bias . . . . .	3-49 3-49
3-7	Geometry for Model 1--Sun Angle Model . . . . .	3-57
3-8	Geometry for Model 3--Nadir Vector Projection Model . . .	3-62
3-9	Geometry for Model 4--Horizon Crossing Time Model. . . .	3-67
3-10	Geometry for Model 5--Sun to Earth-In and Sun to Earth-Out Dihedral Angle Model . . . . .	3-71 3-71
3-11	Geometry for Model 6--Earth Width Model . . . . .	3-76
3-12	Geometry for Model 7--Small Target Model. . . . .	3-78
3-13	Geometry for Model 8--Sun to Earth Mid-Scan Dihedral Angle Model . . . . .	3-80 3-80
3-14	$\rho_c$ Computation Geometry--Spherical Central Body . . . .	3-84
3-15	Resolution of Sign Ambiguity of Horizon Crossing Vector $\hat{D}$ . . . . .	3-90 3-90
4-1	External Interfaces for the MSAD/OABIAS System . . . . .	4-2
5-1	MSAD/OABIAS Baseline Diagram. . . . .	5-2
5-2	DIHMOD Flowchart. . . . .	5-59
5-3	DIAHMOD Flowchart . . . . .	5-73
5-4j	FRAPRO Flowchart . . . . .	5-103
5-5	INITIL Flowchart . . . . .	5-120
5-6	LNMOD Flowchart. . . . .	5-146
5-7	LRMOE Flowchart. . . . .	5-165
5-8	OABIAS Flowchart . . . . .	5-176
5-9	OADRIV Flowchart . . . . .	5-185
5-10	PRINTB Flowchart . . . . .	5-287
5-11	SANMOD Flowchart . . . . .	5-315
5-12	SCBMOD Flowchart . . . . .	5-329
5-13	STMMOD Flowchart. . . . .	5-343

# PRELIMINARY DRAFT

ORIGINAL PAGE IS  
OF POOR QUALITY

## LIST OF ILLUSTRATIONS (Cont'd)

### Figure

7-1	NAMELIST CONTROL . . . . .	7-67
7-2	NAMELIST MAIN . . . . .	7-69
7-3	Input to OABIAS Table . . . . .	7-71
7-4	OABIAS Attitude Summary--Heading Definition . . . . .	7-74
7-5	Attitude and State Vector Table From OABIAS . . . . .	7-75
7-6	Uncertainty Table From OABIAS . . . . .	7-77
7-7	Partial Derivative Table From OABIAS . . . . .	7-79
7-8	Recursive Estimator Gain Table From OABIAS . . . . .	7-80
7-9	Attitude, Observable, and Vector Table From OABIAS . . . . .	7-81
7-10	Residual Table From OABIAS . . . . .	7-82
7-11	Error Messages From OABIAS . . . . .	7-84
7-12	Error Summary Count Table From OABIAS . . . . .	7-86
7-13	OABIAS Filter Response in Right Ascension of Spin Axis . . . . .	7-87
7-14	OABIAS Filter Response in Declination of Spin Axis . . . . .	7-88
7-15	Estimated Uncertainty in Right Ascension of Spin Axis . . . . .	7-89
7-16	Estimated Uncertainty in Declination of Spin Axis . . . . .	7-90
7-17	Residuals of Sun Angle Model . . . . .	7-91
7-18	Residuals of Single Horizon Dihedral Angle Model . . . . .	7-92
7-19	Display Status Flags and Key Assignments . . . . .	7-94
7-20	Array Allocation Sizes . . . . .	7-98
7-21	Main Control Display . . . . .	7-99
7-22	Options for Copying AE Data Set . . . . .	7-100
7-23	Simulator Options . . . . .	7-101
7-24	NAMELIST LIST . . . . .	7-103
7-25	Options for Reading Data . . . . .	7-105
7-26	Header Record Displays . . . . .	7-106
7-27	Data Record Displays . . . . .	7-109
7-28	Data Selection Options for OASYS . . . . .	7-111
7-29	NAMELIST OPMANI . . . . .	7-113
7-30	OASYS Block Average Results . . . . .	7-116
7-31	Alphas Versus Frame Number, Including Rejected Points . . . . .	7-119
7-32	NAMELIST BIASNL . . . . .	7-120
7-33	Final Results From OABIAS . . . . .	7-123
7-34	Table of Errors From OABIAS . . . . .	7-125
7-35	Correlation Coefficients . . . . .	7-127
7-36	Right Ascension Versus Frame Number . . . . .	7-128
7-37	Uncertainty in Right Ascension Versus Frame Number . . . . .	7-129
7-38	Residuals From Sun Angle Model . . . . .	7-130
7-39	Options for Data Prediction . . . . .	7-131

# PRELIMINARY DRAFT

ORIGINAL PAGE IS  
OF POOR QUALITY

## LIST OF ILLUSTRATIONS (Cont'd)

### Figure

7-40	Predicted and Observed Rotation Angles Versus Time . . . .	7-135
7-41	Predicted and Observed Earth Widths Versus Frame Number . . . . .	7-136
7-42	Core Storage and Time Remaining Display . . . . .	7-137
7-43	Error Messages From ODAP . . . . .	7-150
7-44	JCL to Compile, Link, and Execute MSAD/OABIAS . . . . .	7-166
7-45	JCL to Execute MSAD/OABIAS . . . . .	7-171

## LIST OF TABLES

### Table

1-1	Dependence of Observation Models on State Vector Components . . . . .	1-12
3-1	Coordinate Frames, Axes, and Unit Vectors . . . . .	3-39
3-2	Weighting Factor Equation Used in OABIAS . . . . .	3-95
5-1	Identification of the Elements of the Arrays Belonging to the State Vector Class of Arrays . . . . .	5-25
5-2	Identification of the Elements of the Arrays Belonging to the Model Class of Arrays . . . . .	5-26
5-3	Identification of the Elements of the Arrays Belonging to the Diagnostic Output Control Class of Arrays . . . . .	5-27
5-4	Interpretation of Diagnostic Output Control by Array IDIAGN in COMMON INBIAS . . . . .	5-28
7-1	OABIAS Error-Message Error - Table Correlation Matrix . . . . .	7-158

SECTION 1 - INTRODUCTION

**1.1 MOTIVATION FOR BIAS DETERMINATION**

In the simplest, spin-stabilized satellite attitude determination problem, the state vector consists of only two elements which define the orientation of the angular momentum vector in inertial space. In practice it is known that the presence of biases caused by the misalignment of sensors, or by misspecified hardware characteristics, will cause inaccuracies or the complete breakdown of the simple attitude determination computations. This can lead to inaccuracies in attitude control if the spacecraft spin axis orientation cannot be determined to within control system uncertainties, or worse, it can lead to attitude determination blackouts during which computations yield no solution for attitude. Therefore, in more realistic analyses, additional elements, e.g., sensor mounting angles which affect the accuracy of an attitude estimate, are included in the state vector computation to provide improved knowledge of the values of parameters.

Accurate bias determination will permit more accurate spacecraft attitude determination and control than could be accomplished purely on the basis of prelaunch measurements. Highly accurate prelaunch measurements not only are difficult and expensive to obtain but also may be invalidated by postlaunch changes in the spacecraft due to thermal or mechanical shocks. Also, spacecraft dynamic imbalance effects which may appear as sensor biases are expensive to remove completely before launch and may change due to discrete events in the mission profile, such as apogee motor firing or boom deployment.

The Multisatellite Attitude Determination/Optical Aspect Bias Determination (MSAD/OABIAS) System in its present form provides the necessary bias determination and spin axis attitude refinement for spin-stabilized spacecraft with sensor configurations which include Sun sensors and horizon sensors.

**ORIGINAL PAGE IS  
OF POOR QUALITY**

The sensor observables are accurately modeled and are used in a recursive least-squares filter technique to estimate the elements of a state vector, which include the two components of the attitude; Sun sensor azimuth, elevation and plane tilt; Earth sensor azimuth and elevation; Earth sensor-triggering threshold; and fixed time delays on sensor triggerings. In addition, a state vector component is used to correct the in-track orbital position, which is the most likely orbital error as well as the largest single orbital uncertainty.

The interactive graphics capabilities programmed into MSAD/OABIAS provide for a synergistic collaboration between analyst and computer. Generally, it is not feasible to solve for spin axis attitude, sensor misalignments, and orbital position simultaneously. Analyst intervention is required to select the data span and to choose the variables to be solved using that data span. The computer program can best evaluate the numerical parameters and the fit to the data. Analyst scrutiny is required further to detect the possibility of unmodeled effects in the data, which may arise from the use of an early orbit estimate or from anomalous sensor performance.

MSAD/OABIAS is, therefore, an interactive data processing system for determining the maximum information content of a spacecraft attitude sensor data set.

## **1.2 HISTORICAL BACKGROUND**

Prior to the development of the MSAD/OABIAS System, the Optical Aspect Attitude Determination System (OASYS) was used to evaluate biases. During mission support, biases were observed through large dispersions between single-frame deterministic attitude solutions or through large spans of data which yielded no solution. Several trial and error techniques were developed to adjust bias parameter on input to OASYS to reduce the attitude solution dispersion and to improve the quality of the fit to the data. This latter adjustment was accomplished by displaying the raw data superimposed on a computer

**ORIGINAL PAGE 16  
OF POOR QUALITY**

prediction of the data based on the system-determined attitudes and system-estimated biases. In addition, it was possible to determine fixed-angle biases on the Sun angle, the nadir angle, and the dihedral angles calculated for input to the differential correction subsystem of OASYS. Biases which could not be treated as fixed-angle biases due to the Earth sensor-triggering threshold (such as, the sensor-mounting angle bias or the bias on the apparent radius of the Earth) could be determined only by the manual trial and error techniques. Although it was possible to develop considerable analyst expertise in recognizing what biases could be applied to fit the data, these techniques had several drawbacks.

One drawback was that because the nadir angles or dihedral angles are computed through nonlinear transformation of measurements, the biases of these angles were not necessarily physically meaningful. Also, if more than one bias was present, manual trial and error techniques were too slow for real-time support and led to uncertainties about the uniqueness of the bias solution determined.

MSAD/OABIAS was designed to address the above difficulties. It uses as input the true measurements received in the telemetry, and its interactive graphics control structure is designed to speed operational and analytical processing. MSAD/OABIAS evolved from a study of analytical techniques for recursive least-squares Kalman filters (Reference 1). The preliminary design (Reference 2) added a bias determination subsystem to the existing OASYS at the point at which the differential correction subsystem was invoked.

MSAD/OABIAS is a multisatellite system and has been used on data from the Interplanetary Monitoring Platform (IMP), the Small Scientific Satellite (S<sup>3</sup>), the Radio Astronomy Explorer-B (RAE-B), the Atmosphere Explorer-C (AE-C) and the Synchronous Meteorological Satellite-A and -B (SMS-A, -B). The user

**ORIGINAL PAGE IS  
OF POOR QUALITY**

simply supplies MSAD/OBIAS with a sensor-measurement data set in a standard format.<sup>1</sup>

### **1.3 SYSTEM OVERVIEW**

All interactive graphics display services and the interactive control of program flow in MSAD/OBIAS are accomplished through the Graphics Executive Support System (GESS). This system may be considered an overall executive control program or a subsystem of programs which supply graphics support to MSAD/OBIAS at specified points in the program flow. In addition to GESS, five main functional subsystems exist in MSAD/OBIAS. These are

1. Data selection and adjustment subsystem (OADRIV)
2. Data simulator subsystem (ODAP)
3. Deterministic attitude determination processor subsystem (OASYS)
4. Recursive least-squares filter subsystem (OBIAS)
5. Data prediction and solution comparison subsystem (PLOTOC)

Also, an auxiliary routine (AECOPY) copies AE-C spacecraft data in a form readable by the MSAD/OBIAS System. Figure 1-1 shows these major functional subsystems in a program baseline diagram hierarchy. OAMAIN and OPMAIN are drivers and are shown for the sake of accuracy.

In the standard processing sequence, the GESS executive calls the system driver OADRIV. OADRIV either obtains the data to be processed from an OBIAS measurement data set or causes the data simulator ODAP to be invoked. In the case of AE-C data, AECOPY must be invoked by OADRIV to produce the standard OBIAS measurement data set. OADRIV then calls the deterministic processor OASYS (through OPMAIN), and the deterministic solution is used as an a priori estimate in the recursive least-squares filter

---

<sup>1</sup>Due to the exigencies of the AE-C mission, this standard format was violated, necessitating the development of a utility interface routine.

ORIGINAL PAGE IS  
OF POOR QUALITY

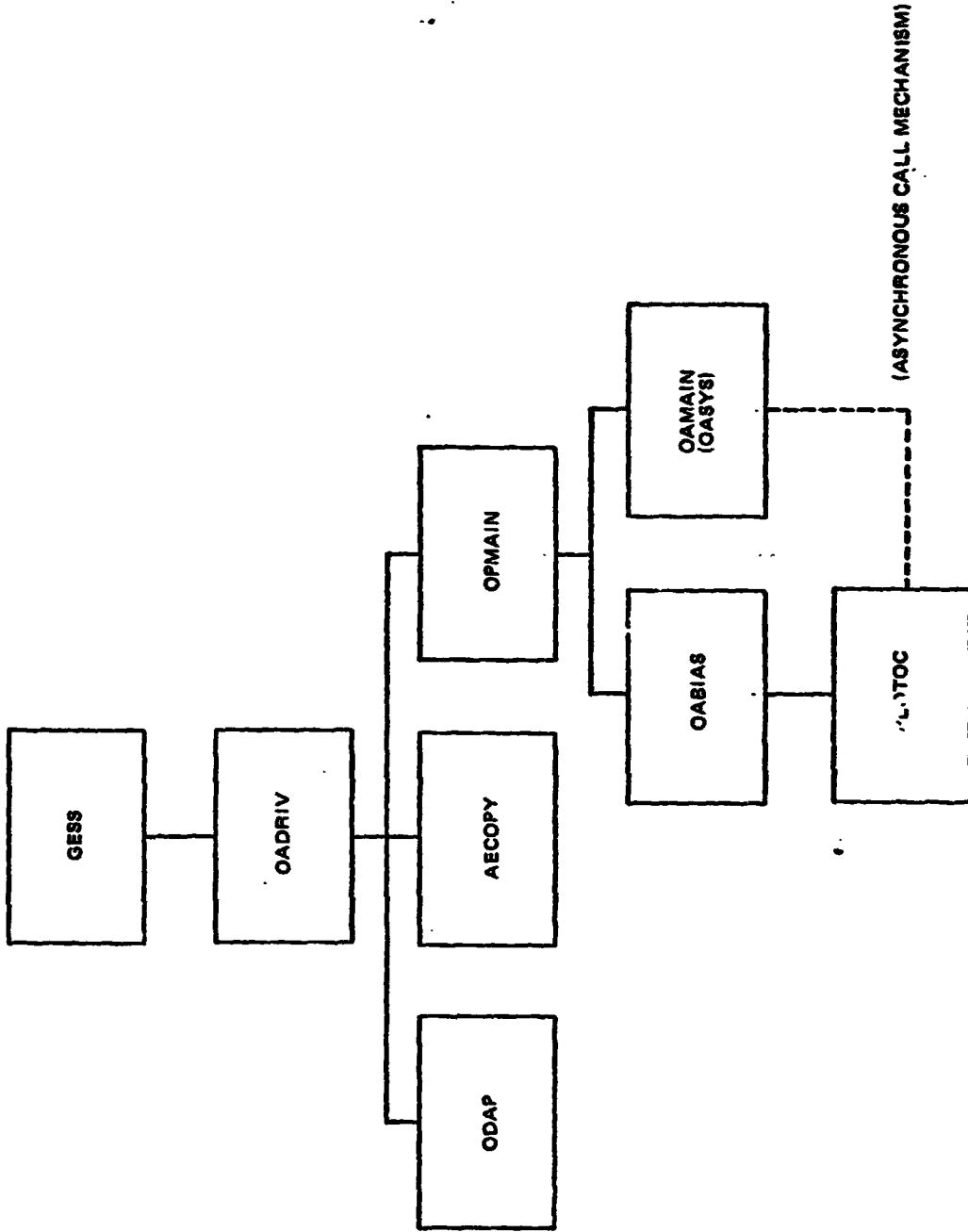


Figure 1-1. MSAD/OABIAS Functional Subsystems

ORIGINAL PAGE IS  
OF POOR QUALITY

subsystem OABIAS. The user may call the data prediction and graphical solution comparison subsystem PLOTOC from OABIAS or asynchronously from OASYS. (Refer to Volume III for a thorough presentation of the mechanics of the graphical processing options.)

MSAD/OABIAS has multiple options for accessing ephemeris data which are required by all of the subsystems. Options are available through the multi-satellite routine EPHENG to read spacecraft ephemerides as well as lunar and solar ephemerides. The position of the spacecraft can be obtained from either the Definitive Orbit Determination System (DODS) file (Reference 3) or the Goddard Trajectory Determination System (GTDS) file (Reference 4). It also can be internally generated through a simple orbit generator (ORBGEN). The positions of the Sun and the Moon can be obtained from a Jet Propulsion Laboratory (JPL) ephemeris file (Reference 5) or a SUNRD file (Reference 6). These positions likewise can be generated internally by using SUN1 for the Sun and ORBGEN for the Moon. Internally-generated ephemerides are useful for simulation purposes. The user is not constrained to use the same ephemeris source in simulating and processing data.

### 1.3.1 OADRIV

OADRIV is the main control subroutine for the MSAD/OABIAS System. Operationally, it serves as the data evaluation, selection, and adjustment subsystem. Although the rest of the MSAD/OABIAS System is limited to 200 frames of data, if core storage is not limited, OADRIV can accept over 1200 frames. This enables rapid and detailed data evaluation and selection by the operator. The OADRIV capacity is limited to approximately 1200 frames because the storage capacity of the IBM 2250 display device buffer is limited.

OADRIV provides a variety of options for sifting the data, including periodic reading of the data by either time or frame number. Also, individual data points in either plot or character displays may be flagged, noise or biases

**ORIGINAL PAGE IS  
OF POOR QUALITY**

may be added to the data (for evaluation or testing purposes), and the appropriate interval may be selected for processing by the attitude and bias determination subsystems.

The capability of the user to edit the data entered in the determination systems is crucial. Because of the variable quality of attitude data and the subtle data rejection decisions which must be made based on knowledge of the hardware or an understanding of spurious events (such as boom reflections), operator intervention in the execution of the program is required. Rejection of spurious data could be done by machine, but undoubtedly, this would require an undeterminable amount of additional storage.

### **1.3.2 ODAP**

ODAP, the data simulator subsystem in MSAD/OABIAS, is a modified graphics version of the program described in Reference 7. It allows all system capabilities to be exercised in the simulation mode, which is essential to any system as large and complex as MSAD/OABIAS. An attached simulator not only facilitates system testing but also makes it feasible. The simulator is also used for prelaunch analysis and simulations. Data can be simulated for any mission conditions, and noise and biases can be applied and passed through to the attitude processors. This simulation-processing sequence can be repeated as necessary during a single execution of the system. The data simulator is not normally used during mission support and can be overlayed when not in use.

### **1.3.3 OASYS**

The OASYS subsystem, an interactive graphics version of the program described in Reference 8, serves as a deterministic attitude determination processor within MSAD/OABIAS. Each data frame consists of the Sun angle, the Sun crossing time, and the Earth-in and Earth-out triggering times, and can be used to compute attitude by four geometric methods--Earth-in, Earth-out, Earth width, and mid-scan dihedral angle. The average of these single

**ORIGINAL PAGE IS  
OF POOR QUALITY**

frame solutions provides an initial estimate to the recursive least-squares filter in OABIAS.

In addition graphical plots of the frame-by-frame attitude solutions obtained through the different methods give insight into what biases may be present. The Earth width method, for example, is sensitive to a bias on the apparent angular radius of the Earth and, in the event of such a bias, yields results which are different from the mid-scan dihedral angle method which is not sensitive to this bias. As a check on the biases determined, the biases can be entered in OASYS and the solutions observed graphically. The correct solution will have the effect of reducing the attitude dispersion in the single-frame solutions and minimizing the difference between the curves for the different solution methods.

#### **1.3.4 OABIAS**

OABIAS is the subsystem which determines the biases and from which the system as a whole takes its name. It is a recursive least-squares filter designed to determine spin axis attitude, sensor biases, and in-track orbit error (Reference 2). The 12-component state vector is composed of the following elements:

- X inertial component of the spin axis<sup>1</sup>
- Y inertial component of the spin axis<sup>1</sup>
- Spin rate
- Phase of rotation measured from the projection of the sunline in the spacecraft spin plane
- Seven sensor bias parameters
- In-track orbital error

---

<sup>1</sup>This component is converted to right ascension and declination of the spin axis in all output displays.

**ORIGINAL PAGE IS  
OF POOR QUALITY**

The OABIAS subsystem uses eight models (functions) of the observables which are dependent on the state vector elements in the filtering scheme. The program provides graphical displays of the state vector elements on a point-by-point basis as well as displays of statistical parameters; e.g., residuals and correlation coefficients. The user has control of all input parameters from the graphics device and can make multiple passes through the data to achieve an optimal solution. (See Section 1.4 for details of the filter and the observation models.)

### **1.3.5 PLOTOC**

The PLOTOC subsystem provides plots of the predicted and observed Earth widths and rotation angles. PLOTOC will display up to three predicted plots simultaneously. Typically this data will be displayed with the deterministic solution input to OABIAS and the OABIAS solution. The degree of fit to the data can then be determined visually.

Parameters can be varied manually to see the effect on the observed fit. Although these parameters--which include height of the atmosphere, oblateness coefficients, and orbital elements--are not in the state vector, their potential effect on the solution must be gauged. The PLOTOC plots clearly show unmodeled effects. PLOTOC provides a check on the validity of the OABIAS solutions and, because all GESS-generated plots can be routed to hardcopy CalComp plots, a way to document the results.

## **1.4 OABIAS RECURSIVE LEAST-SQUARES FILTER**

### **1.4.1 Introduction**

The OABIAS recursive least-squares filter is based on eight distinct observation models. They are

- Model 1--Sun angle model
- Model 2--Sun sighting time model

**ORIGINAL PAGE IS  
OF POOR QUALITY**

- Model 3--Nadir vector projection model
- Model 4--Horizon crossing time model
- Model 5--Sun to Earth-in and Sun to Earth-out dihedral angle model
- Model 6--Earth width model
- Model 7--Small target model
- Model 8--Sun to Earth mid-scan dihedral angle model

(See Section 1.4.2 for individual descriptions.) Any combination of these models may be used. However, statistically independent models should be chosen to obtain valid statistical uncertainties. For example, if the observations available are the Sun angle, the Sun sighting time, and the times at which the horizon sensor acquires and loses the disk of the Earth, a valid choice of statistically independent models would be Models 6, and 8. The addition of any other models, such as Model 5, to process the same observations would yield unrealistically low uncertainties.

Each observation model is formulated as a function of a subset of the 12 state vector components which include two components of the spin axis attitude, the spin rate, the initial phase of the X axis (Sun sensor), and the following eight biases (seven sensor biases and one orbit parameter):

1. Horizon sensor mounting angle bias (equivalent to a bias in the elevation of the sensor relative to the spin plane)
2. Azimuth bias of the horizon sensor relative to the Sun sensor on horizon-in triggering
3. Azimuth bias of the horizon sensor relative to the Sun sensor on horizon-out triggering
4. Bias on the angular radius of the central body (equivalent to a sensor-triggering level bias)
5. Sun angle bias

**ORIGINAL PAGE IS  
OF POOR QUALITY**

6. Sun sensor plane tilt
7. Panoramic attitude sensor plane tilt (used for RAE-B mission)
8. Orbital in-track error

It is not possible to determine all of the state vector elements from any one observation model. The dependence of the observation models on the state vector components is summarized in Table 1-1.

Within OABIAS, data is processed one frame at a time. In order to facilitate analysis, options are available to update the state vector after

- Each observation is processed
- Each frame is processed
- A specified number of frames is processed

If the option is taken to update the state vector on a frame-by-frame basis, an additional option is available to iterate through all data frames since the last update. In this way, any desired degree of recursiveness is provided so that even a batch processing differential correction can be obtained.

#### **1.4.2 Observation Models**

Of the eight OABIAS observation models, two are associated with the Sun and six with the central body (either the Earth or the Moon). The formulation of these observables is summarized here. (See Section 3 of this volume for additional details.)

- Model 1--Sun angle model. The observable for Model 1 is the Sun angle reported with the data. The predicted value is determined by the position of the Sun (from either a solar ephemeris or an algebraic routine) relative to the spacecraft, the spin axis attitude, the Sun sensor plane tilt, and the Sun angle bias.

ORIGINAL PAGE IS  
OF POOR QUALITY

Table 1-1. Dependence of Observation Models on  
State Vector Components

STATE VECTOR COMPONENT	MODEL 1	MODEL 2	MODEL 3	MODEL 4	MODEL 5	MODEL 6	MODEL 7	MODEL 8
$S_1$	X	X	X	X	X	X	X	X
$S_2$	X	X	X	X	X	X	X	X
$\psi_0$		X	X	X	X	X	X	X
$\Delta T$			X	X	X	X	X	X
$I_{\phi H}$			X	X	X	X	X	X
$O_{\phi H}$			X	X	X	X	X	X
$\Delta p$			X	X	X	X	X	X
$\theta_0$	X							
$\omega$		X	X	X	X	X	X	X
$e$	X	X						
$\epsilon_H$			X	X	X	X	X	X
$\Delta t$			X	X	X	X	X	X

X INDICATES DEPENDENCE

**ORIGINAL PAGE IS  
OF POOR QUALITY**

- **Model 2--Sun sighting time model.** The observation for Model 2 is the projection of the Sun vector onto a vector normal to the plane containing the spin axis and Sun sensor slit. The expression for this projection is evaluated at the Sun sighting time. Since the Sun must lie in the plane containing the spin axis and the Sun sensor slit when it is sighted, the observed value is always zero.
- **Model 3--Nadir vector projection model.** The observation for Model 3 is the projection of a unit vector along the optical axis of the horizon sensor onto the nadir vector. The observation is evaluated at the time of a horizon crossing.
- **Model 4--Horizon crossing time model.** The observation for this model is the projection of the horizon vector onto the normal to the plane containing the spin axis and the optical axis of the horizon sensor. It is evaluated at the time of a horizon crossing. Therefore, as in the case of Model 2, the observed value is zero.
- **Model 5--Sun to Earth-in and Sun to Earth-out dihedral angle model.** The two observables for Model 5 are the rotation angles from the Sun to Earth-in crossing and from the Sun to Earth-out crossing. These observables are available directly from the data.
- **Model 6--Earth width model.** The observable for Model 6 is the Earth width dihedral angle, defined as the Earth-out rotation angle minus the Earth-in rotation angle. This model does not depend on a Sun sighting. Therefore, it may be used when the Sun is not visible or when a Sun sighting reference time is not available from the data (as with the AE-C wheel-mounted horizon sensors).
- **Model 7--Small target model.** This model is used when the central body is treated as a point source; e. g., the RAE-B mission. The

ORIGINAL PAGE 19  
OF POOR QUALITY

observable is the sensor mounting angle; i. e. , the angle between the spin axis of the spacecraft and the nadir vector. The nadir vector is assumed to be along the line of sight of the horizon sensor.

- Model 8--Sun to Earth mid-scan dihedral angle model. The observable for this model is the dihedral angle from the Sun to the mid-point between the Earth-in crossing and the Earth-out crossing. For a spherical Earth this would be the same as the dihedral angle from the Sun to the center of the Earth. However, for an oblate Earth the perpendicular bisector of the great circle between the Earth-in crossing and the Earth-out crossing generally does not go through the Earth's center.

Models 6 and 8 are statistically independent whereas the two parts of Models 4 and 5 are not. Therefore, Models 1, 6, and 8 generally would be preferred for processing over Models 1 and 5 or Models 1 and 4. However, Models 6 and 8 depend on both horizon crossings being available, whereas Models 4 and 5 treat the two horizon crossings separately. Thus, Model 4 or 5 would be used when only a single horizon crossing was available; e. g. , a sensor operating in the visible range and triggering on one horizon crossing and the terminator.

## SECTION 2 - SENSOR DESCRIPTIONS

This section describes the Sun sensors and the body-fixed horizon detectors which usually are used onboard satellites supported by the MSAD/OBIAS System. Brief descriptions of the wheel-mounted horizon scanner used by the AE-C satellite and the panoramic attitude scanner (PAS) used on the RAE-B satellite also are included. MSAD/OBIAS supported both the AE-C and the RAE-B missions. The RAE-B PAS application necessitated OBIAS modifications which are described throughout this document.

The geometry of the Sun-sensing and horizon-sensing operations is of primary significance to the MSAD/OBIAS System and, therefore, is emphasized. Detailed physical and internal characteristics of currently available sensors are less important to MSAD/OBIAS and, hence, are not described in this document.

### 2.1 SUN SENSOR

Figure 2-1 shows the main geometric features of the Sun sensor system which has been assumed in the design of MSAD/OBIAS. The sensor's field-of-view (FOV) is fan-shaped and is indicated in Figure 2-1 by the heavy line. The FOV is centered about the face axis  $x_{ss}$  which is at an angle  $\xi_m$  from the satellite equatorial plane. A common value for the total FOV angle  $\tau$  is 128 degrees. The sensor is mounted such that its nominal FOV plane contains the satellite's spin axis  $\hat{S}$ . (In Figure 2-1,  $\hat{S}$  is shown lying in the FOV plane.) Sun sensor systems commonly employ two sensors mounted with their face axis  $x_{ss}$  on opposite sides of the satellite's equatorial plane. This arrangement permits full coverage of the celestial sphere with two 128-degree sensors and provides redundancy over the satellite's equatorial region.

The rotation of the satellite causes the Sun sensor's FOV to sweep out a wide belt on the celestial sphere. In Figure 2-1, this is the area between the two



heavy dashed lines. The sensor sees the Sun once per spin period if the Sun lies within this belt. Otherwise, it does not see the Sun at all. The Sun sighting points occur when the rotating FOV plane crosses the Sun vector  $\hat{U}$ .

Each time the Sun is sighted, the Sun sensor system provides MSAD/OBIAS with two pieces of information--the time  $t_s$  at which the sighting occurred and the elevation angle  $\xi_s$  of the Sun above the sensor face axis  $x_{ss}$  at  $t_s$ . The onboard sensor itself normally does not establish  $t_s$ . It provides a reference pulse at each sighting which is used elsewhere in the spacecraft. Normally,  $t_s$  is a time tag which is placed on the telemetry data on the ground. The satellite spin rate  $\omega$  is computed from the time intervals between successive Sun sighting pulses. The elevation angle  $\xi_s$  is used to determine the desired angle  $\beta$  between the satellite spin axis  $\hat{S}$  and the Sun vector  $\hat{U}$ . Neglecting sensor mounting alignment errors,  $\beta = 90^\circ - \xi_s - \xi_m$ .

## 2.2 HORIZON DETECTOR

Figure 2-2 shows the main geometric features of the horizon detector system which has been assumed in the design of MSAD/OBIAS. The sensor's FOV is narrow and usually is either circular or square. In practice, the FOV diameter or side is commonly in the 1- to 1.5-degree range. A hypothetical unit vector  $\hat{L}$  is located in the center of the FOV;  $\hat{L}$  is fixed in the satellite. The sensor mounting angle  $\gamma$  between the satellite's spin axis  $\hat{S}$  and  $\hat{L}$  is tailored to mission requirements. Satellites which employ horizon scanners commonly include two or more units with different  $\gamma$  angles. This provides redundancy and permits increased coverage throughout the mission since the band swept out by the horizon scanner is small and will miss the central body in some spacecraft orientations.

The rotation of the satellite causes  $\hat{L}$  to sweep out a small circle on the celestial sphere, indicated in Figure 2-1 by the dashed line. The horizon detector system provides output signals (1) at "in-times"  $t_{III}$ , when  $\hat{L}$  crosses the



**ORIGINAL PAGE IS  
OF POOR QUALITY**

boundary from the sky to the central body (Earth or Moon), and (2) at "out-times"  $t_{HO}$ , when  $\hat{L}$  crosses the boundary from the central body to the sky. There will be one in-crossing and one out-crossing in each spacecraft revolution during those portions of the mission when the central body lies within the FOV loci on the celestial sphere (assuming intersection with only one central body). The outputs of the horizon scanner system used by MSAD/OABIAS are the horizon crossing times  $t_{HI}$  and  $t_{HO}$ . In most systems, the horizon crossing parameters measured by the onboard equipment actually are  $t_{HI} - t_s$  and  $t_{HO} - t_s$ . Ground operations convert these measurements to the inputs  $t_{HI}$  and  $t_{HO}$  required by MSAD/OABIAS.

Horizon detectors are designed to be sensitive to either visible light or to infrared radiation. For MSAD/OABIAS operations, the significant difference between the two types of sensors is that visible light sensors detect planetary disk terminators, while infrared sensors detect only the true planetary disk boundary. The OASYS portion of the MSAD/OABIAS System is capable of detecting and rejecting terminator crossings.

### **2.3 AE-C WHEEL-MOUNTED HORIZON SENSORS**

The AE-C spacecraft has one horizon sensor mounted on its body and two sensors that effectively are mounted on the spacecraft's momentum wheel. In fact, the two wheel sensors are mounted on the body of the spacecraft with their field of view nominally parallel to the spin axis of the momentum wheel. Each of these sensors looks into a mirror mounted on the momentum wheel so that the motion of the wheel carries the sensor scan about the celestial sphere.

Within OABIAS, the modeling of the wheel sensors is identical to that of the body sensor. Since there is no wheel-mounted Sun sensor, only Sun angle data (from the body-mounted Sun sensor) and Earth width data are available for attitude determination. The modeling of the wheel-sensor biases is the same as for the body-sensor biases. However, because the bolometer associated

ORIGINAL PAGE IS  
OF POOR QUALITY

with the wheel-mounted sensors is mounted on the body of the spacecraft, an additional physical misalignment is possible. Specifically, the bolometer could be mounted off-axis of the body of the spacecraft and, therefore, be misaligned with the axis of the wheel. This would cause a sinusoidal oscillation in the wheel-sensor, Earth width data as the spin of the spacecraft carried the wheel sensor axis in a small circle about the spin axis. The modeling appropriate to a misalignment of the sensor axis is discussed in detail in Reference 9.

#### 4.4 RAE-B PANORAMIC ATTITUDE SENSOR (PAS)

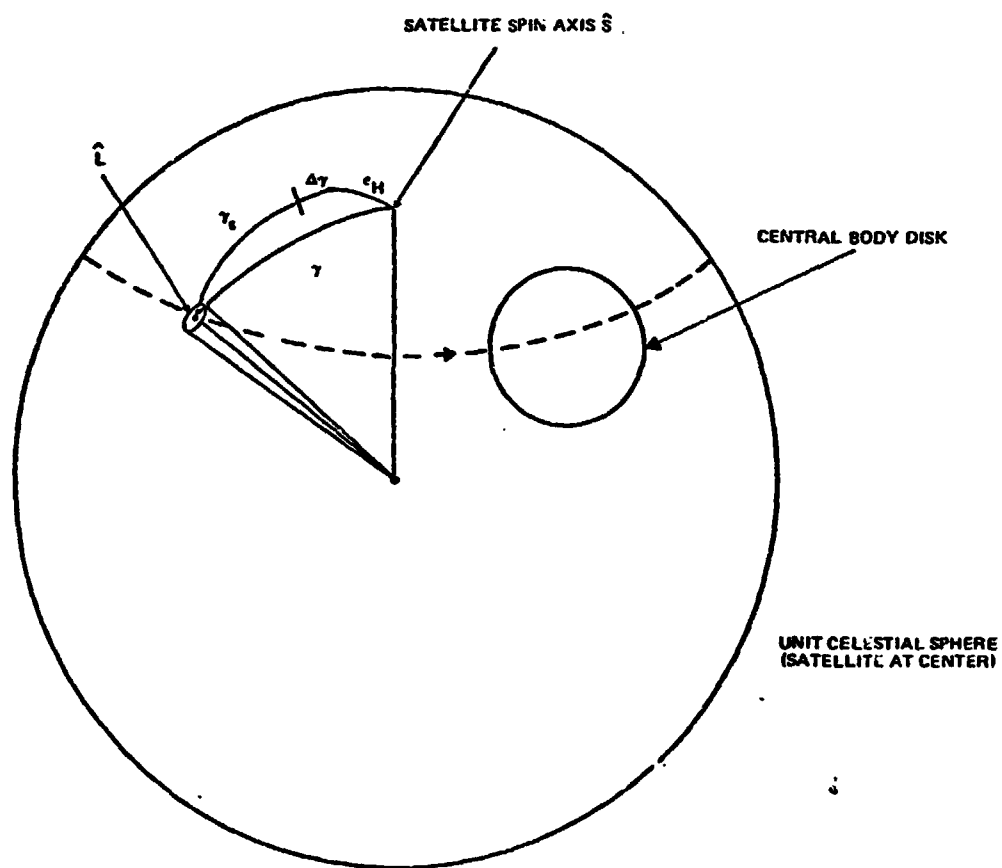
Figure 2-3 shows the geometry of the PAS which was used on the RAE-B satellite. In this figure,  $\epsilon_H$  and  $\Delta\gamma$  are small misalignment angles which will be discussed in detail in Section 3.

One difference between the PAS system and the usual horizon detector is of primary significance to OBIAS; namely, the mounting angle  $\gamma_s$  of the PAS line-of-sight vector  $\hat{L}$  relative to the satellite's spin axis  $\hat{S}$  is not constant. Instead,  $\gamma_s$  can be stepped in a predetermined manner.

On RAE-B, the PAS sensor system supported the translunar phase of the mission during which the central body--the Moon--was sufficiently small to be approximated as a point source for attitude determination purposes. The angle  $\gamma_s$  was advanced 0.7 degree per spin revolution. These steps were actuated by reference pulses from a Sun sensor. The  $\gamma_s$  advance signal was inhibited upon scanner acquisition of a central body. The angle  $\gamma_s$  at which the central body was acquired was the primary information which PAS provided.

The time variation of  $\gamma_s$  on the PAS system made the addition of the misalignment angle  $\epsilon_H$  to the OBIAS mathematical representation of the horizon detector necessary. When modeling the more common body-fixed horizon detectors,  $\epsilon_H$  is not needed. Two new observation models--7 and 8-- were added to OBIAS for use with PAS.

ORIGINAL PAGE IS  
OF POOR QUALITY



NOTE 1:  $e_H$  AND  $\Delta\gamma$  INDICATE MISALIGNMENT ANGLES.

NOTE 2:  $\gamma_s$  VARIES IN 0.7 DEGREE STEPS.

Figure 2-3. RAE-B PAS Geometry

SECTION 2 - ANALYSIS

3.1 INTRODUCTION

This section contains the mathematical algorithms used in the recursive estimator subsystem (OABIAS) of the MSAD/OABIAS System. The logic used in OASYS, the deterministic attitude determination subsystem, is summarized in Section 3.2. Section 3.3 describes the general recursive estimation technique and its application to attitude determination problems. The description covers the following three topics:

1. The recursive and batch processing approaches with a comparison of their merits and drawbacks.
2. The fundamental recursive estimation algorithm on which OABIAS is based. (See Appendix B for the derivation of this algorithm.)
3. The selection or computation of the observation weighting factors.

The general features of the implementation of the estimation algorithm in OABIAS are discussed in Section 3.4. This section describes the modifications made to the algorithm presented in Section 3.3, denotes the main inputs which the program requires, and presents an introduction to the observables and state vector elements which OABIAS employs. Also discussed are the options in OABIAS which enable the user to influence its performance as a recursive estimator, i.e., the state vector updating frequency selection and the iterative operation options.

The remaining portions of Section 3 describe the OABIAS mathematics in more detail. Section 3.5 discusses the satellite and sensor geometry assumed and employed in the OABIAS subsystem. This section includes coordinate frames, transformation matrices, and the mathematical representation of the sensors. It also presents precise definitions of the elements  $x_{\alpha}$  in the state vector  $\underline{x}$ .

**ORIGINAL PAGE IS  
OF POOR QUALITY**

Each of the eight observation models available in OABIAS are discussed in Section 3.6. (See Appendix A for the equations of the observation partial derivatives.) Sections 3.7 through 3.9 cover three additional topics: the computation of the central body angular radius  $\rho_c$ , the horizon crossing vector  $\hat{D}$ , and the weighting factors  $w_j$ . Finally, Section 3.10 summarizes the Section 3 material.

The notation used throughout Section 3 is as follows. General  $3 \times 1$  Cartesian vectors are represented by an overhead arrow ( $\vec{V}$ ), and  $3 \times 1$  Cartesian vectors of unit length are represented by an overhead caret ( $\hat{V}$ ). The magnitude of a vector normally is designated by encasing it with two vertical lines ( $|\vec{V}|$ ); however, a simpler representation ( $V$ ) is used in places where this can be done without ambiguity or confusion. Coordinate frame resolution is signified by superscripts ( $\vec{V}^{GI}$ ).

More general ( $n \times 1$ ) column vectors are designated by an underline ( $\underline{X}$ ). Matrices are signified by upper case letters with no underlines or overhead symbols ( $P$ ). Superscript T designates the transpose of a matrix ( $G^T$ ) or of a column vector ( $\underline{X}^T$ ). Where it is necessary to distinguish between matrices and scalars, the scalars are designated by lower case letters. For example, the elements of matrix (A) are signified by lower case letters with subscripts ( $a_{ij}$ ). The dimensions of vectors and matrices are indicated beneath the symbols the first time they appear in equations.

A state vector estimate is indicated by an overhead caret ( $\hat{\underline{X}}$ ) to distinguish it from the true state vector ( $\underline{X}$ ). This should cause no confusion with the unit vector notation ( $\hat{V}$ ), because the correct meaning should be obvious from the context of the equations.

**ORIGINAL PAGE IS  
OF POOR QUALITY**

The notation distinguishes between variables and algebraic expressions which are used to compute the values of these variables. For example, in the equation

$$\underline{Y}_c = \underline{Y}_c (\underline{M}, \underline{X}, t)$$

$\underline{Y}_c (\underline{M}, \underline{X}, t)$  is a known algebraic expression. The numerical values of the elements of  $\underline{Y}_c$  are computed by inserting values of  $\underline{M}$ ,  $\underline{X}$ , and  $t$  into it. Parentheses ( ) are used in Section 3 almost exclusively in this manner. Also, brackets [ ] usually denote matrices and braces { }, vectors. However, all three--parentheses, brackets, and braces--are used to enclose scalars.

ORIGINAL PAGE IS  
OF POOR QUALITY

### 3.2 OASYS--DETERMINISTIC ATTITUDE DETERMINATION SUBSYSTEM

The analysis required for an overall understanding of MSAD/OABIAS is summarized in this section. (See Reference 8 for a detailed description of the mathematical techniques used in OASYS.)

Attitude computations are based on horizon crossings only; therefore, OASYS must identify and reject terminator crossings. The attitude calculation is based on either a single-horizon crossing method or a double-horizon crossing method. OASYS can process horizon crossings occurring on either the Earth or the Moon, and can determine which central body is being observed, if necessary. In most cases the system will function without the benefit of an initial attitude estimate.

#### 3.2.1 Input to Deterministic Process

Each input frame of preprocessed telemetry is assumed to contain the following information from a single spin period of the spacecraft:

- The Sun angle, or angle between the spin axis and the Sun vector
- The Sun sighting time
- The horizon sensor "on" time
- The horizon sensor "off" time
- The spacecraft spin rate

OASYS processes each frame of data to identify and reject any horizon sensor triggering which occurred at a terminator crossing. For each remaining horizon sensor triggering, the system computes up to two possible deterministic attitudes. After a block of data has been processed in this fashion, a block-averaging technique is used to select from each pair of attitudes a single attitude, such that all chosen attitudes remain approximately constant throughout the block. The chosen attitude vectors are then averaged.

**3.2.2 Design Assumptions**

The following assumptions are necessary for deterministic processing:

1. The spacecraft attitude is assumed to be approximately constant during one spin period. Note, however, that the spacecraft position is not assumed to be constant during one spin period.
2. The spacecraft spin rate is assumed to be approximately constant during one spin period.
3. The spacecraft is assumed to be sufficiently close to the Earth so that the vector from the Earth to the Sun is approximately parallel to the vector from the spacecraft to the Sun.

The quality of the input sensor data and the accuracy of the initial attitude estimate determine the system logic used during any particular execution. For example, the status of the terminator must be checked for each scan. OASYS must handle the following cases: when the Earth is fully sunlit, when the terminator is visible but is not present in the scan, and when the terminator is intersected by the sensor scan. In all cases the logic is based on the computation of attitude from a single-horizon crossing, with either one attitude computation or two, depending on whether the terminator was present in the scan. The ambiguities involved in calculating attitude from a single-horizon crossing are eliminated by logic spanning successive data points. The assumptions are made that the satellite attitude is changing slowly and that successive nadir angle calculations should yield an unambiguous attitude. The presence of the terminator in the scan is determined by a recursive technique utilizing data predictor modules. Singular conditions, which yield ambiguous results for attitude over a short time span, exist both in the case of a sunlit Earth and in the case of the presence of the terminator. In the latter case, an a priori attitude must be used to resolve the ambiguity.

### 3.2.3 Deterministic Logic

#### 3.2.3.1 Single Frame Processing

Attitude computation is characterized by three levels: the level of a single telemetry frame containing one or two valid horizon crossing triggering times, the higher level on which a full block of processed frames is averaged by the system, and the lower level on which the single triggerings are processed.

For each central body under consideration (Earth, Moon), the following functions are performed at the intermediate, single telemetry frame level:

1. The lighting conditions on the central body are computed from ephemeris data. If the central body is dark or not visible, this triggering is rejected.  
  
If a terminator is visible, the terminator flag for this frame is set. If data are not to be included in attitude calculations while a terminator is visible, the triggering is rejected; otherwise, processing continues as for the sunlit case.
2. The attitude determination routine, ATTDET, is called and as many as two attitudes are computed for this crossing.
3. If ATTDET produced no solution, there is no possible attitude consistent with the assumption that this triggering resulted from a sunlit horizon crossing on this central body; therefore, the crossing is rejected.
4. If the central body is fully sunlit, the processing of this crossing is complete. If a terminator is visible, it must be determined whether this triggering resulted from a terminator crossing or a horizon crossing.

### 3.2.3.2 Terminator Rejection Logic

If a terminator is visible, it must be determined whether it is intersected by the spacecraft sensor scan, i.e., whether a particular triggering of the sensor was in fact a horizon crossing or a terminator crossing. The procedure for this determination is a recursive one, utilizing ODAP (data simulator subsystem) (Reference 7) modules as tools. (See Reference 5 for background analysis of ODAP.)

The routine TERCHK is called once for each possible attitude computed in subroutine ATTDET. TERCHK calls the ODAP module with the computed attitude and determines whether a scan of the central body with this attitude would have produced a sunlit horizon crossing for the in or out triggering, as required. If the computed attitude is not consistent with the assumption that this triggering occurred at a sunlit horizon crossing, this attitude is rejected.

Note that it is possible that this test will fail to reject a terminator crossing when the attitude computed from a terminator crossing is so far from the true attitude that a scan with the erroneous attitude would give a sunlit horizon crossing at this triggering. When this occurs, one attitude is consistent with the assumption that this was a terminator crossing, and a second attitude is consistent with the assumption that the triggering was a sunlit horizon crossing. Therefore, there is no deterministic procedure for recognizing this problem.

However, when the problem occurs, the resulting computed attitude generally has a large error. Since the error is large, the erroneous attitude is easily recognized and rejected in the block-averaging module, SPINAV, assuming either an a priori attitude or a large block of data is available.

### 3.2.3.3 Single-Horizon Crossing Computation

Single-horizon crossing events are processed in the module ATTDET. As many as two possible attitudes are calculated for each event, each with corresponding

**ORIGINAL PAGE 19  
OF POOR QUALITY**

nadir angles and dihedral angles. ATTDET is the key module in the interframe processing. (See Reference 8 for a complete discussion of this computation.)

**3.2.3.4 Block-Averaging Procedure**

Once each input telemetry frame has been processed singly, the best estimate of the attitude must be computed based on the single frame results. Each input telemetry frame results in two output measurement frames, each of which may contain zero, one, or two attitudes. The ambiguities which could not be resolved on a single frame basis now can be eliminated if the block of data is large enough.

The module SPINAV processes a block of output frames to resolve the ambiguities and determine the average attitude. For each output frame containing two possible attitudes, SPINAV must determine which of the attitudes, if any, is valid. Note that in some cases both attitudes must be rejected as erroneous.

The assumption inherent to SPINAV is that attitude should remain approximately constant over the duration of a block of data. Therefore, the ambiguities should be resolved in such a way that the selected attitudes are as nearly constant as possible. The following procedure for resolving the ambiguities applies to the most general case, in which each output frame contains two attitudes and no a priori attitude is available.

The first attitude from the first output frame is selected as a trial attitude. In each other output frame the pair of attitudes is examined, and the attitude from that pair which is closer to the trial attitude (in degrees of arc-length) is selected. One attitude is selected in this manner from each output frame.

The set of attitudes thus selected is averaged using SPNAV1. The attitudes are expressed as unit vectors, each component of the vectors is averaged, and the resulting vector is unitized. (If data weighting is employed, a weighted

**ORIGINAL PAGE IS  
OF POOR QUALITY**

average is computed, with each weight equal to  $1/(\text{attitude uncertainty in degrees of arc-length})^2$ .) The resulting unit vector is the average attitude for the set of attitudes selected.

However, the set may include erroneous attitudes, resulting from noisy or biased data, or from terminator crossings which could not be rejected. Therefore, a residual edit must be performed within SPNAV1. First, the standard deviation of the set of attitudes is computed as follows: Let the residual  $\rho_i$  for each attitude be defined as the angle in degrees between that attitude vector and the average attitude vector. Then the weighted standard deviation  $\sigma$  is computed as follows:

$$\sigma = \sqrt{\frac{\sum \omega_i \rho_i^2}{\sum \omega_i}}$$

where  $\omega_i$  denotes the weight for the  $i$ th frame and the summations are taken over all frames in the block.

The resulting value for  $\sigma$  is the standard deviation of the set of attitudes, in degrees of arc-length. Next, each attitude in the set which has a residual  $\rho_i$  greater than  $n\sigma$ , where  $n$  is an input parameter, is rejected. The default value of  $n$  is 3. The attitudes not rejected in this process are then re-averaged. A new standard deviation is computed and the entire procedure is repeated until no further rejections occur.

Then SPNAV1 returns with the block-average attitude, the standard deviation, and the number of frames included in the final average  $M$ . Next, SPINAV computes a goodness-of-fit parameter, which is intended to measure the amount of scatter in the set of selected attitudes. The goodness-of-fit parameter is equal to  $\sigma/M$ . Note that this parameter takes into account both the final standard deviation and the number of frames included in its computation.

ORIGINAL PAGE 13  
OF POOR QUALITY

The above procedure describes the steps followed using the first attitude from the first frame as a trial attitude. This procedure is repeated using each attitude from each frame as a trial attitude. A running comparison is maintained on the goodness-of-fit parameter, and at each step, the block-average attitude associated with the best fit is saved.

The average attitude associated with the best fit is refined further by the following iterative technique. Using the average attitude to resolve the ambiguities, the program selects one attitude from each pair, as above. SPNAV1 is called to average the selected attitudes. The average obtained by SPNAV1 is used as a new average and the sequence is repeated. The process terminates when the set of attitudes selected remains identical for two successive iterations. Convergence normally occurs in two or three iterations.

The following discussion is intended to clarify the theory behind the block-averaging procedure and explain its strengths and weaknesses.

Consider a block of  $N$  output frames, with each frame having two attitude solutions. The ambiguities can be resolved in  $2^N$  different ways, if one attitude is selected from each pair. If a possibility exists that neither attitude in the pair is correct, then there are  $3^N$  different ways to resolve the ambiguities. A goodness-of-fit parameter can be defined which measures the amount of scatter in the selected attitudes and defines the "correct" way for resolving the ambiguities as the way which minimizes this parameter. An exhaustive search of the  $2^N$  (or  $3^N$ ) choices is the only procedure guaranteed to yield this correct solution. Clearly such a procedure is impractical unless  $N$  is very small. (Note that if  $N = 2$ , the procedure is quite practical. In fact, it corresponds to the case of two horizon crossings, each yielding two attitudes. In that case, a check of the four possible pairings will reveal which pair of attitudes is optimal. When  $N = 2$ , the method in SPINAV reduces to the same situation.) If  $N$  is large, some simplifying assumption must be

ORIGINAL PAGE IS  
OF POOR QUALITY

introduced. The method in SPINAV assumes that at least one of the attitudes in the block is close to the final desired block average, i. e., the block average which would be obtained if the ambiguities were correctly resolved. Clearly, it would be very unusual for a set of attitudes to yield an average which did not lie close to any attitude in the set. Therefore, this simplifying assumption is reasonable, and in virtually all cases it should yield the same result as an exhaustive search of all  $2^N$  cases.

The computation time required for SPINAV is approximately proportional to  $N^2$ . (The number of trial attitudes is  $2N$ . For each trial attitude, SPINAV requires a computation time proportional to  $N$ .) Therefore, the block-averaging method is impractical when  $N$  is large. In practice it has been found that a block with 200 useful output frames requires several minutes of processing time on the IBM S/360-95. In most cases such exhaustive processing of a large block is unnecessary. A small subset of the block can be processed, and the average of this block can be used as an a priori attitude. If an a priori attitude is available, it is used as a trial attitude, and the search for a trial attitude is eliminated. The short iterative procedure described above can be used without searching for a trial attitude. The results in most cases will be identical to those which would be obtained using the complete method.

Finally, no method for resolving the ambiguities, not even an exhaustive search of all  $2^N$  combinations, will yield correct results in all cases. If the attitude is allowed to change in an arbitrary manner from one frame to the next, resolving ambiguities is clearly impossible, even if the data are perfect. Also, if the attitude is constant, but systematic or random errors in the data cause the "correct" attitude solutions to vary within the block by an amount comparable to the difference between the two attitudes in each pair, ambiguities cannot be resolved.

### 3.2.3.5 Other Deterministic Attitude Computations

OASYS provides four methods of independently calculating attitude: one using the Earth-in triggering, one using the Earth-out triggering, a third requiring both triggerings to calculate an Earth width angle and then a nadir angle, and a fourth using the Earth scan mid-time as computed from the two Earth triggerings. This latter method is the double-horizon dihedral angle method. (See Reference 8 for the mathematical details of these methods.)

### 3.2.3.6 Data Weighting

An option is provided in OASYS to compute data weights to be used in the block-averaging procedure. These data weights are computed from user-specified values for the uncertainties in the observables. If the data weighting option is selected, five uncertainties are computed for each single-horizon crossing solution: the arc-length uncertainty in attitude, the uncertainty in right ascension of the spin vector, the uncertainty in declination of the spin vector  $\delta$ , the uncertainty in the nadir angle, and the uncertainty in the dihedral angle. For each double horizon solution, the uncertainty in the nadir angle and the uncertainty in the dihedral angle are computed.

In the block-averaging procedure (SPINAV), the unit spin vectors are averaged with each spin vector assigned a weight equal to  $1/(\text{arc-length uncertainty in degrees})^2$ .

In addition to providing weighting factors, OASYS provides a measure of the uncertainty in the block-average attitude, by computing a weighted average of the uncertainties for all frames. A weighted average is computed for the uncertainties in arc-length,  $\alpha$ , and  $\delta$ . The weights used in computing these weighted averages are the same weights used in the block-averaging procedure,  $1/(\text{arc-length uncertainty in degrees})^2$ .

ORIGINAL PAGE IS  
OF POOR QUALITY

The following technique is used to compute uncertainties: Let  $f$  be a function describing some computed quantity in terms of observed quantities. For example,  $f$  might be the function which expresses the right ascension of a unit vector along the spin axis  $\alpha$  in terms of the observables  $\beta$ ,  $\gamma$ ,  $\rho$ ,  $A$ , and  $t$ .

$$\alpha = f(\beta, \gamma, \rho, A, \vec{R}(t))$$

where  $\beta$  = Sun angle

$\gamma$  = sensor mounting angle

$\rho$  = effective angular radius of the Earth

$A$  = rotation angle from Sun crossing to horizon crossing

$\vec{R}(t)$  = spacecraft position at time  $t$

Strictly speaking, not all of these quantities are directly observed. For example, the Sun angle  $\beta$  is computed from a coded field in the telemetry, and the rotation angle  $A$  is computed from a spin rate and crossing times, which in turn are computed from clock counts in the telemetry. However, this set of observables has the advantage that uncertainties in each observable may be conveniently estimated and treated as constant, at least over a single block of data.

Standard error analysis yields the following expression for the uncertainty in  $\alpha$ :

$$\sigma_{\alpha}^2 = \left( \sigma_{\beta} \frac{\partial \alpha}{\partial \beta} \right)^2 + \left( \sigma_{\gamma} \frac{\partial \alpha}{\partial \gamma} \right)^2 + \dots$$

where  $\sigma_{\alpha}$  = standard deviation of  $\alpha$

$\sigma_{\beta}$  = standard deviation of  $\beta$

and similarly for each observable.

**ORIGINAL PAGE IS  
OF POOR QUALITY**

This analysis is based on the assumption that the errors in the observables are normally distributed, uncorrelated errors which are small enough so that the function  $f$  may be treated as linear, i. e. ; the partial differentials  $\partial\alpha/\partial\beta$ , etc., may be treated as constant.

Given that the function can be treated as linear in the desired region, the derivatives may be computed numerically, as follows:

$$\left(\sigma_{\beta} \frac{\partial\alpha}{\partial\beta}\right)^2 \cong [f(\beta, \gamma, \dots) - f(\beta + \sigma_{\beta}, \gamma, \dots)]^2$$

This technique is easily applied to any function  $f$  which can be evaluated numerically.

In actual implementation the method works as follows: the attitude, the nadir angle, and the dihedral angle are computed using the observed data. Then the specified uncertainty in the Sun angle is added to the observed Sun angle, and the attitude, the nadir angle, and the dihedral angle are re-computed, using the perturbed Sun angle with all other parameters as before. The changes in attitude, nadir angle, and dihedral angle are saved. Next the specified uncertainty in some other parameter is added to the observed value, and attitude is computed again, using a perturbed value for only one observable at a time. After each observable has been perturbed in this manner, the uncertainty in  $\alpha$ , for example, is computed as

$$\sigma_{\alpha} = \sqrt{\sum \Delta\alpha_i^2}$$

where  $\Delta\alpha_i$  = the change in  $\alpha$  resulting from a perturbation to the  $i$ th observable

**ORIGINAL PAGE IS  
OF POOR QUALITY**

Note that for the uncertainty in time  $t$  the ephemeris routines must be called to obtain the position at the perturbed time  $t + \sigma_t$ . This error in time can be used to represent both the effect of an absolute timing error (i. e., the absolute times from the attitude telemetry are not consistent with the absolute times used for orbit determination) and the effect of an in-track orbit error of a given time magnitude (i. e., the spacecraft is 30 seconds ahead of or behind the orbit tape prediction).

This method of uncertainty computation breaks down if attitude cannot be computed from the perturbed data (i. e., if the function  $f(\beta + \sigma_\beta, \gamma, \dots)$  is undefined). In this case, the function  $f$  is certainly not linear over the region  $\beta$  to  $\beta + \sigma_\beta$ , because  $f$  is not defined over the entire interval. When this condition occurs, OASYS assigns a very large uncertainty (99999.0 degrees) to the attitude, nadir angle, and dihedral angle, resulting in a very low weight for the frame. This is a reasonable action in most cases, because the uncertainties are generally very large in the region close to the point at which attitude becomes undefined. That is, for the functions under consideration, the derivatives go to infinity at the point where the function becomes undefined. (This is true, for example, for the square root, arc sine, and arc cosine functions, all of which are involved in the attitude computations. These are also the only functions which can cause the attitude computation to be undefined.) The problem of perturbed data yielding no solution can always be avoided by using sufficiently small values for the uncertainties in the observables. For example, if the uncertainty in each observable is reduced by a factor of 10, the relative weights will remain accurate, and the probability that the perturbed data will yield no solution is reduced. The user must then remember to multiply the computed attitude uncertainties by a factor of 10 to obtain realistic values.

### 3.3 THE RECURSIVE ESTIMATOR APPROACH

#### 3.3.1 Comparison Between Recursive Processing and Batch Processing Estimation Methods

This section compares, nonmathematically, the batch processing and recursive processing methods for estimating the time-invariant state vector  $\underline{x}$  of a system using, as input, a block  $\underline{Y}$  of noisy observations  $y_i$  obtained on that system. The discussion of batch processors infers the usual least-squares differential correction (DC) algorithm employed, for example, by the GCONES program and GTDS. The discussion of recursive processors infers the usual nonlinear recursive least-squares algorithm employed by OABIAS.

With the batch processing algorithms, all observations  $y_i$  in  $\underline{Y}$  are, in effect, handled simultaneously. Batch processors which take into account observation geometry nonlinearity (to be defined in Section 3.3.2) require an a priori estimate  $\hat{\underline{x}}_0$  of  $\underline{x}$  to start the operation. A batch processor does not provide a new estimate  $\hat{\underline{x}}$  until the complete set of observations  $\underline{Y}$  has been processed.

With the recursive processing algorithms,  $\underline{Y}$  is separated into a number of mutually exclusive subsets. For example, in a system such as OABIAS which processes the observations one at a time, the subsets are the scalar observations  $y_i$ . They usually are arranged in chronological order and are processed sequentially. Updated and improved estimates  $\hat{\underline{x}}$  are obtained continually during the processing operation. In the most common operating mode,  $\hat{\underline{x}}$  is updated after processing each  $y_i$ , and this updated value is employed in computing the partial derivatives  $G$  required for processing the next observation  $y_{i+1}$ . In other modes,  $\hat{\underline{x}}$  may be updated less often, e.g., as infrequently as after the full data set  $\underline{Y}$  is processed. When the observation geometry is nonlinear, the  $\hat{\underline{x}}$  updating frequency is of some significance, because its influence on the  $G$ s affects the dynamics of the filter. Recursive processors always require an a priori estimate  $\hat{\underline{x}}_0$  to start the processing operation.

**ORIGINAL PAGE IS  
OF POOR QUALITY**

An iterative processing technique is one in which the observation set  $\underline{Y}$  is reprocessed several times. The state vector estimate  $\hat{\underline{X}}$  obtained at the end of each complete pass of  $\underline{Y}$  through the processor is used as the initial input for the following pass. Iterative processing is useful in improving the accuracy of the final estimate when the result obtained by only a single pass would be degraded by the nonlinearity in the observation equations and the error in the a priori estimate  $\hat{\underline{X}}_0$ . In practice, batch processors used for attitude determination problems usually must be operated iteratively to yield trustworthy results; the procedure is called differential correction (DC). The nature of the recursive processing algorithms makes iterative operation of recursive processors less essential in attitude determination problems, because the estimate  $\hat{\underline{X}}$  is continually being updated. However, iterative operation of recursive processors is possible, often advantageous, and sometimes necessary.

Recursive estimation algorithms have a number of potential operational advantages over batch processing algorithms. The main ones are as follows:

1. Recursive processors handle only a small number of observations at a time. Therefore, because they need to store only a small number of observations at any one time, recursive processors can require less computer core space than batch processors and have no a priori limit on the size of the data arrays they can process.
2. Recursive processors are better suited for real-time operations, because the operation need not be delayed until a block of observations is accumulated. Individual observations can be processed immediately, thus providing immediate estimates of the attitude state of the spacecraft with various measures of the accuracy of that estimate.

**ORIGINAL PAGE IS  
OF POOR QUALITY**

3. The series of successive state estimates provided by the recursive processor allow the operator to watch the convergence of the solutions and develop an intuitive feeling for the quality of the solutions that is not possible with the single output of the batch processor.

The potentiality for the real-time operation of a recursive processor is deterred when iterative processing is required. Also, both the real-time and core storage advantages of recursive processors can vanish if preprocessing of the input data is required or if storing the input data in large blocks is necessary rather than passing the data to the recursive processor on receipt. This has been the case with MSAD/OABIAS. Hence, the development of an intuitive feeling for the quality of the solutions has been the main advantage of recursive processing over batch processing in the OABIAS application.

The principal advantage of batch processors is stability. Because recursive processors can update their state vector estimate  $\hat{x}$  continually (after processing each  $y_i$ , if necessary), in iterative operation, they tend to converge to a final  $\hat{x}$  estimate faster than batch processors. Because batch processors update  $\hat{x}$  only at the end of each iteration they are more likely to converge to a valid solution in difficult problems, i. e., to be more stable. In a recursive processing operation, however, updating  $\hat{x}$  only at the end of each iteration will overcome this difference and yield dynamics virtually identical to that of batch processing.

In addition to stability, batch processors have two other potential advantages over recursive processors. The first is running speed. Because batch processors generally require fewer numerical operations than recursive processors, to process a block of data they tend to run faster. Secondly, batch processors can take into account the effects of correlated errors in  $y_i$  better than recursive processors. This capability, however, is not utilized often and, therefore, can rarely be considered a significant advantage.

### 3.3.2 The Basic Recursive Estimator Algorithm

This section discusses the concept of observation equations and geometry non-linearity, defines some terminology to be used in the remainder of Section 3, and presents and discusses the fundamental recursive estimation algorithm on which OABLAS is based.

Recursive estimators require a set of observations  $\underline{Y}$  as inputs. Let the individual scalar observations  $y_j$  be designated as  $y_j$  where  $j = 1, 2, \dots, p$ . Associated with each observation  $y_j$  is an algebraic expression  $y_{cj}(\underline{X}, t)$  which enables the value of  $y_j$  to be predicted.  $y_{cj}(\underline{X}, t)$  is a mathematical model of the satellite and its pertinent sensors. Thus, for each observation  $j$  there is an equation of the form

$$y_j = y_{cj}(\underline{X}, t_j) + v_j \quad (3-1)$$

where  $t_j$  is the time at which observation  $j$  was obtained, and  $y_j$  is the actual "measured" value of the observation.  $v_j$  is an error term which must be included to make the two sides of the equation balance.  $v_j$  results from the error in the  $y_j$  measurement and from modeling errors, i. e., from approximations in the  $y_{cj}(\underline{X}, t)$  expression. The actual value of  $v_j$  of course is unknown.

In some problems Equation (3-1) can be placed in the form

$$y_j = \underline{a}_j(t_j)^T \cdot \underset{s \times 1}{\underline{X}} + b_j(t_j) + v_j \quad (3-2)$$

where  $\underline{a}_j$  and  $b_j$  are constant or time-dependent coefficients, but are not explicit functions of  $\underline{X}$ .

ORIGINAL PAGE IS  
OF POOR QUALITY

In this case it is said that the observation geometry is linear. When Equation (3-1) cannot be placed in the above form it is said that the observation geometry is nonlinear. Recursive estimation problems in which the observation geometry is linear tend to present fewer difficulties than those in which it is nonlinear because there is a fully developed and rigorous body of theory for generating mathematically optimal results in the linear case. Unfortunately, the observation geometry in attitude determination problems usually is sufficiently nonlinear that its effect must be taken into account in the basic algorithms of the recursive system and/or compensated for by ad hoc procedures.

It is necessary at this point to define some terms which will be used in the remainder of Section 3. This terminology is nearly identical to that used in Reference 1. The word "measurements" will be used when referring to the independent inputs  $m_\alpha$  supplied, via telemetry and preliminary ground processing, to the overall attitude determination system. To be specific, the measurements supplied to MSAD/OABIAS are the Sun angles  $\beta$ , Sun sighting times  $t_s$ , central body-in horizon crossing times  $t_{HI}$ , and central body-out horizon crossing times  $t_{HO}$ . The word "observables" will be used when referring to the basic variables which serve as inputs to the recursive estimator portion of the attitude determination system. The terms "real observations" or merely "observations"  $y_j$  will be used to designate the measured values of the observables. The term "model observations" will be used to designate the predicted values  $y_{cj}$  of the observations. The word "model" is used here, because  $y_{cj}$  is obtained using mathematical models of the satellite and its sensors. In Equation (3-1),  $y_{cj}(X, t)$  is the algebraic expression which is used to compute  $y_{cj}$ .

In most estimation studies, a distinction is not made between measurements  $m_\alpha$  and observations  $y_j$ . Instead, the observables are considered to be the basic parameters which are measured. A distinction is being made in the

**ORIGINAL PAGE IS  
OF POOR QUALITY**

present analysis, however, because the observables used by OABIAS (and also those used by OASYS/GCONES and OASYS/GRECRS) are not the basic measured parameters  $t_s$ ,  $t_{HI}$ , and  $t_{HO}$ . The direct use of event times, such as  $t_s$ ,  $t_{HI}$ , and  $t_{HO}$ , as observables is difficult because of the difficulty in predicting these times via algebraic models as is required by Equation (3-1). The easier and more usual approach is to convert  $t_s$ ,  $t_{HI}$ , and  $t_{HO}$  (via preliminary processing) into parameters which can be handled more easily as observables by the estimator portion of the system. For example, in OASYS/GCONES and OASYS/GRECRS the observables are Sun angles, nadir angles, and dihedral angles. (The observables used by OABIAS will be discussed in detail in Section 3.6.) One of the drawbacks of transforming measurements  $m_\alpha$  into new observables is that it tends to increase the statistical correlation between the observables. This difficulty occurs in OASYS and GRECRS which process the observations one at a time.

The equations of the basic recursive processing algorithm used by OABIAS follow. (A derivation of these equations is given in Appendix B.)

$$y_{cjR} = y_{cj}(\underline{x}_{jR}) \quad (3-3a)$$

$$\underline{G}_{jR} = \underline{G}_j(\underline{x}_{jR}) \quad (3-3b)$$

$s \times 1$

$$z_{jR} = y_j - y_{cjR} \quad (3-3c)$$

$$\underline{K}_j = \left[ w_j^{-1} + \underline{G}_{jR}^T P_{j-1} \underline{G}_{jR} \right]^{-1} P_{j-1} \underline{G}_{jR} \quad (3-3d)$$

$s \times 1$

ORIGINAL PAGE IS  
OF POOR QUALITY

$$P_j = \begin{bmatrix} I & -K_j G_{jR}^T \\ \text{sxs} & \text{ } \end{bmatrix} P_{j-1} \quad (3-3c)$$

$$\Delta \hat{X}_j = K_j \left\{ z_{jR} - G_{jR}^T \left( \hat{X}_{j-1} - X_{jR} \right) \right\} \quad (3-3f)$$

$$X_j = \hat{X}_{j-1} + \Delta \hat{X}_j \quad (3-3g)$$

s x 1

where

$$G_j(X) = \frac{\partial y_{cj}(X)^T}{\partial X} \quad (3-4)$$

s x 1

The above equations are applicable only to estimators, such as OBIAS, which (1) assume that  $X$  is constant in time and (2) process the scalar observations  $y_j$  one at a time. Equations (3-3f) and (3-3g) are not identical to the equations actually implemented in OBIAS; the modified equations used in OBIAS are discussed in Section 3.4.4. The Equations (3-3f) and (3-3g) are used in this introductory discussion because they are more basic and easier to comprehend than the corresponding OBIAS equations.

The computations denoted by Equation (3-3) are performed sequentially on each observation  $y_j$ . In other words,  $y_1$  is run through the equations, then  $y_2$  and so on until the complete observation vector  $\underline{y}$  has been processed. Initial values of  $\hat{X}_0$  and  $P_0$  must be provided for processing observation  $y_1$ . ( $\hat{X}_0$  is used as the initial reference vector  $X_{1R}$ .) In addition, a weighting factor  $w_j$  must be provided or computed for each  $y_j$ . The computations must be performed in the order shown in Equation (3-3) except  $y_{cjR}$  and the innovative

ORIGINAL PAGE IS  
OF POOR QUALITY

residual  $z_{jR}$  can be computed at any point prior to the  $\Delta \underline{X}_j$  computation. Also, the covariance matrix  $P_j$  can be computed at any point after calculation of the gain vector  $K_j$ .  $P_j$  is not used in calculation, but is used instead in processing the next  $j + 1$  observation.

The individual equations of Equation (3-3) now will be discussed. In Equation (3-3a)  $y_{cjR}$  is the aforementioned model observation. The subscript R in Equation (3-3) indicates that the parameter is computed using a reference value  $\underline{X}_{jR}$  of the state vector. In most estimation systems,  $\underline{X}_{jR}$  is the previous estimate  $\hat{\underline{X}}_{j-1}$ . OABIAS, however, has the capability of updating the reference vector less often than this; this capability will be discussed in Section 3.4.

In Equation (3-3b),  $\underline{G}_{jR}$  is an  $s \times 1$  partial derivative vector where  $s$  is the dimension of the state vector  $\underline{X}$ . Its value is computed by inserting  $\underline{X}_{jR}$  into the algebraic expression  $\underline{G}_j(\underline{X})$  which is formed by differentiating the  $y_c(\underline{X})$  expression with respect to  $\underline{X}$  as indicated in Equation (3-4). Essentially,  $y_{cjR}$  and  $\underline{G}_{jR}$  are the first two coefficients of the Taylor series expansion of the observation Equation (3-1); i. e.,

$$y_j = y_{cjR} + \underline{G}_{jR}^T \{ \underline{X} - \underline{X}_{jR} \} + v_j + \text{higher order terms in } (\underline{X} - \underline{X}_{jR}) \quad (3-5)$$

In Equation (3-3c),  $z_{jR}$  is called the residual, or innovative residual, of observation  $j$ .  $z_{jR}$  provides an indication of the deviation of the true state vector  $\underline{X}$  from the reference vector  $\underline{X}_{jR}$ . This can be seen more clearly by combining Equations (3-3c) and (3-5) to yield

$$z_{jR} = \underline{G}_{jR}^T \{ \underline{X} - \underline{X}_{jR} \} + v_j + \text{higher order terms in } (\underline{X} - \underline{X}_{jR}) \quad (3-6)$$

**ORIGINAL PAGE IS  
OF POOR QUALITY**

In Equation (3-3f), it is seen that, to first order,  $z_{jR}$  is converted to an  $\hat{x}_{j-1}$  reference prior to its use in updating the state vector. In other words, the terms within the outer braces { } on the right side of Equation (3-3f) were obtained by truncating the series

$$z_j(\hat{x}_{j-1}) = z_j(x_{jR}) - G_{jR}^T [\hat{x}_{j-1} - x_{jR}] + \text{higher order terms} \quad (3-7a)$$

where

$$G_{jR} = G_j(x_{jR}) = \frac{\partial y_{cj}}{\partial \underline{x}}(x_{jR})^T = - \frac{\partial z_y}{\partial \underline{x}}(x_{jR})^T \quad (3-7b)$$

Equations (3-3f) and (3-3g) show that the updated state vector estimate  $\hat{x}_j$  is obtained by adding a correction vector  $\Delta \hat{x}_j$  to the previous estimate  $\hat{x}_{j-1}$ .  $\Delta \hat{x}_j$  is the product of the modified residual vector  $z_j(\hat{x}_{j-1})$  and a gain vector  $K_j \cdot K_j$  is computed using Equation (3-3d); the computation also requires a matrix  $P_{j-1}$  which was computed, via Equation (3-3e), when processing the previous observation  $j - 1$ . Except for degradation due to observation geometry nonlinearity, establishing the gain vector through Equations (3-3d) and (3-3e) is an optimal technique because the resulting estimate  $\hat{x}_j$  is optimal according to the several statistical and nonstatistical criteria. With the nonstatistical approach taken in Appendix B, this method is optimal because the resulting  $\hat{x}_j$  minimizes a generalized least-squares loss function.

The term  $w_j$  of Equation (3-3d) tells the processor how heavily to weight observation  $j$  in generating the new estimate  $\hat{x}_j$ . The matrix  $P_{j-1}$ , which was computed via Equation (3-3e) when processing observation  $j - 1$ , tells the processor how much weight to attach to the preceding estimate  $\hat{x}_{j-1}$ .

**ORIGINAL PAGE IS  
OF POOR QUALITY**

Statistical considerations indicate that optimally (1) the initial input matrix  $P_0$  should be the covariance  $E\{\underline{X} - \hat{\underline{X}}_0\} \{\underline{X} - \hat{\underline{X}}_0\}^T$  of the uncertainty in  $\hat{\underline{X}}_0$  and (2) each  $w_j$  should be the inverse of the variance  $\sigma_{y_j}^2$  in  $y_j$  due to random errors in the basic measurements  $m_\alpha$ . If these conditions are satisfied for each observation  $y_j$ , the resulting matrices  $P_j$  will be the covariance  $E\{\underline{X} - \hat{\underline{X}}_j\} \{\underline{X} - \hat{\underline{X}}_j\}^T$  of the uncertainty in the estimate  $\hat{\underline{X}}_j$ . Analyses which lead to these conclusions usually assume that (1) the observation geometry is linear, (2) the  $y_j$  errors are uncorrelated, and (3) the input measurements  $m_\alpha$  enter directly into the  $y_j$ , not the  $y_{cj}$ , computations.

**3.3.3 Discussion of Weighting Factors**

The question of observation errors, optimal weighting factors  $w_j$ , and the conditions under which processing the observations one at a time is an optimal technique will be considered at this point. The results of this development will be used in the discussion of the OABIAS observables and weighting factors (see Section 3.6). Let  $\underline{M}$  be the composite  $n \times 1$  measurement vector of a block of data and let  $m_\alpha$ , where  $\alpha = 1 \dots n$ , be the individual scalar measurements; i.e.,  $m_\alpha$  is an element of  $\underline{M}$ . Let  $dm_\alpha$  and  $d\underline{M}$  be the scalar and vector measurement errors. Let  $\underline{Y}$  be the  $p \times 1$  observation vector. Neglect the degenerate case in which each element  $y_j$  of  $\underline{Y}$  is identical to a corresponding scalar measurement  $m_\alpha$ . It is assumed that each observation  $y_j$  is computed using one or more  $m_\alpha$ 's; i.e.,

$$y_j = y_j(\underline{M}) \quad (j = 1 \text{ to } p) \quad (3-8)$$

Let  $dy_j$  and  $d\underline{Y}$  be the scalar and vector observation vectors. Assume that they result entirely from the measurement errors  $d\underline{M}$ .

**ORIGINAL PAGE IS  
OF POOR QUALITY**

Then, to first order

$$\begin{matrix} d\mathbf{Y} = \mathbf{H} \cdot d\mathbf{M} \\ p \times 1 \quad p \times n \quad n \times 1 \end{matrix} \quad (3-9a)$$

where

$$h_{j\alpha} = \frac{\partial y_j}{\partial m_\alpha}(\mathbf{M}) \quad (3-9b)$$

Let  $R_M$  and  $R_Y$  be the covariance matrices of  $d\mathbf{M}$  and  $d\mathbf{Y}$ . From Equation (3-9a), to first order

$$\begin{matrix} R_Y = \mathbf{H} R_M \mathbf{H}^T \\ p \times p \quad n \times n \end{matrix} \quad (3-10)$$

Statistical approaches to the estimation problem indicate that processing the observations  $y_j$  one at a time, as has been assumed in the current section, can be optimal only if the  $dy_j$ 's are statistically uncorrelated; i.e., if  $R_Y$  is diagonal. In this case, the inverses of the diagonal elements of  $R_Y$  are the optimum weighting values  $w_j^*$ .

Using Equation (3-10), the necessary conditions for a diagonal  $R_Y$  can be shown to be that (1) each scalar observation  $y_j$  is computed from its own set of measurements  $\underline{M}_j$  whose elements  $m_{j\alpha}$ , where  $\alpha = 1, 2, \dots, n_j$ , are not used in the computations of any other observation  $y_k$ , where  $k \neq j$  and (2) the measurement subsets  $\underline{M}_1, \underline{M}_2, \dots, \underline{M}_p$  are statistically uncorrelated. Then, the variance  $\sigma_{y_j}^2$  and optimum weighting factor  $w_j^*$  of observation  $j$  are

$$w_j^{*-1} = \sigma_{y_j}^2 = \mathbf{h}_j^T R_{M_j} \mathbf{h}_j \quad (3-11a)$$

ORIGINAL PAGE IS  
OF POOR QUALITY

where

$$h_{j\alpha} = \frac{\partial y_j}{\partial m_{j\alpha}} (M_j) \quad (3-11b)$$

In the special case where the elements of  $M_j$  are uncorrelated with variances  $\sigma_{m_{j\alpha}}^2$ , Equation (3-11a) reduces to

$$w_j^{*-1} = \sigma_{y_j}^2 = \sum_{\alpha=1}^{n_j} h_{j\alpha}^2 \sigma_{m_{j\alpha}}^2 \quad (3-11c)$$

### 3.4 IMPLEMENTATION OF THE RECURSIVE ESTIMATOR ALGORITHM IN OABIAS

This section discusses the general features of the implementation of the recursive estimator algorithm in OABIAS, including the main options which are available to influence its performance as an estimator.

#### 3.4.1 Principal Inputs

Preprocessed telemetry information is the principal input required by OASYS/OABIAS. Each frame in this data set must contain the following information from a single spin period of the satellite:

- The measured angle  $\beta$  between the Sun vector and the satellite's spin axis
- The time  $t_s$  at which the Sun was sighted
- The central body-in crossing time  $t_{HI}$ ; i.e., the time at which the line of sight of the horizon detector crossed the sky-to-central-body horizon
- The central body-out crossing time  $t_{HO}$
- The satellite spin rate  $\omega$

$\beta$ ,  $t_s$ ,  $t_{HI}$ , and  $t_{HO}$  constitute the elements  $m_\alpha$  of the measurement vector  $\underline{M}$  noted in Section 3.3.2. Thus, if there are  $n$  useful frames in the telemetry data set and none of the measurements in any of the frames is discarded, in the dimension of  $\underline{M}$  is  $4n$ . In this context, the spin rates  $\omega$  in the data set are not considered measurements because they normally are computed algebraically using the  $t_s$  measurements and, more significantly, because they are used only in preliminary processing in OASYS, not in OABIAS.

In addition to the telemetry inputs  $\underline{M}$ , the OABIAS recursive estimation subsystem requires the unit Sun vectors in geocentric inertial (GI) coordinates  $\hat{U}^{GI}$

**ORIGINAL PAGE IS  
OF POOR QUALITY**

at each Sun sighting and the central-body-to-satellite vectors in GI coordinates  $\vec{R}^{GI}$  at each horizon crossing. These are obtained from ephemeris data or an orbit generator. The OABIAS recursive estimation subsystem also requires the angular radius  $\rho_c$  of the central body on the unit celestial sphere at the horizon crossings.  $\rho_c$  is computed by the program from the orbit data. In addition, the nominal value of the horizon detector mounting angle  $\gamma_s$  and the initial estimates  $\hat{\underline{X}}_0$  of the state vector  $\underline{X}$  and of the covariance matrix  $P_0 = E (\underline{X} - \hat{\underline{X}}_0) (\underline{X} - \hat{\underline{X}}_0)^T$  are required. Program operating instructions and  $m_\alpha$  error parameters which are supplied by the user through the NAMELIST are also needed.

### 3.4.2 Observation Models

OABIAS uses eight different observables, commonly referred to as "models." (See Section 3.6 for a detailed discussion of the mathematics of the eight models.) When running OABIAS, the user has the option of selecting which models are to be used. These models are analogous to and replace the Sun angle, nadir angle, and dihedral angle models employed in GCONES (Reference 8) and OASYS/GRECRS (Reference 10).

OABIAS possesses models with error-free real observations--a feature which is not commonly found in recursive estimation systems. In the usual estimation system, the measurements  $\underline{M}$  and their errors enter into the computations through the real observations  $\underline{Y}$ ; i.e.,  $\underline{Y} = \underline{Y}(\underline{M})$  and  $\underline{Y}_c = \underline{Y}_c(\underline{X})$ .<sup>1</sup> In OABIAS Models 2, 3, and 4, however, the real observations are error-free and  $\underline{M}$  enters solely through  $\underline{Y}_c$ ; i.e.,  $\underline{Y}_c = \underline{Y}_c(\underline{M}, \underline{X})$ . The Appendix B least-squares derivation of the OABIAS recursive estimator algorithm shows that this unorthodoxy does not alter the validity or optimality of the algorithm

---

<sup>1</sup>Refer to Section 3.3.2 for the distinction between measurements, real observations, and model observations.

**ORIGINAL PAGE IS  
OF POOR QUALITY**

because the essential properties of the computed residual vector  $\underline{z}$  are retained.

### 3.4.3 State Vector Elements

The state vector  $\underline{x}$  used by OABIAS contains 12 elements  $x_\eta$ . These elements with their alternative symbols are defined as follows:

- $x_1 (s_1)$  and  $x_2 (s_2)$  which define the attitude of the satellite; i. e., the orientation of its angular momentum vector
- $x_3 (\psi_0)$  which defines the phase of the satellite in its spin cycle at the start of the run
- $x_9 (\omega)$  which is the satellite's spin rate
- $x_4 (\Delta\gamma)$ ,  $x_5 (\phi_H^I)$ ,  $x_6 (\phi_H^O)$ ,  $x_{11} (\epsilon_H)$  which define the effective mounting alignment of the horizon scanner
- $x_8 (\Delta\beta)$  and  $x_{10} (\epsilon)$  which define the effective mounting alignment of the Sun sensor
- $x_7 (\Delta\rho)$  which is the effective error in the central body angular radius  $\rho_c$  computed in OABIAS using orbit information
- $x_{12} (\Delta t)$  which is a timing-bias due to an effective error in the computed location of the satellite in its orbit

The precise mathematical definitions of the 12 state vector elements are given in Section 3.5. Note that  $\phi_H^I$  and  $\phi_H^O$  are the effective azimuth angles of the horizon scanner, relative to a body-fixed reference frame, at the Earth-in and Earth-out horizon crossings, respectively. OABIAS considers these as distinct parameters. Also,  $\epsilon_{II}$  is an alignment error of PAS and is not required with conventional horizon detectors.

The initial covariance matrix  $P_0$  which the user supplies to OABIAS is diagonal. When selected diagonal elements of this matrix are set to zero, the

ORIGINAL PAGE IS  
OF POOR QUALITY

corresponding elements of  $\underline{X}$  remain constant, at their a priori values, throughout the run. Thus, the user can select the components of  $\hat{\underline{X}}$  to be updated. This is a powerful and necessary tool for the proper use of OABIAS.

OABIAS also provides the user with the option of not updating the state vector estimate  $\hat{\underline{X}}$  after each observation. Equation (3-3) shows that a reference vector  $\underline{X}_{jR}$  is used in the processing operations performed on each observation  $j$ .  $\underline{X}_{jR}$  enters into the mathematics primarily through the partial derivative vector  $\underline{G}_{jR}$ . Most recursive processors which model the observation geometry nonlinearity (i.e., which make each  $\underline{G}_j$  a function of  $\hat{\underline{X}}$ ) update  $\underline{X}_{jR}$  at each observation using  $\underline{X}_{jR} = \hat{\underline{X}}_{j-1}$ . In OABIAS, however,  $\underline{X}_{jR}$  may be updated after each observation, after each telemetry frame, or after every  $N$  telemetry frames, where  $N$  is a user-selected integer. These options have been included in OABIAS to provide additional flexibility of operation, particularly when observation geometry nonlinearity is significant. OABIAS computes an updated state vector estimate  $\hat{\underline{X}}$  only at those points where the reference vector (now to be denoted as  $\underline{X}_R$ ) is updated. For this reason, previous CSC reports have called the operation state vector updating rather than reference vector updating. The reference vector is updated by setting it equal to the updated state vector.

To derive the state vector updating equations implemented in OABIAS, combine Equations (3-3f) and (3-3g) into a single equation. Replace  $\underline{X}_{jR}$  by  $\underline{X}_R$  and replace the  $j$  subscripts by  $k$ 's. The first observation after the most recent updating is signified by  $k = 1$ . Subtracting  $\underline{X}_R$  from both sides of the equation yields

$$\Delta \hat{\underline{X}}_k = \Delta \hat{\underline{X}}_{k-1} + \underline{K}_k \left\{ z_{kR} - \underline{G}_{kR}^T \Delta \hat{\underline{X}}_{k-1} \right\} \quad (3-12a)$$

where, by definition

$$\begin{aligned}\Delta \hat{\underline{x}}_k &= \hat{\underline{x}}_k - \underline{x}_R \\ \Delta \hat{\underline{x}}_{k-1} &= \hat{\underline{x}}_{k-1} - \underline{x}_R\end{aligned}\tag{3-12b}$$

and

$$\Delta \hat{\underline{x}}_0 = \underline{0}\tag{3-12c}$$

It should be noted that the  $\Delta \hat{\underline{x}}_k$  of Equation (3-12) is not the same variable as the  $\Delta \hat{\underline{x}}_j$  of Equations (3-3f) and (3-3g) because it is defined relative to a different reference. OBIAS sets  $\Delta \hat{\underline{x}}$  equal to 0 when the state vector is updated and then processes the observations sequentially using Equations (3-3a) through (3-3e) and (3-12a). Let the number of observations between updates be  $n$ . When  $k = n$ , OBIAS updates  $\hat{\underline{x}}$  and  $\underline{x}_R$  using

$$\hat{\underline{x}}_n = \hat{\underline{x}}_0 + \Delta \hat{\underline{x}}_n\tag{3-13a}$$

$$\underline{x}_R = \hat{\underline{x}}_n\tag{3-13b}$$

where  $\hat{\underline{x}}_0$  is now the previous state vector estimate.

#### 3.4.4 Iterative Operation

When the effect of observation geometry nonlinearity is significant, the performance of a recursive filter can often be improved by iterative operation. With this technique, the composite block  $\underline{y}$  of observations, or subsets of

ORIGINAL PAGE IS  
OF POOR QUALITY

this block, are run through the filter several times. The state vector estimate  $\hat{\underline{x}}_f^\lambda$  obtained at the end of any one pass  $\lambda$  is used as the a priori input  $\underline{x}_o^{\lambda+1}$  for the next pass. If the procedure is successful, the estimates  $\hat{\underline{x}}_f^\lambda$  will converge toward a constant value as  $\lambda$  increases.

Recursive filters require, as inputs, not only a priori state vector estimates  $\hat{\underline{x}}_o$  but also an a priori covariance matrix  $P_o$ . For iterative operation, a technique for establishing the matrix input  $P_o^\lambda$  to be used at the start of each pass  $\lambda$  must be decided upon. The two simplest approaches are: (1) to reset  $P$  to its original a priori value (i. e.,  $P_o^\lambda = P_o$ , where  $\lambda = 1, 2, \dots$ ) or (2) to use the value obtained at the end of the previous pass (i. e.,  $P_o^\lambda = P_f^{\lambda-1}$ , where  $\lambda = 1, 2, \dots$ ).

Three types of iteration capability are provided in OABIAS. In the first, the complete block  $\underline{y}$  is run through the processor in each pass. For this method of iteration, the user has the option of employing either of the two  $P_o^\lambda$  updating schemes noted in the above paragraph. The number of iterations are selected a priori by the user; the program has not been given the capability of using the  $\hat{\underline{x}}_f^\lambda$  convergence as a criteria for automatically ending the operation.

In the second type of iteration, the iterations are performed on subsets  $\underline{y}_\alpha$  of  $\underline{y}$ . The  $\underline{y}_\alpha$ 's are composed of the observations between state vector updates. Thus, if  $\hat{\underline{x}}$  is being updated every seven frames,  $\underline{y}_1$  will contain the observations obtained from frames 1 to 7. The program will continue to reprocess  $\underline{y}_1$ , until the estimate  $\hat{\underline{x}}_{1f}^\lambda$  converges or until the specified limit on the number of passes is reached. It then will move on to set  $\underline{y}_2$  which is composed of the observations obtained from frames 8 to 14. For this mode of iteration, OABIAS has not been given the  $P_o^\lambda = P_o^1$  covariance matrix resetting capability; it employs only the  $P_o^\lambda = P_o^{\lambda-1}$  method.

### 3.4.5 Single Observation Iteration

In addition to the two iteration techniques discussed above, OABIAS has a third iterative method called the linearity fix (Reference 11). Although conceptually and mathematically similar to the other two iteration methods, the linearity fix should be distinguished from them. With this third technique, the program iterates the scalar observations one at a time. That is, any single observation, e.g., observation  $j$ , is re-run through the filter ( $\lambda = 1, 2, \dots$ ) until the state vector estimate  $\hat{\underline{x}}_j^\lambda$  converges to a constant value or until the user-specified limit on the number of passes is reached. The program then moves to observation  $j + 1$ , etc. After these operations on observation  $j$  have been completed, it is never necessary to recall observation  $j$  for further processing. As a result, the method provides the advantages of block iteration with less degradation to the capability for real-time operation. The algorithm employed in OABIAS for single observation iteration was obtained directly from Reference 1.

The mathematics of the single observation iteration method can be delineated using the basic recursive estimator equations (Equation 3-3) as a starting point. Assume that the processing of observation  $j - 1$  has been completed to yield  $\hat{\underline{x}}_{j-1}$  and  $P_{j-1}$ . Observation  $j$  is to be processed next. Let superscript  $\lambda$  signify the  $\lambda$ th pass (of observation  $j$ ) through the filter. In pass  $\lambda$ , the single observation iteration algorithm uses the state vector estimate  $\hat{\underline{x}}_j^{\lambda-1}$  from pass  $\lambda - 1$  as the reference vector. (In other words, the  $\underline{x}_{jR}$  of Equation (3-3) is now  $\hat{\underline{x}}_j^{\lambda-1}$ .) Equation (3-3) now can be rewritten to encompass the single observation iteration option.

$$y_{cj}^\lambda = y_{cj} \left( \hat{\underline{x}}_j^{\lambda-1} \right) \quad (3-14a)$$

$$\underline{G}_j^\lambda = \frac{\partial y_{cj}}{\partial \underline{X}_j} \left( \hat{\underline{X}}_j^{\lambda-1} \right)^T \quad (3-14b)$$

$s \times 1$

$$z_j^\lambda = y_j - y_{cj}^\lambda \quad (3-14c)$$

$$\underline{K}_j^\lambda = P_{j-1} \underline{G}_j^\lambda \left[ w_j^{-1} + \underline{G}_j^{\lambda T} P_{j-1} \underline{G}_j^\lambda \right]^{-1} \quad (3-14d)$$

$$\hat{\underline{X}}_j^\lambda = \hat{\underline{X}}_{j-1} + \underline{K}_j^\lambda \left\{ z_j^\lambda - \underline{G}_j^{\lambda T} \left( \hat{\underline{X}}_{j-1} - \hat{\underline{X}}_j^{\lambda-1} \right) \right\} \quad (3-14e)$$

where

$$\hat{\underline{X}}_j^0 = \hat{\underline{X}}_{j-1} \quad (3-14f)$$

While the filter is operating on observation  $j$ , the subscript  $j$  in the above equations is constant;  $\lambda$  takes on values 1, 2, 3, etc. The covariance matrix  $P$  is not updated during the  $\lambda$  passes. Instead, it is updated only after  $\hat{\underline{X}}_j^\lambda$  has converged or the limit on the number of passes has been reached. Letting  $n$  be the total number of passes of observation  $j$  through the filter, the  $P$  updating equation is

$$P_j = \left[ I - \underline{K}_j^{nT} \underline{G}_j^n \right] P_{j-1} \quad (3-15)$$

$s \times s$

### 3.5 BASIC GEOMETRY

This section delineates the coordinate frames, direction cosine matrices, and main geometric variables used in the OABIAS subsystem and/or employed in the discussions in Section 3.6 of the eight OABIAS observation models. Exact definitions of the 12 elements of the OABIAS state vector  $\underline{x}$  also are included.

#### 3.5.1 Coordinate Frame Flow Diagram

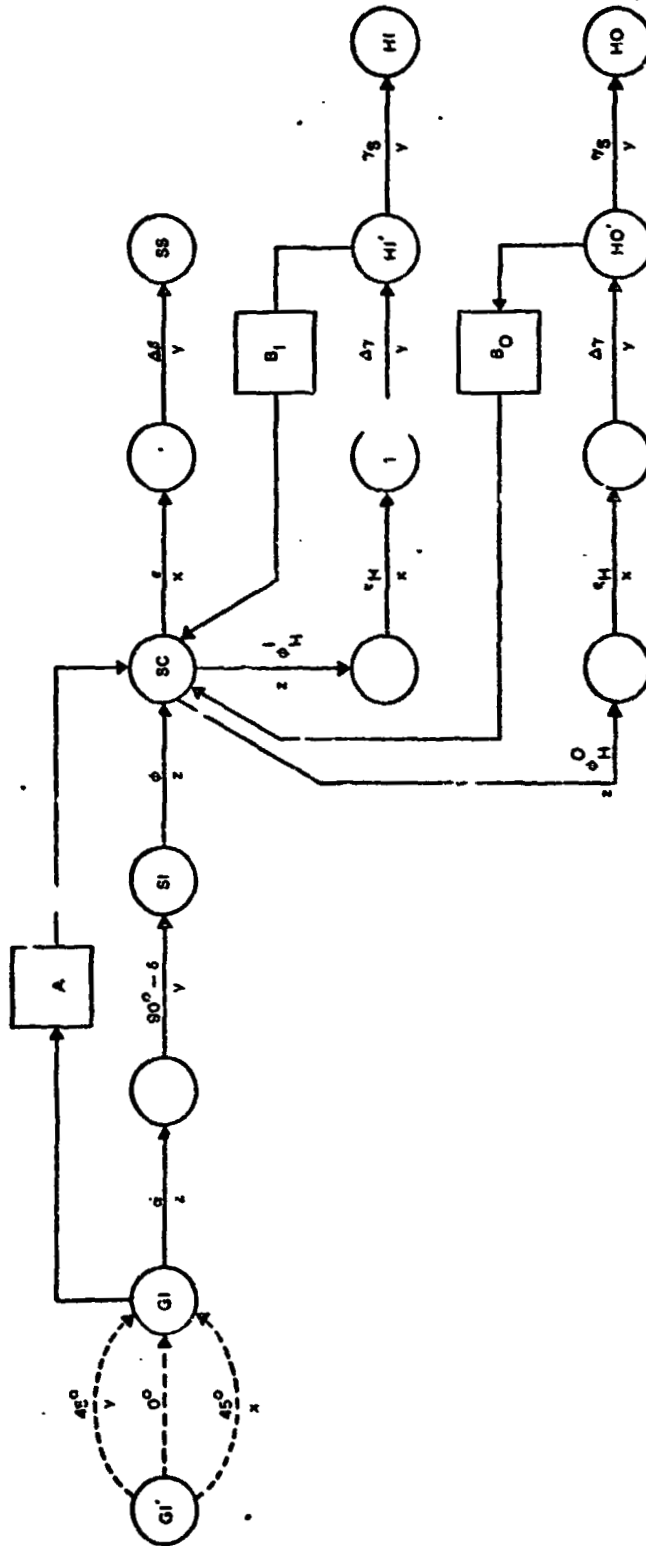
The Cartesian coordinate frames and the main geometric variables to be used in the remainder of this section are shown in Figure 3-1. This figure uses a standard technique for displaying the relationships between coordinate frames. The circles in the figure represent the coordinate frames. A straight line between any two circles defines the rotation by which the coordinate frame on the left is transformed to the frame on the right. For example, rotating frame spacecraft inertial (SI) about its z-axis through the angle  $\phi$  yields frame spacecraft reference (SC). In the interest of simplicity, only the coordinate frames which are fundamentally significant have been given names and symbols; the remaining frames are intermediate ones of lesser importance.

The rotation angles shown in Figure 3-1 are to be regarded as the true angles of the satellite being studied rather than as OABIAS time-varying estimates of these angles. Thus, the angles are time-invariant except for the rotation angle  $\phi$  and (in RAE-B problems) the detector mounting angle  $\gamma_s$ .

The squares in Figure 3-1 indicate direction cosine matrices. For example,  $A$  is the direction cosine matrix which transforms vector components from GI resolution to SC resolution.

$$\vec{V}^{SC} = A \vec{V}^{GI}$$

ORIGINAL PAGE IS  
OF POOR QUALITY



NOTE: THE ANGLES IN THIS DIAGRAM ARE DEFINED IN TEXT. THE COORDINATE FRAMES ARE DEFINED IN TABLE 4-1 AND IN TEXT.

Figure 3-1. Coordinate Frame Flow

ORIGINAL PAGE IS  
OF POOR QUALITY

Similarly,  $B_1$  ( $B_0$ ) transforms vector components from horizon-in crossing prime (III') [horizon-out crossing prime (HIO')] resolution to SC resolution.

$$\vec{V}^{SC} = B_1 \vec{V}^{III'}$$

Table 3-1, which supplements Figure 3-1, defines the directions of the most significant axes of the main coordinate frames. In this section, coordinate frame axes will normally be indicated by  $x$ ,  $y$ , and  $z$  with appropriate subscripts. When it is necessary to specify unit vectors along coordinate frame axes, those shown in Table 3-1 will be used. Unit vectors along axes of particular significance, such as the one along the satellite's spin axis, have been given special symbols as shown in the table.

### 3.5.2 Coordinate Frames GI' and GI

Frame GI' is the conventional geocentric inertial frame defined with respect to the celestial equator and poles. Let  $\alpha'$  and  $\delta'$  (not shown in Figure 3-1) be the conventional right ascension and declination of the satellite's spin axis relative to frame GI'. When  $\delta'$  is close to 0 degree or  $\pm 90$  degrees, the coordinates which OABIAS uses to specify satellite attitude encounter discontinuities (see Section 3.5.8). OABIAS avoids these difficulties by automatically performing a 45-degree rotation of frame GI' to frame GI in runs where  $\delta'$  is close to (i. e., within a user-specified tolerance of) 0 degree or  $\pm 90$  degrees. Frame GI in Figure 3-1 is the geocentric inertial frame, rotated or not, which is used in the OABIAS calculations. The 45-degree rotation entails the transformation of the unit Sun vector  $\hat{U}$  and the orbit radius vector  $\vec{R}$  from frame GI' to frame GI.

The 45-degree rotation of frame GI' normally is taken about the  $x_{GI}$ -axis. However, rotation about this axis produces an insufficient change in declination when  $\delta'$  is close to 0 degree and  $\alpha'$  is close to 0 degree or 180 degrees.

**ORIGINAL PAGE IS  
OF POOR QUALITY**

Table 3-1. Coordinate Frames, Axes, and Unit Vectors.

NAME OF COORDINATE FRAME	SYMBOL	AXES	DIRECTION OF SIGNIFICANT AXES	DESIGNATION OF UNIT VECTORS ALONG AXES	ALTERNATE DESIGNATION OF SIGNIFICANT UNIT VECTORS
STANDARD GEOCENTRIC INERTIAL <sup>1</sup> (SEE NOTE 1)	GI'	$x_{GI}'$ $y_{GI}'$ $z_{GI}'$	TOWARD VERNAL EQUINOX  TOWARD NORTH CELESTIAL POLE	— — —	— — —
ROTATED GEOCENTRIC INERTIAL <sup>1</sup> (SEE NOTE 1)	GI	$x_{GI}$ $y_{GI}$ $z_{GI}$	— — —	$\hat{e}_1$ $\hat{e}_2$ $\hat{e}_3$	— — —
SPACECRAFT INERTIAL <sup>1</sup>	SI	$x_{SI}$ $y_{SI}$ $z_{SI}$	SEE NOTE 2 SEE NOTE 2 ALONG SATELLITE SPIN AXIS	$\hat{i}$ $\hat{j}$ $\hat{k}$	— — $\hat{s}$
SPACECRAFT REFERENCE <sup>2</sup>	SC	$x_{SC}$ $y_{SC}$ $z_{SC}$	SEE NOTE 2 SEE NOTE 2 ALONG SATELLITE SPIN AXIS	$\hat{e}_1$ $\hat{e}_2$ $\hat{e}_3$	— — $\hat{s}$
SUN SENSOR <sup>2</sup>	SS	$x_{SS}$ $y_{SS}$ $z_{SS}$	PERPENDICULAR TO SUN SENSOR FACE SEE NOTE 2 SEE NOTE 2	— — —	— $\hat{N}_S$ —
HORIZON-IN CROSSING <sup>3</sup>	HI	$x_{HI}$ $y_{HI}$ $z_{HI}$	SEE NOTE 2 SEE NOTE 2 ALONG HORIZON IN-CROSSING LOS	— — —	— $\hat{N}_{HI}$ $\hat{L}_I$
HORIZON-OUT CROSSING <sup>3</sup>	HO	$x_{HO}$ $y_{HO}$ $z_{HO}$	SEE NOTE 2 SEE NOTE 2 ALONG HORIZON-OUT CROSSING LOS	— — —	— $\hat{N}_{HO}$ $\hat{L}_O$

<sup>1</sup>FIXED IN INERTIAL SPACE

<sup>2</sup>FIXED IN THE BODY OF THE SPACECRAFT

<sup>3</sup>FIXED IN THE BODY OF THE SPACECRAFT FOR NORMAL HORIZON DETECTORS; ROTATES RELATIVE TO THE SPACECRAFT BODY ON RAE-8

NOTE 1: THE DISTINCTION BETWEEN FRAMES GI' AND GI IS DISCUSSED IN SECTION 3.5.2.

NOTE 2: THE DIRECTIONS OF THESE AXES FOLLOW FROM THE BASIC COORDINATE FRAME GEOMETRY SUMMARIZED IN FIGURE 4.1 AND DISCUSSED IN TEXT.

Thus, whenever a rotation is necessary and  $\alpha'$  is within  $\pm 15$  degrees of 0 degree or 180 degrees, the 45-degree rotation is taken about  $y_{GI}$ , rather than  $x_{GI}$ . Figure 3-2 summarizes the  $GI'$  to  $GI$  rotation criteria. It should be noted that the transformation from  $GI'$  to  $GI$  coordinates affects only the internal workings of OABIAS; it does not affect the inputs provided by the user or the outputs generated by the program.

### 3.5.3 Coordinate Frames SI and SC and State Vector Elements $x_3(\phi)$ and $x_9(\omega)$

Frame SI is fixed in inertial space in any single OABIAS run. Frame SC is the basic body-fixed reference frame of the spacecraft. Figure 3-3 shows the relation among frames GI, SI, and SC. The  $z_{SI}$ - and  $z_{SC}$ -axes both lie along the unit spin vector  $\hat{S}$  of the spacecraft. Since OABIAS does not include nutation effects, frame SC is obtained from frame SI by a single rotation angle  $\phi$  which defines the instantaneous phase of the spacecraft in its spin cycle. The  $x_{SC}$ - and  $y_{SC}$ -axes are oriented such that the azimuth (measured in the  $x_{SC}$ - $y_{SC}$  plane from the  $+x_{SC}$ -axis) of the center of the spacecraft's Sun sensor is zero.

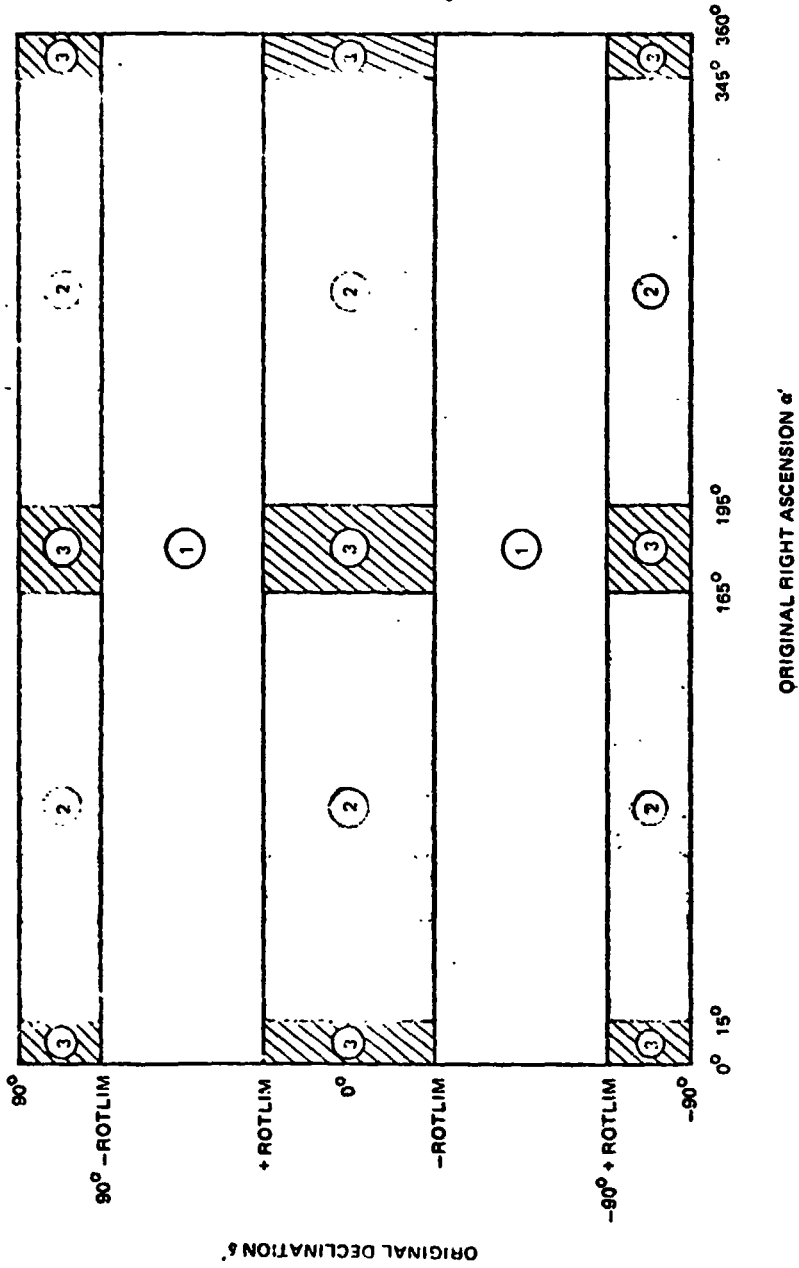
OABIAS assumes that  $\phi$  is a linear function of time

$$\phi = \psi_0 + \omega \{t - t_0\} \quad (5-16)$$

where  $\psi_0$  and  $\omega$  are constant, and  $t_0$  is the time at the start of the run.

The value of  $\psi_0$  is normally of little or no direct interest. It must be included in  $\underline{X}$ , however, because it is an essential component in three of the eight OABIAS observation models. Similarly,  $\omega$  is an essential component of six of the eight models.

ORIGINAL PAGE 19  
OF POOR QUALITY



LEGEND:  
 ROTLIM - USER-SPECIFIED TOLERANCE  
 1 - NO ROTATION  
 2 - ROTATE 45° ABOUT XGI'  
 3 - ROTATE 45° ABOUT YGI'

Figure 3-2. Criteria for Rotation of Frame GI

ORIGINAL PAGE 18  
OF POOR QUALITY

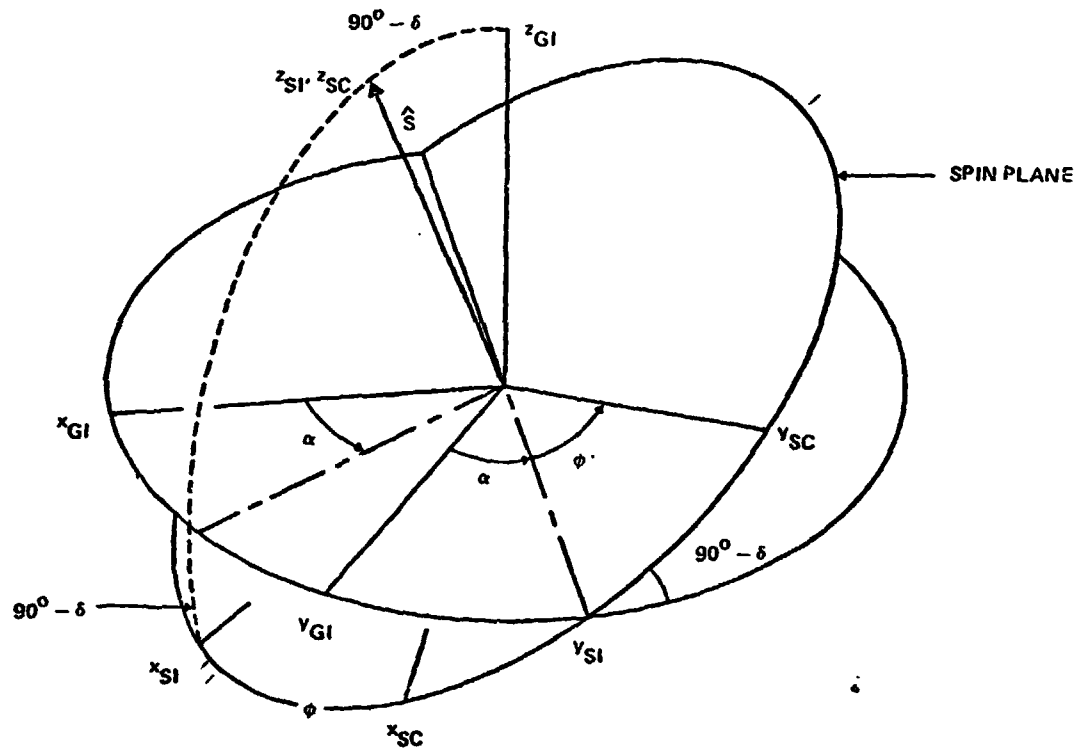


Figure 3-3. Geometry of Frames GI, SI, and SC

ORIGINAL PAGE IS  
OF POOR QUALITY

### 3.5.4 Sun Sensor Geometry and State Vector Elements $x_8$ ( $\Delta\beta$ ) and $x_{10}$ ( $\epsilon$ )

Figure 3-4 shows the Sun sensor geometry at a Sun sighting time.  $\beta_M$  on this figure is the angle measured by the Sun sensor, and  $\beta$  is the true Sun angle; i. e., the angle between  $\hat{U}$  and  $\hat{S}$ .  $\epsilon$  and  $\Delta\beta$  are bias errors which cause the variation between  $\beta$  and  $\beta_M$ .

This document employs a coordinate frame Sun sensor (SS) whose axes are attached to the Sun sensor. The  $x_{SS}$ - and  $z_{SS}$ -axes form the sensor's reference slit plane. Ideally, the Sun sensor is mounted such that the spacecraft's spin vector  $\hat{S}$  lies in this reference slit plane. The sensor sights the Sun and measures the angle  $\beta_M$  at those instants when (1) the spinning  $x_{SS}$ - $z_{SS}$  plane crosses the unit Sun vector  $\hat{U}$  and (2) the angle between  $\hat{U}$  and  $x_{SS}$  is within the range limits of the sensor. If the Sun does lie within the sensor's FOV, it is sighted once per spin cycle.

OBIAS models the Sun sensor biases as actual or effective alignment errors  $\epsilon$  and  $\Delta\beta$ .  $\epsilon$  and  $\Delta\beta$  are included in the state vector  $\underline{X}$  as elements  $x_{10}$  and  $x_8$ , respectively.  $\epsilon$  is an alignment tilt of the reference slit plane, and  $\Delta\beta$  is a rotation of the instrument in this plane.  $\Delta\beta$  is, in effect, an alignment error of the main slit plane of the sensor.

### 3.5.5 Horizon Detector Geometry and State Vector Elements $x_4$ ( $\Delta\gamma$ ), $x_5$ ( $\phi_H^I$ ), $x_6$ ( $\phi_H^O$ ), and $x_{11}$ ( $\epsilon_H$ )

Parameters which are related to horizon crossings--either central-body in or central-body out--are signified by the subscript H. Indices I and O are used, as necessary, to indicate in-crossings and out-crossings, respectively.

The horizon scanner representation used in OBIAS employs separate coordinate frames for in-crossing and out-crossing conditions. In Figure 3-1, horizon-in crossing (IH) and horizon-out crossing (HO) are the main coordinate frames of the horizon scanner. IH' and HO' are the intermediate frames and

ORIGINAL PAGE IS  
OF POOR QUALITY

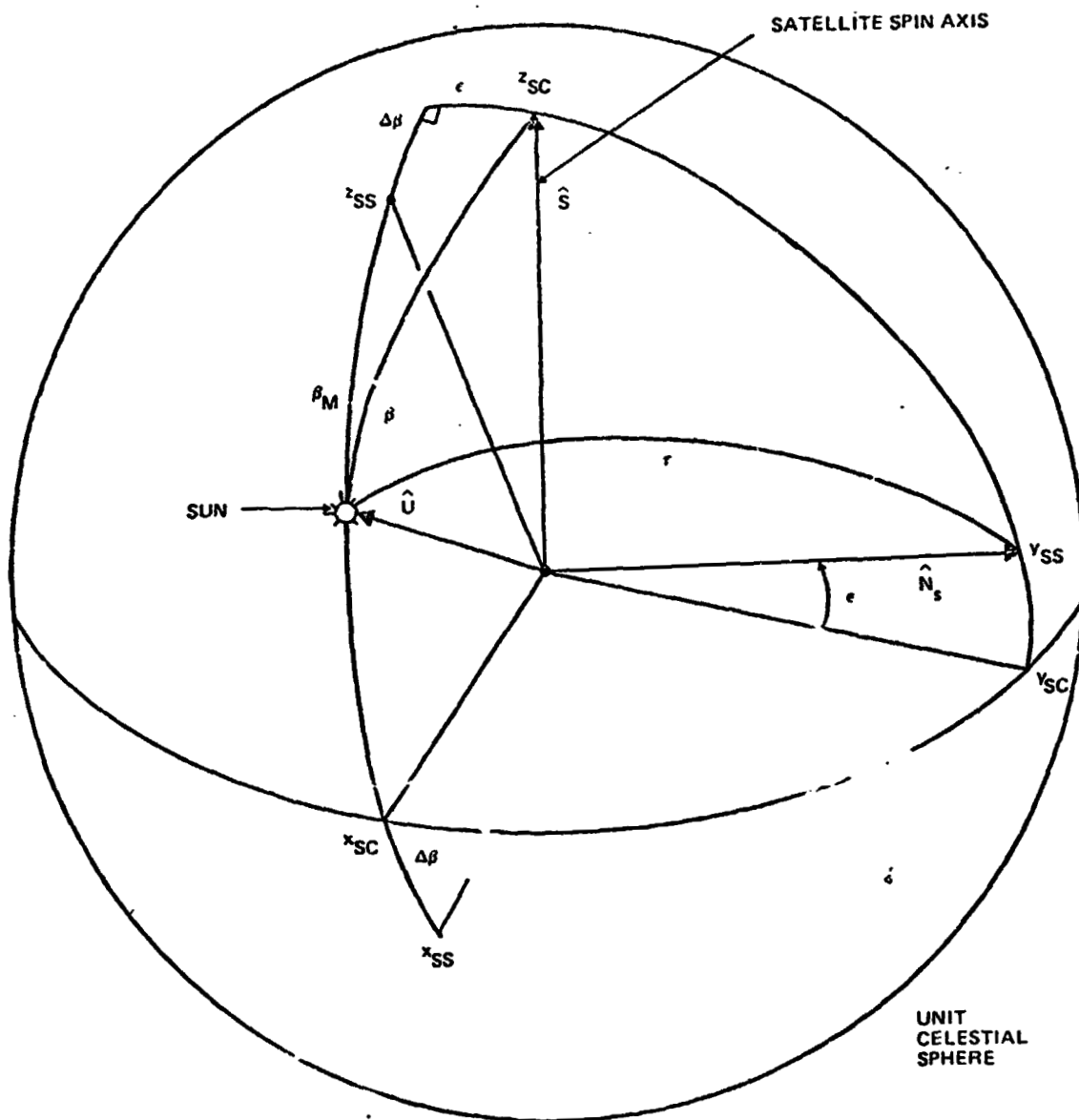


Figure 3-4. Sun Sensor Geometry at Sun Sighting

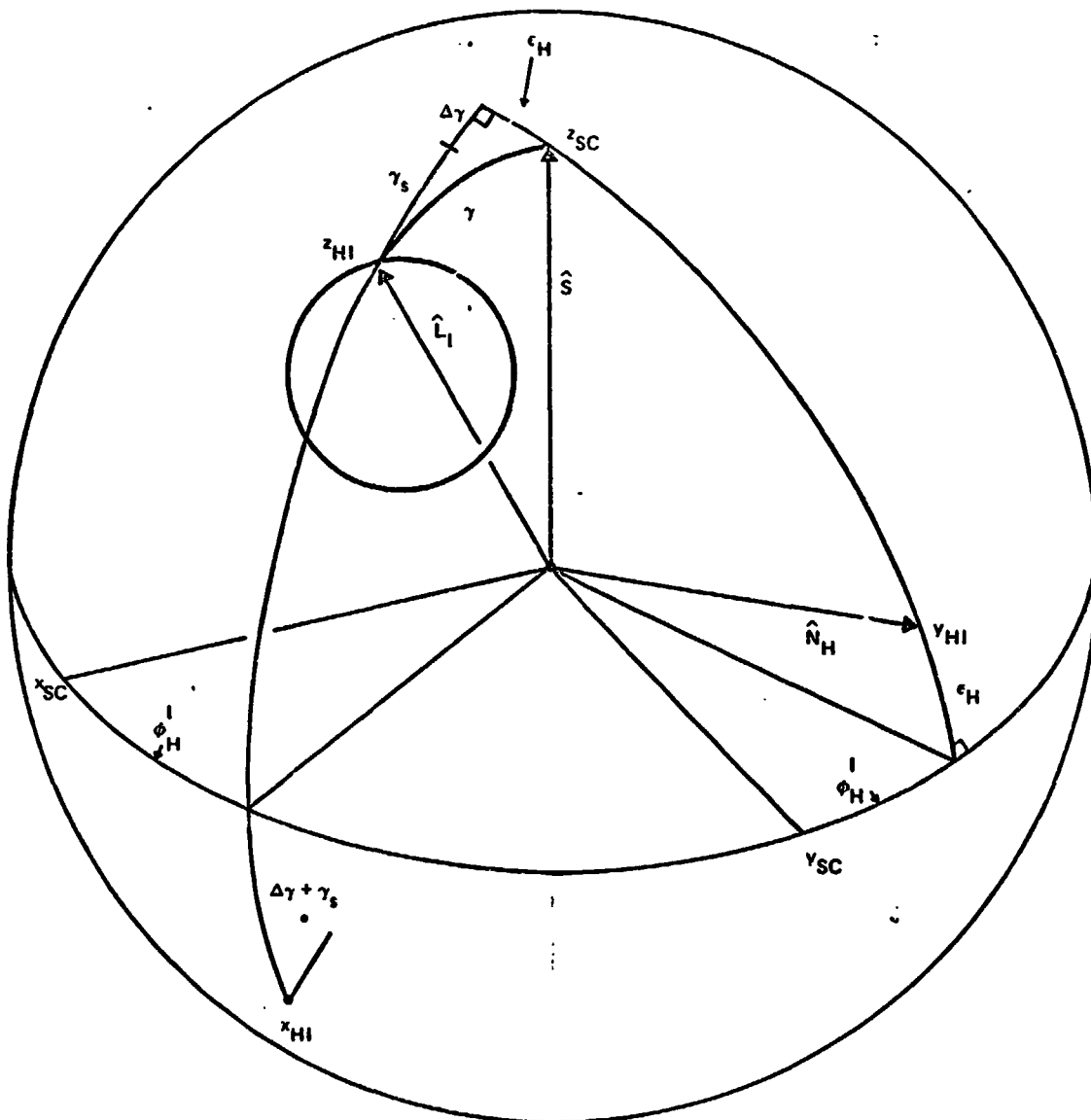
are designated only because later sections utilize the matrices  $B_I$  and  $B_O$  which transform vector resolution from  $III'$  and  $HO'$  back to SC coordinates.

The geometry of a horizon-in crossing is shown in Figure 3-5.  $\hat{L}_I$  and  $\hat{L}_O$  designate unit vectors along the  $z_{III}$ - and  $z_{HO}$ -axes, respectively. A horizon-in crossing occurs when  $\hat{L}_I$  crosses the sky-to-central-body boundary. A horizon-out crossing occurs when  $\hat{L}_O$  crosses the central-body-to-sky boundary.

The orientation of frame III relative to the satellite body-fixed reference frame SC is specified by angles  $\phi_H^I$ ,  $\epsilon_H$ ,  $\Delta\gamma$ , and  $\gamma_S$ . The orientation of HO relative to SC is specified by  $\phi_H^O$ ,  $\epsilon_H$ ,  $\Delta\gamma$ , and  $\gamma_S$ .  $\gamma_S$  is the nominal mounting angle of the horizon detector's line of sight relative to the satellite's spin axis. For normal horizon detectors  $\gamma_S$  is constant. Thus, frames III and HO and the intermediate frames  $III'$  and  $HO'$  are invariant relative to frame SC. For the RAE-B PAS, however,  $\gamma_S$  is stepped in 0.7-degree increments. Hence, in PAS problems, frames  $III'$  and  $HO'$  are fixed relative to frame SC, but III and HO are time-varying relative to SC.

OABIAS models the horizon scanner bias errors through the rotation angles  $\epsilon_H$ ,  $\Delta\gamma$ ,  $\phi_H^I$ , and  $\phi_H^O$ . These are included in  $X$  as elements  $x_{11}$ ,  $x_4$ ,  $x_5$ , and  $x_6$ , respectively.  $\epsilon_H$  and  $\Delta\gamma$  are regarded as alignment errors of the unit and are considered to be identical for both in-crossings and out-crossings.  $\epsilon_H$ , however, is used only with PAS. As can be seen in Figure 3-5, when  $\Delta\gamma$ ,  $\gamma_S$ , and  $\gamma$  are constant (as they are with normal horizon detectors), a non-zero  $\epsilon_H$  affects the horizon triggering times in the same way as a bias  $\Delta\phi_H$  on the azimuth angle  $\phi_H$ . Hence, it is not possible for OABIAS to distinguish between  $\epsilon_H$  and  $\Delta\phi_H$ , and only one of the pair is observable from the available horizon crossing time data. When running OABIAS, the usual technique for circumventing this difficulty is to constrain  $\epsilon_H$  to zero. In PAS runs, however,  $\epsilon_H$ , in principle, is distinguishable from  $\Delta\phi_H^I$  and

ORIGINAL PAGE IS  
OF POOR QUALITY



NOTE: THE RELATION BETWEEN THE SC AND HI FRAMES CAN BE SEEN MORE CLEARLY IN FIGURE 4-1.

Figure 3-5. Horizon Detector Geometry at Central-Body-In Crossing

**ORIGINAL PAGE IS  
OF POOR QUALITY**

$\Delta\phi_{\text{H}}^{\text{O}}$  because of the time variation of  $\gamma_{\text{S}}$ ; hence  $\epsilon_{\text{H}}$  is not constrained to zero in RAF-B problems.

$\phi_{\text{H}}^{\text{I}}$  and  $\phi_{\text{H}}^{\text{O}}$  are azimuth angles of the horizon detector and can be regarded as the sum of the nominal azimuth angle  $\phi_{\text{HNOM}}$  and smaller perturbation angles  $\Delta\phi_{\text{H}}^{\text{I}}$  and  $\Delta\phi_{\text{H}}^{\text{O}}$ ; i.e.,

$$\phi_{\text{H}}^{\text{I}} = \phi_{\text{HNOM}} + \Delta\phi_{\text{H}}^{\text{I}}$$

$$\phi_{\text{H}}^{\text{O}} = \phi_{\text{HNOM}} + \Delta\phi_{\text{H}}^{\text{O}}$$

The biases  $\Delta\phi_{\text{H}}^{\text{I}}$  and  $\Delta\phi_{\text{H}}^{\text{O}}$  result not only from physical instrument misalignment, but also from improperly predicted electronic phenomena associated with horizon detector triggering. The latter type of bias is not necessarily identical for Earth-in and Earth-out crossings, and for this reason OABIAS uses distinct azimuth angles  $\phi_{\text{H}}^{\text{I}}$  and  $\phi_{\text{H}}^{\text{O}}$  for in-crossings and out-crossings.

As indicated above, horizon detector azimuth bias errors  $\Delta\phi_{\text{H}}^{\text{I}}$  and  $\Delta\phi_{\text{H}}^{\text{O}}$  are included in  $\underline{X}$ . However, an analogous azimuth bias  $\Delta\phi_{\text{S}}$  of the Sun sensor is not included. Instead, the  $x_{\text{SC}}$ -axis has been defined in such a manner that  $\Delta\phi_{\text{S}} = 0$ . As shown in Figure 3-4, the  $x_{\text{SC}}$ -axis employed internally in OABIAS lies along the intersection of the Sun sensor reference slit ( $x_{\text{SS}}$ - $z_{\text{SS}}$ ) plane with the plane perpendicular to the spin vector  $\hat{S}$ . The OABIAS state vector has been set up in this manner because it is not possible to determine absolute azimuth misalignments (relative to an arbitrary body-fixed reference frame with an axis along  $\hat{S}$ ) of both the Sun sensor and the horizon detector from the available Sun sighting and horizon crossing time data. Instead, only the azimuth misalignments of one instrument relative to the other can be determined. The OABIAS solution has been to constrain the azimuth alignment angle of the Sun sensor to zero.

### 3.5.6 State Vector Element $x_7$ ( $\Delta\rho$ )

Using horizon crossing time data in attitude determination computations requires that the values of the angular radius  $\rho$  of the central body on the unit celestial sphere as seen from the satellite be known. (The technique used in OASYS/OABIAS to compute  $\rho$  is discussed in Section 3.7.) State vector element  $x_7$  is a constant angular bias  $\Delta\rho$  on the computed values  $\rho_c$  of  $\rho$ .

The assumption that a  $\rho_c$  might have a constant bias is realistic because a constant bias on the triggering threshold of the horizon scanner is the main error source which generates a  $\Delta\rho$ . Figure 3-6 demonstrates this phenomena. The attitude determination algorithms assume that the sensor triggers whenever the center point of its FOV crosses the boundary of the central body disk. Figure 3-6 shows the result when the triggering occurs significantly early on the in-crossing and late on the out-crossing. The figure indicates that this triggering time error increases the apparent  $\rho$  of the Earth by a constant value, i. e.,  $\Delta\rho$ , which is independent of the path of the sensor across the Earth's disk. This, of course, is a simplified view of the triggering phenomena and is based on a number of assumptions and approximations which include the following:

1. The FOV is circular
2. The oblateness of the central body is negligible
3. The change in the true angular radius  $\rho$  of the central body during the run is negligible
4. The sensor triggers, on the average, when a given fraction  $dA$  of its FOV is illuminated
5.  $dA$  is identical for both in-crossings and out-crossings<sup>1</sup>
6.  $dA$  does not change significantly during the run

---

<sup>1</sup>This is usually the most important assumption.

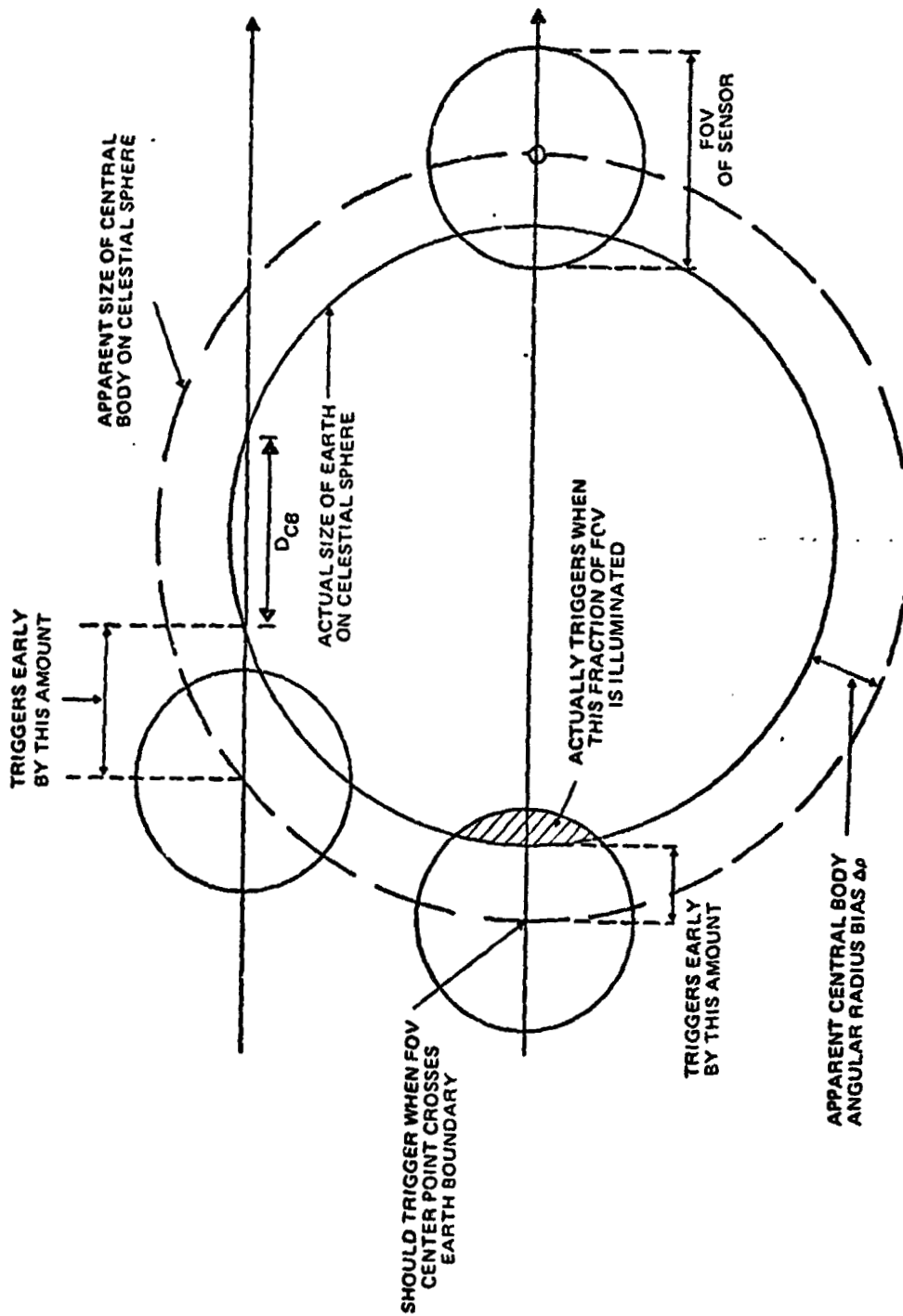


Figure 3-6. Generation of Earth Radius Bias  $\Delta p$  by Sensor Triggering Level Bias

**ORIGINAL PAGE IS  
OF POOR QUALITY**

From the above paragraph, it should be evident that  $\Delta\rho$  is largely a result of sensor behavior rather than of an actual uncertainty in the true Earth radius.

**3.5.7 State Vector Element  $x_{12}(\Delta t)$**

State vector element  $x_{12}$  is a time bias  $\Delta t$  in the location of the satellite in its orbit. It represents either a lag or a lead of the true in-track location of the satellite in its orbit, relative to either the location predicted by the OABIAS orbit generator or the location specified by the orbit data supplied to OABIAS. The use of such a bias is convenient for approximating simulated orbit data errors which result from aerodynamic drag near the perigees of highly elliptical orbits.  $\Delta t$  has been included in  $\underline{X}$  mainly to handle this type of problem.

It should be emphasized that  $\Delta t$  is not an error in the telemetered sensor event times  $t_s$ ,  $t_{HI}$ , or  $t_{HO}$ .  $\Delta t$  enters the OABIAS mathematics only through the orbit radius vector  $\vec{R}^{GI}$ .

**3.5.8 Transformation Matrix A and State Vector Elements  $x_1(s_1)$  and  $x_2(s_2)$**

The OABIAS algorithms require computation of the transformation matrix A shown in Figure 3-1. This section discusses this computation and includes the parameters  $s_1$  and  $s_2$  which OABIAS uses as the  $x_1$  and  $x_2$  components of  $\underline{X}$  to specify spin vector attitude.

Using Figure 3-1 and elementary rotation matrix techniques, A may be determined as a function of the angles  $\alpha$ ,  $\delta$ , and  $\phi$ . The result is

$$A = \begin{bmatrix} c\phi s\delta c\alpha - s\phi s\alpha & c\phi s\delta s\alpha + s\phi c\alpha & -c\phi c\delta \\ -s\phi s\delta c\alpha - c\phi s\alpha & -s\phi s\delta s\alpha + c\phi c\alpha & s\phi c\delta \\ c\delta c\alpha & c\delta s\alpha & s\delta \end{bmatrix} \quad (3-17)$$

where  $s = \text{sine}$  and  $c = \text{cosine}$ .

A can also be expressed in the following form:

$$A = \begin{bmatrix} \hat{e}_1^{GI, T} \\ \hat{e}_2^{GI, T} \\ \hat{e}_3^{GI, T} \end{bmatrix} \quad (3-18)$$

where  $\hat{e}_1^i$ ,  $\hat{e}_2^i$ , and  $\hat{e}_3^i$  are unit vectors along the x-, y-, and z-axes of frame SC, and superscript GI signifies resolution along the axes of frame GI. Superscript T signifies that the elements are  $1 \times 3$  row vectors rather than  $3 \times 1$  column vectors.  $\hat{e}_3^i$  lies along the spin axis of the satellite. Thus  $\hat{e}_3^i = \hat{S}$ .

Let the scalars  $s_1$ ,  $s_2$ , and  $s_3$  signify the components of  $\hat{S}^{GI}$ . Then Equations (3-17) and (3-18) show that

$$s_1 = c\delta c\alpha \quad (3-19a)$$

$$s_2 = c\delta s\alpha \quad (3-19b)$$

$$s_3 = s\delta = \pm \sqrt{1 - s_1^2 - s_2^2} \quad (3-19c)$$

The plus sign is used with the radical sign in Equation (3-19c) when  $\delta \geq 0$ , and the minus sign is used when  $\delta \leq 0$ .

- In place of the usual  $\alpha$  and  $\delta$  angles, OABIAS uses  $s_1$  and  $s_2$  as the spin vector attitude coordinates  $x_1$  and  $x_2$  of  $\underline{X}$ . Therefore it is necessary to rewrite Equation (3-17) to yield A as a function of  $s_1$ ,  $s_2$ , and  $\phi$ .

**ORIGINAL PAGE IS  
OF POOR QUALITY**

This can be done, element by element, using Equations (3-17) and (3-19). The result is

$$A = \begin{bmatrix} a_{11} & a_{12} & a_{13} \\ a_{21} & a_{22} & a_{23} \\ a_{31} & a_{32} & a_{33} \end{bmatrix} \tag{3-20a}$$

$$= \frac{1}{\sqrt{s_1^2 + s_2^2}} \begin{bmatrix} s_1 s_3 \cos \phi - s_2 s \phi & s_2 s_3 \cos \phi + s_1 s \phi & -\left[ \frac{s_1^2 + s_2^2}{s_1 + s_2} \right] \cos \phi \\ -s_1 s_3 \sin \phi - s_2 s \phi & -s_2 s_3 \sin \phi + s_1 s \phi & \left[ \frac{s_1^2 + s_2^2}{s_1 + s_2} \right] \sin \phi \\ s_1 \sqrt{s_1^2 + s_2^2} & s_2 \sqrt{s_1^2 + s_2^2} & s_3 \sqrt{s_1^2 + s_2^2} \end{bmatrix}$$

where

$$s_3 = \pm \sqrt{1 - s_1^2 - s_2^2} \tag{3-20b}$$

Equations (3-20a) and (3-20b) are the ones actually used in OBIAS to compute the elements  $a_{\mu\nu}$  of A.  $\phi$  is computed using Equation (3-16).

Equations (3-19a) and (3-19b) show that  $s_1$  and  $s_2$  approach zero as  $\delta$  approaches  $\pm 90$  degrees. Equations (3-20a) and (3-20b) show that the elements  $a_{11}$ ,  $a_{12}$ ,  $a_{21}$ ,  $a_{22}$  of A then approach a singular condition (zero divided by zero). The net result is that the use of coordinates  $s_1$  and  $s_2$  does not eliminate the well known singularity at  $\delta = 90$  degrees which is encountered with  $\alpha$  and  $\delta$  coordinates. The purpose of the 45-degree coordinate rotation when the user-supplied declination estimate  $\hat{\delta}_0$  is close to  $\pm 90$  degrees is to avoid this difficulty.

ORIGINAL PAGE IS  
OF POOR QUALITY

As noted previously, the correct sign of the square root term in Equation (3-20b) is positive when  $\delta > 0$  and negative when  $\delta < 0$ . OBIAS determines the correct sign of  $s_3$  at the start of each run and maintains this sign throughout the run. Thus, erroneous computations would result if the filter's transient response were such that the sign for  $s_3$  had to change during the run. OBIAS prevents this from occurring by performing the aforementioned 45-degree rotation whenever the user-supplied declination angle estimate  $\hat{\delta}_0$  is close to zero. The proper sign of  $s_3$  is determined from the sign of the initial declination angle  $\hat{\delta}_0$  of the rotated coordinate frame GI. As a result of the rotation,  $s_3$  is sufficiently large that it will not pass through zero during the run; hence the potential change difficulty is avoided.

### 3.5.9 Transformation Matrices $B_I$ and $B_O$

The derivation of the equations for the direction cosines matrices  $B_I$  and  $B_O$  of Figure 3-1 requires only straightforward rotation matrix techniques. Because the form of the equations for  $B_I$  and  $B_O$  is identical, only a single matrix, to be designated as  $B_H$ , is shown. The azimuth angle is signified by  $\phi_H$ . The result is

$$\begin{aligned}
 B_H &= \begin{bmatrix} b_{11} & b_{12} & b_{13} \\ b_{21} & b_{22} & b_{23} \\ b_{31} & b_{32} & b_{33} \end{bmatrix} = T_{\phi_H}(z)^T T_{\epsilon_H}(x)^T T_{\Delta\gamma}(y)^T \\
 &= \begin{bmatrix} c\Delta\gamma c\phi_H - s\Delta\gamma s\epsilon_H s\phi_H & -c\epsilon_H s\phi_H & s\Delta\gamma c\phi_H + c\Delta\gamma s\epsilon_H s\phi_H \\ c\Delta\gamma s\phi_H + s\Delta\gamma s\epsilon_H c\phi_H & c\epsilon_H c\phi_H & s\Delta\gamma s\phi_H - c\Delta\gamma s\epsilon_H c\phi_H \\ -s\Delta\gamma c\epsilon_H & s\epsilon_H & c\Delta\gamma c\epsilon_H \end{bmatrix} \quad (3-21)
 \end{aligned}$$

where  $T(\ )$  signifies the matrix for the rotation about the axis within the parentheses and superscript  $T$  signifies matrix transpose.

### 3.6 OBSERVATION MODELS

This section discusses each of the eight OABIAS observation models. Also included are the derivations of the  $y$  and  $y_c$  algorithms for each of the models. First, however, the pertinent features of the general observation model equation used by OABIAS will be recapitulated.

The OABIAS observation model equations are in the form

$$y(\underline{m}) = y_c(\underline{m}, \underline{X}) + v \quad (3-22)$$

where  $y$  = the real observation

$y_c$  = the model observation

$\underline{m}$  = the  $4 \times 1$  vector of the basic measurements for the frame being processed

$v$  = the net error due to the error in  $\underline{m}$  and to modeling approximations and inaccuracy

$$\underline{m}^T = \{m_1, m_2, m_3, m_4\} = \{\beta_M, t_s, t_{HI}, t_{HO}\} \quad (3-23)$$

OABIAS processes the telemetry frames individually. Assuming no Sun angle smoothing, no observation model utilizes measurements  $m_\alpha$  from more than one telemetry frame in any single processing operation. For this reason, in the remainder of this section, single frame measurement vectors  $\underline{m}$  will be referred to rather than the composite block measurement vector  $\underline{M}$  used earlier in this report. Also, the form of Equation (3-22) will be maintained throughout this section with the real observation on the left and the model observation on the right.

For each of the eight models there is an observation equation of the general form shown above. In Models 1, 5, 6, and 8,  $y$  is calculated using one or

**ORIGINAL PAGE IS  
OF POOR QUALITY**

more elements of  $\underline{m}$ . In Model 7,  $y$  is the telemetered horizon detector angle. In Models 2, 3, and 4,  $y$  is zero by definition.  $y_c$  is computed in each model from an algebraic expression involving one or more elements of  $\underline{X}$  and, directly or indirectly, one or more elements of  $\underline{m}$ . In Models 2, 3, and 4, the  $\underline{m}$  dependency enters solely through  $y_c$ .

When running OABIAS, the user selects the elements of  $\underline{X}$  to be used and the models to be employed. These must be compatible with each other and with the attitude determination problem being pursued. Because knowledge of the elements of  $\underline{X}$  which appear in each of the models is important, they will be noted explicitly in the discussion of each model. (See Table 3-2 for a summary of these elements.)

The OABIAS recursive estimation algorithm also requires computations of partial derivatives of the form

$$g_{\eta} = \frac{\partial y_c}{\partial x_{\eta}}$$

$$\eta = 1 \text{ to } 12$$

The 12  $g_{\eta}$ 's are comprised in the  $G$  vector used elsewhere in the report. Because there are 8 models and 12 state vector elements, there are 96 partial derivatives including some which are zero. (Because of the number and complexity of the partial derivative equations, they are contained in Appendix A.)

### 3.6.1 Model 1--Sun Angle Model

The angle which is measured by the Sun sensor  $\beta_M$  is the observable for Model 1 and is clearly the most significant element of  $\underline{m}$  used by Model 1. Model 1 is similar to the Sun angle models used in OASYS/GCONES and OASYS/GRECRS except Model 1 includes the Sun sensor misalignment angles  $\epsilon$  and  $\Delta\beta$ .

ORIGINAL PAGE 53  
OF POOR QUALITY

The basic geometry at a Sun sighting is shown in Figure 3-4. The features of this figure essential to Model 1 are repeated in Figure 3-7.

The Sun angle observation equation is obtained by applying the law of cosines of sides to the spherical triangle shown in Figure 3-7. Thus,

$$\beta_M = -\Delta\beta + \arccos(\sec \epsilon \cos \beta) \quad (3-24)$$

A suitable equation for  $\cos \beta$  now must be derived. This equation should include elements of  $\underline{X}$  but not the measured Sun angle  $\beta_M$ . The derivation starts by expressing  $\cos \beta$  as the dot product of  $\hat{U}$  and  $\hat{S}$

$$\cos \beta = \hat{U} \cdot \hat{S} \quad (3-25)$$

Let  $\hat{U}$  and  $\hat{S}$  be resolved along the axes of frame GI and let their components be designated as  $u_1, u_2, u_3$  and  $s_1, s_2, s_3$ , respectively. In OABIAS, an ephemeris file or orbit generator provides the unit Sun vector components  $u'_1, u'_2, u'_3$  (at Sun sighting time  $t_s$ ) along the axes of frame GI'. These are identical to  $u_1, u_2, u_3$  in runs in which the 45-degree frame GI rotation is not made. In runs in which this rotation is made, the OABIAS transforms  $u'_1, u'_2, u'_3$  into  $u_1, u_2, u_3$  using standard rotation equation methods. Hence  $u_1, u_2$ , and  $u_3$  are not functions of  $\underline{X}$ .  $s_3$  is computed using Equation (3-19c) given previously.

In summary, the Model 1 equations are

$$y = \beta_M \quad (3-26a)$$

$$y_c = -\Delta\beta + \arccos[(u_1 s_1 + u_2 s_2 + u_3 s_3) \sec \epsilon] \quad (3-26b)$$

ORIGINAL PAGE IS  
OF POOR QUALITY

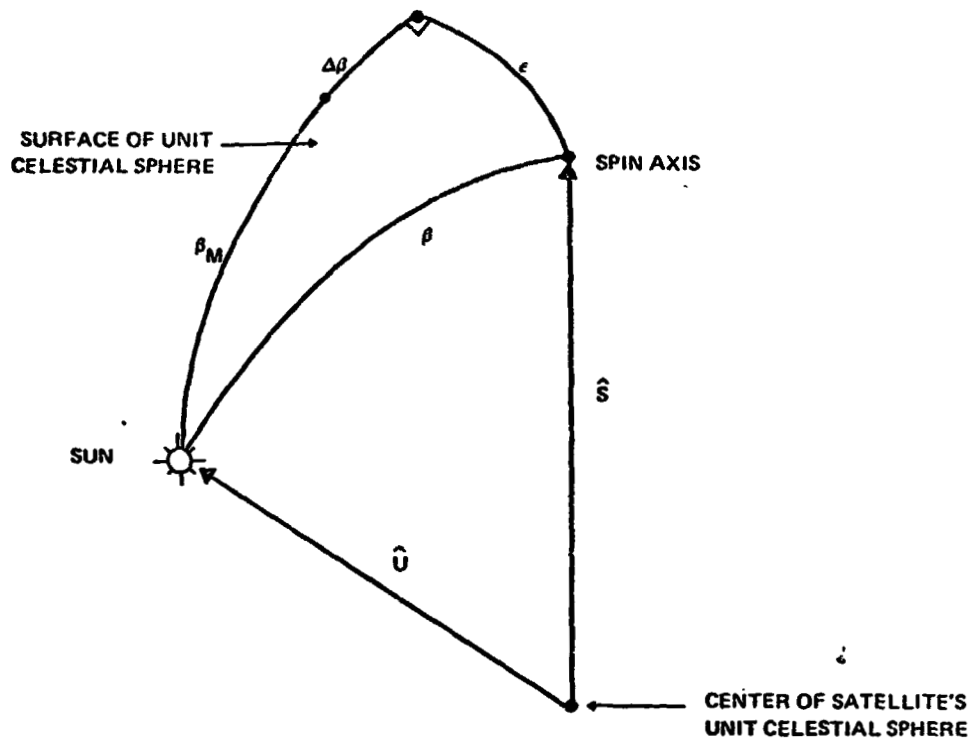


Figure 3-7. Geometry for Model 1--Sun Angle Model

where

ORIGINAL PAGE IS  
OF POOR QUALITY

$$s_3 = \pm \sqrt{1 - s_1^2 - s_2^2} \quad (3-26c)$$

The correct sign in Equation (3-26c) is determined at the start of each OABIAS run.

Equation (3-26) shows that Model 1 contains the following  $\underline{X}$  elements:

$$s_1, s_2, \Delta\beta, \text{ and } \epsilon$$

Model 1 is the only model which contains  $\Delta\beta$ , and it is the only model that uses the Sun angle measurement  $\beta_M$ . Hence, Model 1 normally is included in all OABIAS runs.

### 3.6.2 Model 2--Sun Sighting Time Model

Model 2 employs only the Sun time measurement  $t_s$ . The essential features of the geometry are shown in Figure 3-4. In this figure, the Sun sensor reference plane  $x_{SS}-z_{SS}$  rotates in inertial space due to the spin of the satellite. The Sun is sighted when this plane crosses the unit Sun vector,  $\hat{U}$ .

$\hat{N}_s$  is the unit vector along the Sun sensor axis  $y_{SS}$  which is perpendicular to  $x_{SS}$  and  $z_{SS}$ .  $\hat{N}_s$  is perpendicular to  $\hat{U}$  at Sun sighting times  $t_s$ . Therefore,

$$0 = \left. \hat{U} \cdot \hat{N}_s \right|_{t=t_s} \quad (3-27)$$

The observable for Model 2 is  $\hat{U} \cdot \hat{N}_s = \cos\tau$ , where  $\tau$  is the angle between  $\hat{U}$  and  $\hat{N}_s$  as shown in Figure 3-4. The value of  $\cos\tau$  varies as a function

of the angle  $\phi$  of the satellite in its spin cycle. Assuming the orientation of  $\hat{U}$  and  $\hat{S}$  to be constant,  $\cos\tau$  is a periodic function of time; its fundamental period is the satellite's spin period  $2\pi/\omega$ .  $\cos\tau$  is observed only at those times  $t_s$  when the Sun is sighted. However,  $\cos\tau$  is zero at  $t = t_s$  as was indicated in Equation (3-27). Therefore, the real observation  $y$  and model observation  $y_c$  for Model 2 are

$$y = 0 \quad (3-28a)$$

$$y_c = \hat{U} \cdot \hat{N}_s \quad (3-28b)$$

where  $y_c$  is evaluated at the measured Sun sighting time  $t_s$ .

It should be apparent that there is a fundamental difference between Models 1 and 2. In Model 1, the significant measured parameter  $\beta_M$  entered into the mathematics through the real observation  $y$ . Thus,  $y$  was not known perfectly. In Model 2, the measured parameter  $t_s$  enters the mathematics solely through the model observation  $y_c$  rather than through  $y$ . With Model 2,  $y$  is zero by definition. Hence the name "observation" as applied to  $y$  in Model 2, in a sense, is a misnomer. However, this difference between the methods of Models 1 and 2 does not affect the performance of the system as a least-squares recursive estimator; in both cases the residuals  $y - y_c$  have equivalent properties.

A suitable equation for  $y_c$  containing  $t_s$  and elements of  $\underline{X}$  now must be derived. Using frame GI resolution, Equation (3-28b) becomes

$$y_c = \hat{U}^{GI} \cdot \hat{N}_s^{GI} = u_1 n_1 + u_2 n_2 + u_3 n_3 \quad (3-29)$$

ORIGINAL PAGE #  
OF POOR QUALITY

As was noted in the Model 1 discussion, the components  $u_1, u_2, u_3$  of  $\hat{U}^{GI}$  are provided by ephemeris data. Hence, the remaining problem is to develop equations for the components  $n_1, n_2, n_3$  of  $\hat{N}_s^{GI}$ .

Because  $N_s$  lies along  $y_{SS}$ ,

$$\hat{N}_s^{SS} = \begin{Bmatrix} 0 \\ 1 \\ 0 \end{Bmatrix} \quad (3-30)$$

The  $n_1, n_2, n_3$  equations now can be developed with the aid of Figure 3-1 and standard coordinate frame transformation methods. The result is

$$\hat{N}_s^{GI} = \begin{Bmatrix} n_1 \\ n_2 \\ n_3 \end{Bmatrix} = A^T T_\epsilon(x)^T T_{\Delta\beta}(y)^T \begin{Bmatrix} 0 \\ 1 \\ 0 \end{Bmatrix} \quad (3-31)$$

where superscript T signifies a matrix transpose and

$$T_{\Delta\beta}(y) = \begin{bmatrix} c\Delta\beta & 0 & -s\Delta\beta \\ 0 & 1 & 0 \\ s\Delta\beta & 0 & c\Delta\beta \end{bmatrix} \quad (3-32a)$$

$$T_\epsilon(x) = \begin{bmatrix} 1 & 0 & 0 \\ 0 & c\epsilon & s\epsilon \\ 0 & -s\epsilon & c\epsilon \end{bmatrix} \quad (3-32b)$$

A is the direction cosine matrix defined in Figure 3-1 and discussed in Section 3.5.8. It is computed in OABIAS by Equation (3-20).

**ORIGINAL PAGE IS  
OF POOR QUALITY**

The final equation for  $n_1, n_2, n_3$  is obtained by substituting Equations (3-32a) and (3-32b) into Equation (3-31) and performing the multiplications. By indicating the elements of  $A$  by lower case letters, as shown in Equation (3-20), the result is

$$N_s^{GI} = \begin{Bmatrix} n_1 \\ n_2 \\ n_3 \end{Bmatrix} = \begin{Bmatrix} a_{21} c\epsilon + a_{31} s\epsilon \\ a_{22} c\epsilon + a_{32} s\epsilon \\ a_{23} c\epsilon + a_{33} s\epsilon \end{Bmatrix} \quad (3-33)$$

$\Delta\beta$  does not appear in the result.

The final equations for Model 2 are Equations (3-28a), (3-29), and (3-33). Equations (3-33) and (3-20) show that Model 2 includes the following elements of  $\underline{X}$ :  $s_1, s_2, \psi_0, \omega$ , and  $\epsilon$ . When computing  $\phi$  and, hence,  $A$  for Model 2, the measured Sun sighting time  $t_s$  is used. This is the mechanism through which  $\underline{m}$  enters the Model 2 mathematics.

### 3.6.3 Model 3--Nadir Vector Projection Model

The central body horizon-in crossing time  $t_{HI}$  or the horizon-out crossing time  $t_{HO}$  are the elements of  $\underline{m}$  which are used in Model 3. When the user requests Model 3, separate calculations using first  $t_{HI}$  and then  $t_{HO}$  are performed. In the interest of simplicity, the present discussion and notation will not distinguish explicitly between the horizon-in crossing and horizon-out crossing cases.

Figure 3-8 summarizes the essential geometry for Model 3. In this figure,  $\hat{L}$  is the unit vector along the line of sight of the horizon scanner and rotates in inertial space due to the satellite's rotation. Figure 3-8 shows the locus traced out on the unit celestial sphere by the tip of  $\hat{L}$ .  $-\hat{R}$  is the unit nadir vector of the central body; it moves relatively slowly on the celestial sphere

ORIGINAL PAGE IS  
OF POOR QUALITY

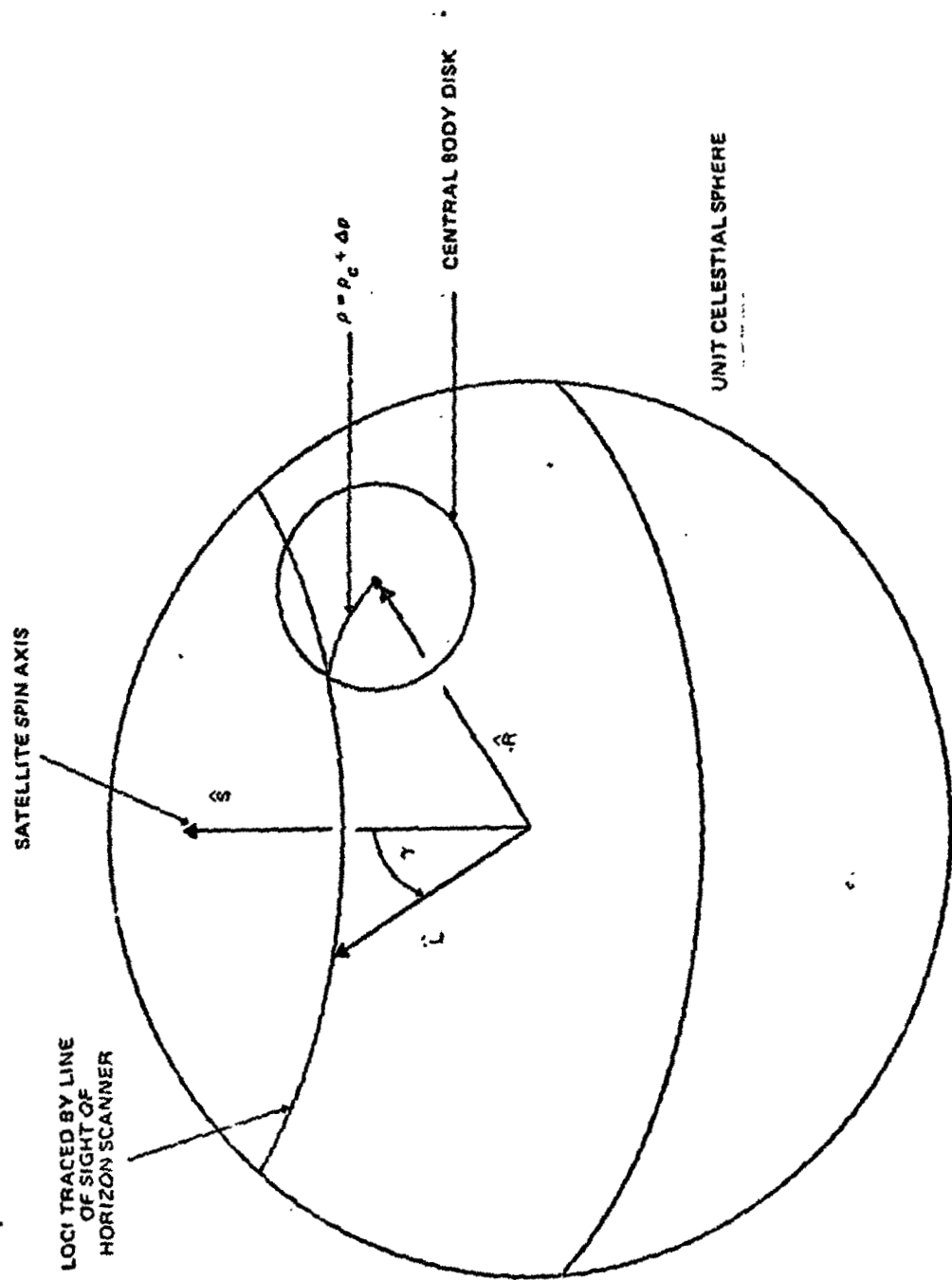


Figure 3-8. Geometry for Model 3--Nadir Vector Projection Model

**ORIGINAL PAGE IS  
OF POOR QUALITY**

due to the in-track motion of the satellite around its orbit.  $\rho$  is the apparent angular radius of the central body on the unit celestial sphere as seen from the satellite.

The observable for Model 3 is the parameter  $\cos \rho + \hat{R} \cdot \hat{L}$ . This parameter varies cyclically at the orbit period  $2\pi/\omega$ . There is also a slow variation due to the motion of  $\hat{R}$  on the celestial sphere and (in elliptic orbits) the changing magnitude of  $\rho$ . The measurements of this observable are contained in the horizon crossing times  $t_H$ . A check of the geometry in Figure 3-8 will show that the observable is zero at these times. In this respect, Model 3 is analogous to Model 2. The equations for  $y$  and  $y_c$ , therefore, are

$$y = 0 \quad (3-34a)$$

$$y_c = \cos \rho + \hat{R} \cdot \hat{L} \quad (3-34b)$$

where  $y_c$  is computed at the horizon crossing times  $t_H$ .

OABIAS uses the following equation to obtain  $\cos \rho$  for the  $y_c$  computation:

$$\cos \rho = \cos (\rho_c + \Delta\rho) = \cos \rho_c \cos \Delta\rho - \sin \rho_c \sin \Delta\rho \quad (3-35)$$

where  $\rho_c$  is the computed value of  $\rho$  obtained using orbit data. (See Section 4.6 for a discussion of this computation.)  $\Delta\rho$ , which is element  $x_7$  of  $\underline{X}$ , is a bias on  $\rho_c$ .

To derive the equation for  $\hat{R} \cdot \hat{L}$ , frame GI resolution is used. Let  $\vec{R}$  be the distance vector from the Earth's center to the satellite. Then

$$\hat{R}^{GI} = \frac{1}{|\vec{R}|} \vec{R}^{GI} \quad (3-36)$$

**ORIGINAL PAGE IS  
OF POOR QUALITY**

Letting the components of  $\vec{R}^{GI}$  be designated as  $R_1, R_2, R_3,$

$$|\vec{R}| = \sqrt{R_1^2 + R_2^2 + R_3^2} \quad (3-37)$$

The  $R_1, R_2, R_3$  values are generated for the OBIAS recursive estimator via an ephemeris file or orbit generator; these data are transformed as necessary in those applications where the 45-degree GI' to GI transformation is made.

Let the components of  $\hat{L}^{GI}$  be designated as  $l_{1GI}, l_{2GI}, l_{3GI}$ . Use of Equations (3-35) and (3-36) now enables the  $y_c$  expression in Equation (3-34b) to be written as follows:

$$y_c = \cos \rho_c \cos \Delta\rho - \sin \rho_c \sin \Delta\rho + \frac{1}{|\vec{R}|} \{ R_1 l_{1GI} + R_2 l_{2GI} + R_3 l_{3GI} \} \quad (3-38)$$

Suitable equations for the components  $l_{1GI}, l_{2GI}, l_{3GI}$  of  $\hat{L}^{GI}$  are derived using Figure (3-1) and the usual rotation matrix techniques. The intermediate result is

$$\hat{L}^{H'} = T_\gamma(y)^T \hat{L}^H = T_\gamma(y)^T \begin{Bmatrix} 0 \\ 0 \\ 1 \end{Bmatrix} \quad (3-39a)$$

$$\hat{L}^{SC} = \begin{Bmatrix} l_{1SC} \\ l_{2SC} \\ l_{3SC} \end{Bmatrix} = B \hat{L}^{H'} \quad (3-39b)$$

$$\hat{L}^{GI} = \begin{Bmatrix} l_{1GI} \\ l_{2GI} \\ l_{3GI} \end{Bmatrix} = A^T \hat{L}^{SC} \quad (3-39c)$$

where

ORIGINAL PAGE #  
OF POOR QUALITY

$$T_y(y) = \begin{bmatrix} cy_s & 0 & -sy_s \\ 0 & 1 & 0 \\ sy_s & 0 & cy_s \end{bmatrix} \quad (3-40)$$

The second part of Equation (3-39a) follows from the fact that  $\hat{L}$  lies along the  $z_H$ -axis. The equations for the elements  $a_{\lambda\mu}$  and  $b_{\lambda\mu}$  of matrices A and B are Equations (3-20) and (3-21). The final scalar equations for  $l_{1GI}$ ,  $l_{2GI}$ ,  $l_{3GI}$  are obtained by performing the matrix multiplications of Equations (3-38), (3-39), and (3-40). The result is

$$\hat{L}^{SC} = \begin{bmatrix} b_{11} sy_s + b_{13} cy_s \\ b_{21} sy_s + b_{23} cy_s \\ b_{31} sy_s + b_{33} cy_s \end{bmatrix} = \begin{bmatrix} l_{1SC} \\ l_{2SC} \\ l_{3SC} \end{bmatrix} \quad (3-41a)$$

$$\hat{L}^{GI} = \begin{bmatrix} l_{1GI} \\ l_{2GI} \\ l_{3GI} \end{bmatrix} = \begin{bmatrix} a_{11} l_{1SC} + a_{21} l_{2SC} + a_{31} l_{3SC} \\ a_{12} l_{1SC} + a_{22} l_{2SC} + a_{32} l_{3SC} \\ a_{13} l_{1SC} + a_{23} l_{2SC} + a_{33} l_{3SC} \end{bmatrix} \quad (3-41b)$$

The final equations for Model 3 are Equations (3-34), (3-37), (3-38), and (3-41). Equations (3-16), (3-20), and (3-21) also are needed for computation of the elements of the A and B matrices.

In using Equation (3-16) to compute the angle  $\phi$  which appears in A, the time  $t$  is the measured horizon crossing  $t$ .

$$\phi_{\text{model 3}} = \psi_0 + \omega \left( t_{11} - t_0 \right) \quad (3-42)$$

C-2

The elements of  $\vec{R}^{GI}$ , however, are evaluated at  $t_{II} + \Delta t$  where  $\Delta t$  is element  $x_{12}$  of  $\underline{X}$ . These are the two mechanisms through which  $\underline{m}$  enters into Model 3.

A check of the equations will show that Model 3 includes the following elements of  $\underline{X}$ :  $s_1, s_2, \psi_0, \Delta\gamma, \phi_H^I$  or  $\phi_H^O, \Delta\rho, \omega, t_H$ , and  $\Delta t$ .

#### 3.6.4 Model 4--Horizon Crossing Time Model

As with Model 3, Model 4 employs the central body horizon crossing times  $t_{HI}$  or  $t_{HO}$ . Likewise, separate calculations using  $t_{HI}$  and  $t_{HO}$  are made with Model 4. Once again, the present discussion and notation will not distinguish explicitly between horizon-in crossings and horizon-out crossings.

Figure 3-9 shows the essential geometry for Model 4.  $\hat{N}_H$  is a unit vector along the y-axis of frame H and the horizon detector line of sight vector  $\hat{L}$  lies along the z-axis of frame H. Hence,  $\hat{N}_H$  and  $\hat{L}$  are perpendicular to one another and  $\hat{N}_H \cdot \hat{L} = 0$ . Both vectors rotate in inertial space due to the spin of the satellite.

Figure 3-9 shows the locus swept out on the unit celestial sphere by the tip of  $\hat{L}$ .  $\hat{D}$  is a unit vector whose tip is at the intersection of the perimeter of the central body disk and the locus of  $\hat{L}$ .  $\hat{D}$  moves (relatively slowly) due to the motion of the satellite in its orbit which produces motion of the central body disk on the unit celestial sphere. It is important to realize that the  $\hat{D}$  motion is not a function of the satellite's spin rate  $\hat{\omega}$ .

The observable for Model 4 is  $\cos \zeta$  where  $\zeta$  is the angle between  $\hat{N}_{II}$  and  $\hat{D}$ . Thus  $\cos \zeta = \hat{N}_{II} \cdot \hat{D}$ .  $\cos \zeta$  varies as a function of the angle  $\phi$  of the satellite in its spin cycle. The motion is near-periodic with the fundamental period being the satellite's spin period  $2\pi/\omega$ . There also is a slow variation due to the motion of  $\hat{D}$ .  $\cos \zeta$  is observed at the horizon crossing times  $t_{II}$

ORIGINAL PAGE IS  
OF POOR QUALITY

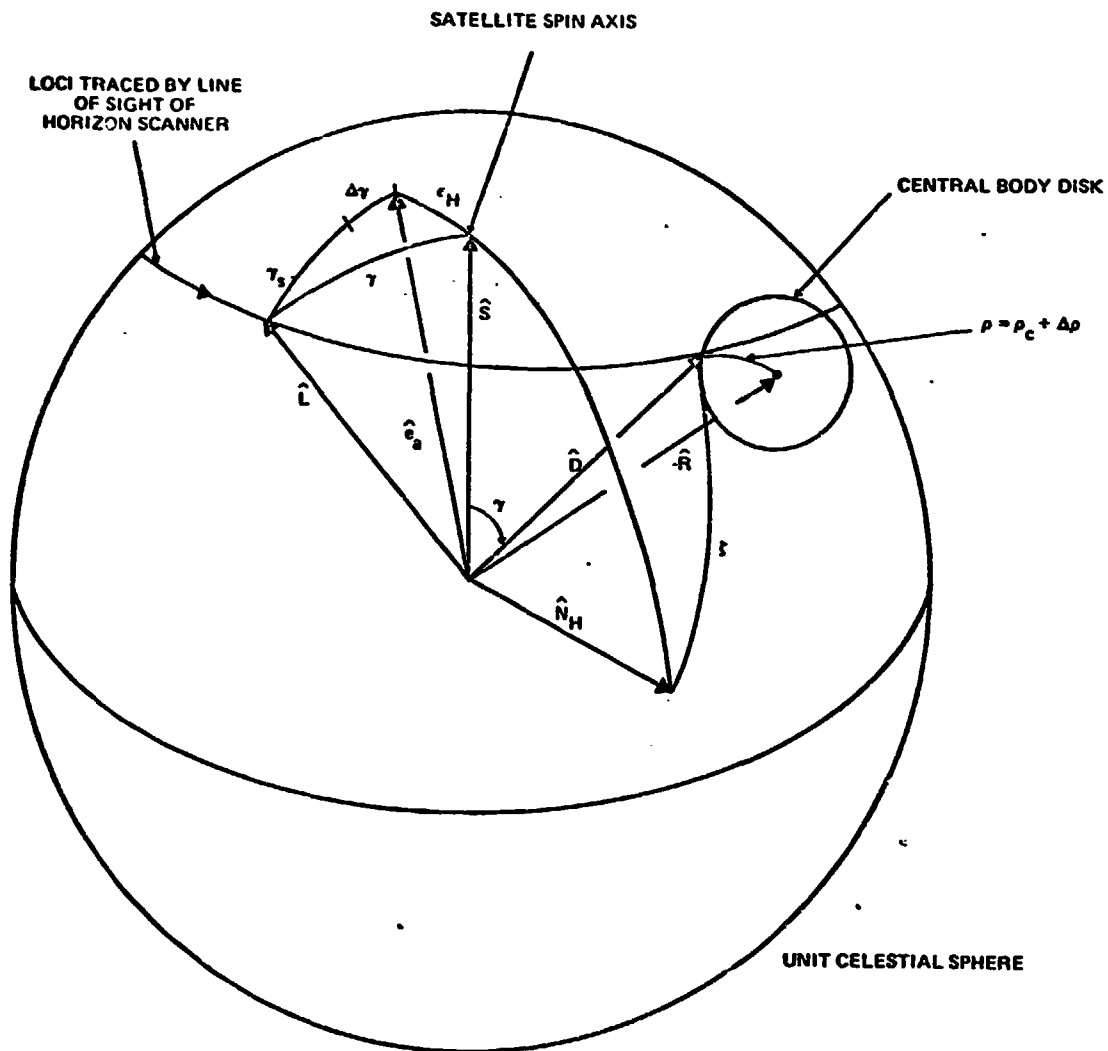


Figure 3-9. Geometry for Model 4--Horizon Crossing Time Model

ORIGINAL PAGE IS  
OF POOR QUALITY

when  $\hat{L}$  and  $\hat{D}$  coincide. Because  $\hat{L}$  is orthogonal to  $\hat{N}_H$ ,  $\cos \zeta = 0$  at  $t = t_H$ . Therefore, the  $y$  and  $y_c$  equations are

$$y = 0 \quad (3-43a)$$

$$y_c = \hat{N}_H \cdot \hat{D} \quad (3-43b)$$

where  $y_c$  is evaluated at the horizon crossing times  $t_H$ .

Resolution on frame GI is employed in the  $y_c$  computation. Thus,

$$y_c = \hat{N}_H^{GI} \cdot \hat{D}^{GI} \quad (3-44)$$

Referring to Figure 3-1,

$$\hat{N}_H^{SC} = T_{\phi_H}(z)^T T_{\epsilon_H}(x)^T T_{\Delta\gamma}(y)^T \hat{N}_H^{H'} \quad (3-45a)$$

$$\hat{N}_H^{GI} = A^T \hat{N}_H^{SC} \quad (3-45b)$$

where  $\phi_H(z)$ ,  $\epsilon_H(x)$ , and  $\Delta\gamma(y)$  are the usual coordinate frame transformation matrices. From the definition of frame  $H'$  and the vector  $N_H$ ,

$$N_H^{H'} = \begin{Bmatrix} 0 \\ 1 \\ 0 \end{Bmatrix} \quad (3-46)$$

**ORIGINAL PAGE IS  
OF POOR QUALITY**

The scalar equations for  $\hat{N}_H^{GI}$  are obtained by substituting Equation (3-46) into Equation (3-15) and performing the matrix multiplications. The result is

$$\hat{N}_H^{SC} = \begin{pmatrix} n_{H1SC} \\ n_{H2SC} \\ n_{H3SC} \end{pmatrix} = \begin{pmatrix} -s\phi_H c\epsilon_H \\ c\phi_H c\epsilon_H \\ s\epsilon_H \end{pmatrix} \quad (3-47a)$$

$$\hat{N}_H^{GI} = \begin{pmatrix} n_{H1GI} \\ n_{H2GI} \\ n_{H3GI} \end{pmatrix} = \begin{pmatrix} a_{11} n_{H1SC} + a_{21} n_{H2SC} + a_{31} n_{H3SC} \\ a_{12} n_{H1SC} + a_{22} n_{H2SC} + a_{32} n_{H3SC} \\ a_{13} n_{H1SC} + a_{23} n_{H2SC} + a_{33} n_{H3SC} \end{pmatrix} \quad (3-47b)$$

The scalar equations involving  $\hat{D}^{GI}$  can be obtained with the aid of Figure 3-9.

$$\hat{S}^{GI} \cdot \hat{D}^{GI} = c(\gamma_s + \Delta\gamma) c\epsilon_H \quad (3-48a)$$

$$\hat{R}^{GI} \cdot \hat{D}^{GI} = -c(\rho_c + \Delta\rho) \quad (3-48b)$$

$$\hat{D}^{GI} \cdot \hat{D}^{GI} = 1 \quad (3-48c)$$

At any stage of the OBIAS computations, numerical values (or estimates) for all parameters in Equations (3-18), except  $\hat{D}^{GI}$ , are available. Hence, Equations (3-48a), (3-48b), and (3-48c) constitute a set of scalar equations which can be solved for the three components of  $\hat{D}^{GI}$ . Because the derivation of the algorithm for  $\hat{D}^{GI}$  is lengthy and not essential for the discussion of Model 4, it will be deferred to Section 3.8. However, it should be noted that  $\hat{D}^{GI}$  is a function of the following elements of  $\underline{X}$ :  $s_1$ ,  $s_2$ ,  $\Delta\gamma$ ,  $\Delta\rho$ ,  $\epsilon_H$ , and  $\Delta t$ .

**ORIGINAL PAGE IS  
OF POOR QUALITY**

The equations for Model 4 are (3-43a), (3-44), and (3-47), plus the solution of Equation (3-48) for  $D^{\hat{G}I}$ . In addition, Equation (3-20) is required to calculate the elements of  $\Lambda$ , and a supplementary calculation of  $\rho_c$  is needed. The algorithm also requires  $\vec{R}^{GI}$  and the nominal mounting angle  $\gamma_s$  as inputs.

As in Model 4,  $\phi$  (and hence  $\Lambda$ ) is evaluated at the measured horizon crossing time  $t_H$ .  $\vec{R}^{GI}$  (and hence  $\rho_c$ ) is evaluated at  $t_H + \Delta t$  where  $\Delta t$  is element  $x_{12}$  of  $\underline{X}$ . These are the two places where  $\underline{m}$  enters into the Model 4 mathematics. A check of the equations should show that the  $\underline{X}$  elements which appear in Model 4 are the same as in Model 3:  $s_1, s_2, \psi_0, \Delta\gamma, \phi_H^I$  or  $\phi_H^O, \Delta\rho, \omega, \epsilon_H$ , and  $\Delta t$ .

**3.6.5 Model 5--Sun to Earth-In and Sun to Earth-Out Dihedral Angle Model**

Model 5 uses two elements of  $\underline{m}$ : the Sun sighting time  $t_s$  and either the horizon-in crossing time  $t_{HI}$  or the horizon-out crossing time  $t_{HO}$ . When the user requests Model 5, separate calculations using  $t_s$  and  $t_{HI}$  and then  $t_s$  and  $t_{HO}$  are performed. In the interest of simplicity, the present discussion and notation will not distinguish explicitly between horizon-in crossings and horizon-out crossings.

The geometry for Model 5 is shown in Figure 3-10. The left portion of the figure shows the geometry at a Sun sighting time  $t_s$ ; the right portion shows the geometry at a horizon crossing time  $t_H$ . Since the spin rate  $\omega$  is constant, the total spin angle change between  $t_s$  and  $t_H$  will be  $\omega(t_H - t_s)$ . The observable for Model 5 is  $(t_H - t_s)$ . Thus

$$y = t_H - t_s \tag{3-49}$$

ORIGINAL PAGE IS  
OF POOR QUALITY

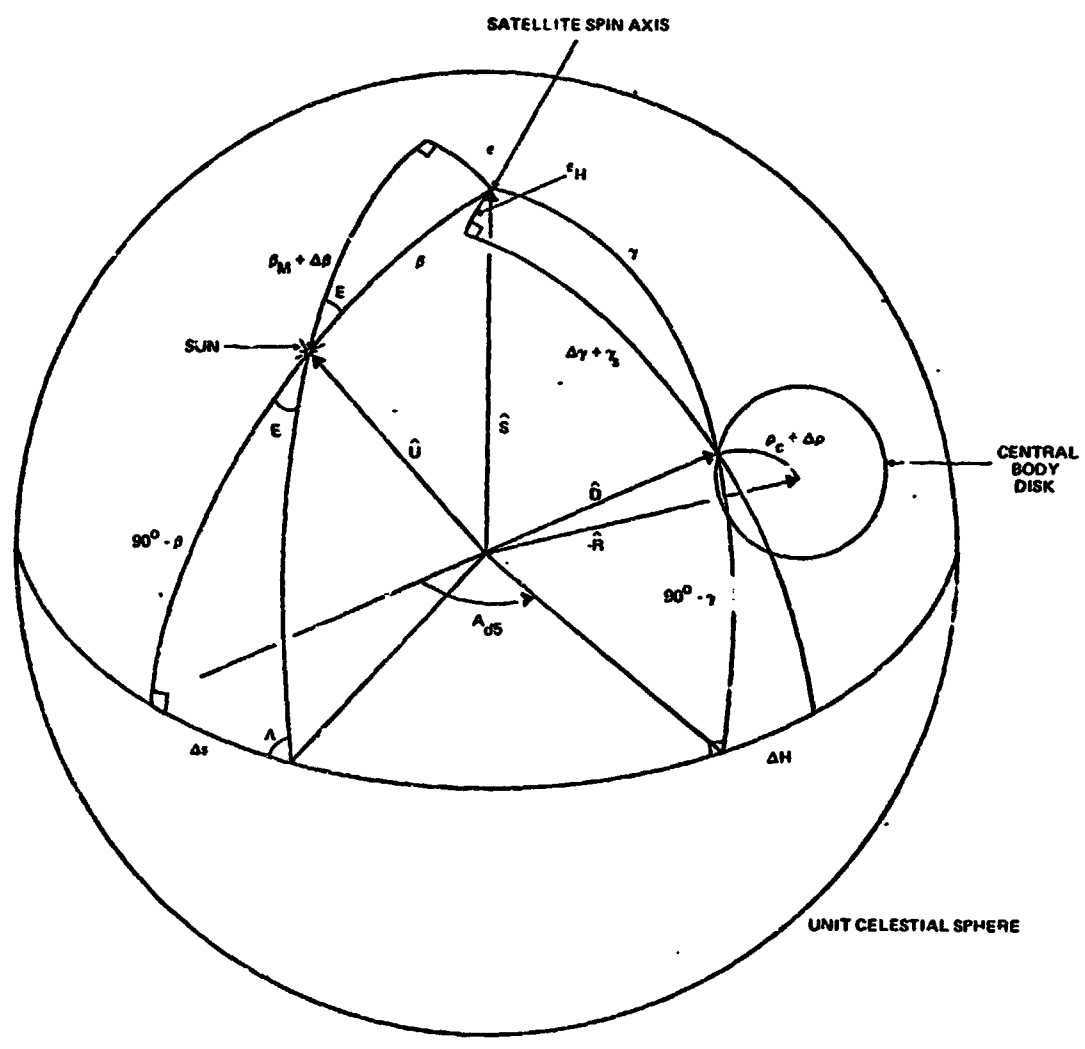


Figure 3-10. Geometry for Model 5--Sun to Earth-In and Sun to Earth-Out Dihedral Angle Model

**ORIGINAL PAGE IS  
OF POOR QUALITY**

The basic equation for the model observation  $y_c$  can be developed with the aid of Figure 3-10.

$$y_c = \frac{1}{\omega} \{A_{d5} - \Delta s + \Delta H - \phi_H - 2\pi n\} \quad (3-50)$$

$A_{d5}$ , as shown in Figure 3-10, is the dihedral angle between the  $\hat{U}-\hat{S}$  plane and the  $\hat{S}-\hat{D}$  plane.  $\Delta s/\omega$  is the change in the Sun sighting time  $t_s$  due to Sun sensor misalignments  $\epsilon$  and  $\Delta\beta$ . Similarly,  $\Delta H/\omega$  is the change in  $t_H$  due to horizon scanner misalignments  $\epsilon_H$  and  $\Delta\gamma$ .  $\phi_H/\omega$  is the time required for the satellite to spin through the azimuth angle  $\phi_H$  between the Sun sensor and the horizon scanner.  $2\pi n$ , where  $n = 1, 0, \text{ or } +1$ , is an additional term which is required to make the angle inside the braces fall within the proper range under all conditions.

$A_{d5}$  in Equation (3-50) is computed using the well known dihedral angle expression

$$A_{d5} = \arctan \left\{ \frac{\hat{S} \cdot [\hat{U} \times \hat{D}]}{\hat{U} \cdot \hat{D} - [\hat{D} \cdot \hat{S}][\hat{U} \cdot \hat{S}]} \right\} \quad (3-51)$$

where all vectors are resolved on frame GI.

As noted previously,  $\hat{U}^{GI}$  is provided by ephemeris data and is evaluated at  $t = t_s$ . The elements of  $\hat{S}^{GI}$  are  $s_1$  and  $s_2$ , which are the state vector elements, and  $s_3$  which is obtained via  $s_3 = \pm \sqrt{1 - s_1^2 - s_2^2}$ .  $\hat{D}^{GI}$  is computed using the technique summarized in the Model 4 discussion and delineated in Section 3.8. When computing  $\hat{D}^{GI}$ , the vector  $\hat{R}^{GI}$  is evaluated at  $t = t_H + \Delta t$ .

ORIGINAL PAGE IS  
OF POOR QUALITY

The term  $\Delta s$  in Equation (3-50) is computed using the two spherical triangles associated with the Sun sensor in Figure 3-10. From the upper triangle and the law of sines,

$$\sin E = \sin \epsilon / \sin \beta \quad (3-52a)$$

From the lower triangle and the law of sines,

$$\sin \Delta s = \frac{\sin E \sin (90 - \beta)}{\sin \Lambda} \quad (3-52b)$$

Combining Equations (3-52a) and (3-52b),

$$\sin \Delta s = \frac{\sin \epsilon \cos \beta}{\sin \beta \sin \Lambda} \quad (3-52c)$$

From the lower triangle and the law of cosines of angles,

$$\cos \Lambda = \sin \epsilon \sin \beta \quad (3-52d)$$

Comparing Equations (3-52a) and (3-52d) shows that

$$\Lambda = 90 - \epsilon \quad (3-52e)$$

The final equation for  $\Delta s$  is obtained by substituting Equation (3-52e) into (3-52c).

$$\Delta s = \arcsin (\tan \epsilon \cot \beta) \quad (3-53)$$

**ORIGINAL PAGE IS  
OF POOR QUALITY**

When using Equation (3-53),  $\beta$  is computed as follows:

$$\beta = \text{arc cos} (\hat{U}^{\text{GI}} \cdot \hat{S}^{\text{GI}}) \quad (3-54)$$

The remaining task is to develop the equation for  $\Delta H$  to be used in Equation (3-50). Figure 3-10 shows that this task is geometrically identical to the development just completed for computing  $\Delta s$ . Hence, Equation (3-53) can be employed directly with appropriate changes in variables. The result is

$$\Delta H = \text{arc sin} [\tan \epsilon_H \text{ctn } \gamma] \quad (3-55)$$

where  $\gamma$  is calculated from

$$\gamma = \text{arc cos} [\hat{S}^{\text{GI}} \cdot \hat{D}^{\text{GI}}] \quad (3-56)$$

In summary, the equations for Model 5 are Equations (3-49) through (3-51) and (3-53) through (3-56). A check of these equations shows that Model 5 uses the following elements of  $\underline{X}$ :  $s_1$ ,  $s_2$ ,  $\Delta\gamma$ ,  $\phi_H^I$  or  $\phi_H^O$ ,  $\Delta\rho$ ,  $\omega$ ,  $\epsilon$ ,  $\epsilon_H$ , and  $\Delta t$ .

### 3.6.6 Model 6--Earth Width

Model 6 uses two elements of  $\underline{m}$ : the horizon-in crossing time  $t_{HI}$  and the horizon-out crossing time  $t_{HO}$ . The observable is the difference between these two times. Thus

$$y = t_{HO} - t_{HI} \quad (3-57)$$

ORIGINAL PAGE IS  
OF POOR QUALITY

Figure 3-11 shows the geometry for Model 6. Model 6 is mathematically identical to Model 5 except the Sun time and geometric variables of Model 5 are replaced by the Sun time and geometric variables associated with the other horizon crossing.

The basic  $y_c$  equation for Model 6 can be written with the aid of Figure 3-11. The result is

$$y_c = \frac{1}{\omega} \left[ A_{d6} - \phi_H^O + \phi_H^I + 2\pi n \right] \quad (3-58)$$

Equation (3-58) is analogous to Equation (3-50) for Model 5. Equation (3-55) shows that  $\Delta H_I$  and  $\Delta H_O$  are identical in value. Hence, they cancel one another and do not appear in Equation (3-58).  $\phi_H^I$  and  $\phi_H^O$  are elements  $x_5$   $x_6$  of  $\underline{X}$ .

$A_{d6}$  in the  $y_c$  equation is computed from  $\hat{D}_I^{GI}$ ,  $\hat{S}^{GI}$ , and  $\hat{D}_O^{GI}$  using the usual dihedral angle expression

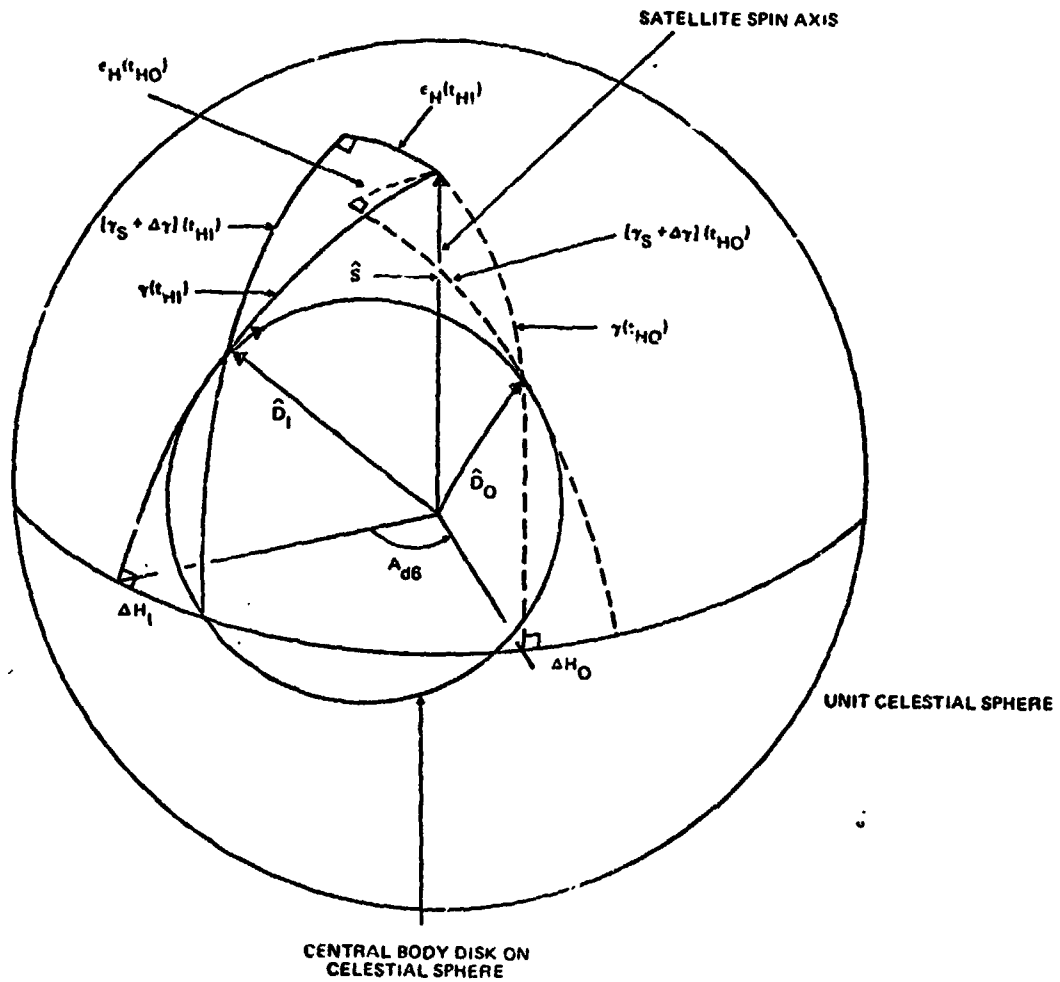
$$A_{d6} = \arctan \left\{ \frac{\hat{S} \cdot [\hat{D}_I \times \hat{D}_O]}{\hat{D}_I \cdot \hat{D}_O - [\hat{D}_I \cdot \hat{S}][\hat{S} \cdot \hat{D}_O]} \right\} \quad (3-59)$$

where all vectors are resolved on frame GI.

$\hat{D}_I^{GI}$  in the above equation is computed by the usual method (see Section 3.8), with  $\hat{R}^{GI}$  and  $\rho_c$  evaluated at  $t_{HI} + \Delta t$ .  $\hat{D}_O^{GI}$  is computed by the same technique with  $\hat{R}^{GI}$  and  $\rho_c$  evaluated at  $t_{HO} + \Delta t$ .

A check of the equations shows that Model 6 contains the following elements of  $\underline{X}$ :  $s_1$ ,  $s_2$ ,  $\Delta\gamma$ ,  $\phi_H^I$  and  $\phi_H^O$ ,  $\Delta\rho$ ,  $\omega$ ,  $\epsilon_H$ , and  $\Delta t$ .

ORIGINAL PAGE IS  
OF POOR QUALITY



NOTE: MOTION OF CENTRAL BODY DISK BETWEEN  $t_{HO}$  AND  $t_{HI}$  NOT SHOWN.

Figure 3-11. Geometry for Model 6--Earth Width Model

### 3.6.7 Model 7--Small Target Model

Model 7 was developed for the translunar phase of the RAE-B mission. In this phase, the angular radius of the central body (the Moon) was sufficiently small that it could be approximated as a point source for attitude determination purposes. The PAS horizon detector angle  $\gamma$  was stepped in a predetermined manner. The telemetered data included the relative times  $(t_H - t_s)$  when the central body horizon was detected and the scanner angles  $\gamma_s$  at these times.

The geometry for Model 7, shown in Figure 3-12, is mathematically similar to Model 1. The observable for Model 7 is the horizon scanner angle  $\gamma_s$ . The observation equation can be derived using Figure 3-12 and the law of cosines of sides. The result is

$$\gamma_s = -\Delta\gamma + \arccos \left[ \frac{\cos \gamma}{\cos \epsilon_H} \right] \quad (3-60)$$

$\cos \gamma$  can be computed as follows:

$$\cos \gamma = -\hat{R}^{GI} \cdot \hat{S}^{GI} \quad (3-61)$$

Therefore, the Model 7 equations for  $y$  and  $y_c$  are

$$y = \gamma_s \quad (3-62a)$$

$$y_c = -\Delta\gamma + \arccos \left[ \frac{-\hat{R}^{GI} \cdot \hat{S}^{GI}}{\cos \epsilon_H} \right] \quad (3-62b)$$

In the RAE-B application,  $\hat{R}^{GI}$  was computed at frame times which were accurate to  $\pm 0.5$  spin period.

ORIGINAL PAGE IS  
OF POOR QUALITY

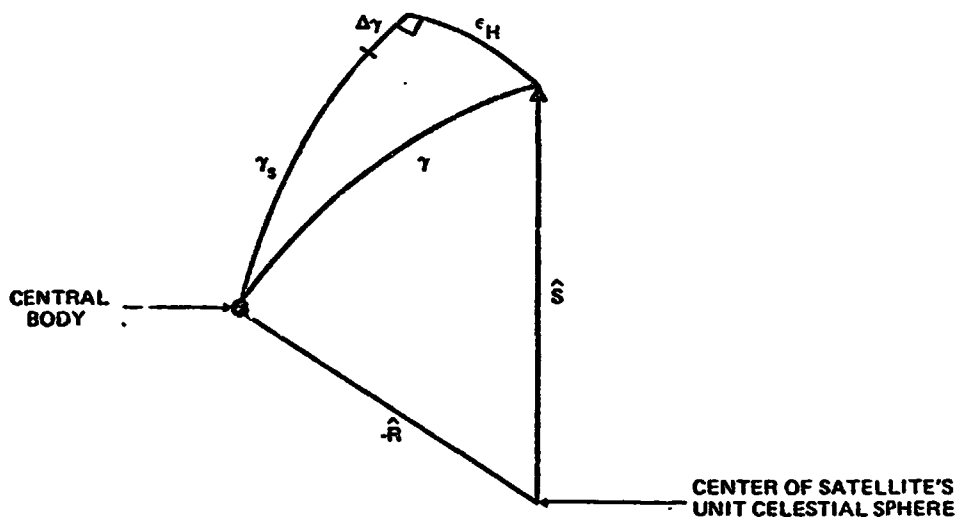


Figure 3-12. Geometry for Model 7--Small Target Model

**ORIGINAL PAGE IS  
OF POOR QUALITY**

Equation (3-62) shows that the following elements of  $\underline{x}$  appeared in Model 7:

$s_1$ ,  $s_2$ ,  $\Delta\gamma$ , and  $\epsilon_{II}$ .

**3.6.8 Model 8--Sun to Earth Mid-Scan Dihedral Angle Model**

Model 8 originally was designed for the RAE-B mission and, like Model 7, approximated the central body as a point. However, Model 8 has recently been modified to eliminate the restriction that the central body must be small. The present discussion covers only the new version of Model 8.

Model 8 uses three elements of  $\underline{m}$ : the Sun sighting time  $t_s$  and the two horizon crossing times  $t_{HI}$  and  $t_{HO}$ . The geometry for Model 8 is shown in Figure 3-13. The Model 8 observable is the time interval between  $t_s$  and the midtime between the horizon-in crossing and the horizon-out crossing  $0.5 [t_{HI} + t_{HO}]$ . Thus

$$y = 0.5 [t_{HI} + t_{HO}] - t_s \quad (3-63)$$

Model 8 is mathematically similar to Model 5 except  $t_{HI}$  and  $t_{HO}$  of Model 5 are replaced in Model 8 by  $0.5 [t_{HI} + t_{HO}]$ . Also  $\hat{D}_I$ ,  $\hat{D}_O$  of Model 5 are used for the Model 8 dihedral angle ( $A_d$ ) computation. The equation for the model observation  $y_c$  can be obtained with the aid of Figure 3-13 or by analogy to the corresponding Model 5 result--Equation (3-50). It is

$$y_c = \frac{1}{\omega} \left[ A_{d8} - 0.5 \left( \phi_{HI}^O + \phi_{HI}^I \right) - \Delta s + \Delta H + 2\pi n \right] \quad (3-64)$$

In Equation (3-64),  $\phi_{II}^O$  and  $\phi_{II}^I$  are the horizon detector azimuth angle elements  $x_5$  and  $x_6$ . Model 8 thus employs the average azimuth angle of the horizon detector.

ORIGINAL PAGE #  
OF POOR QUALITY

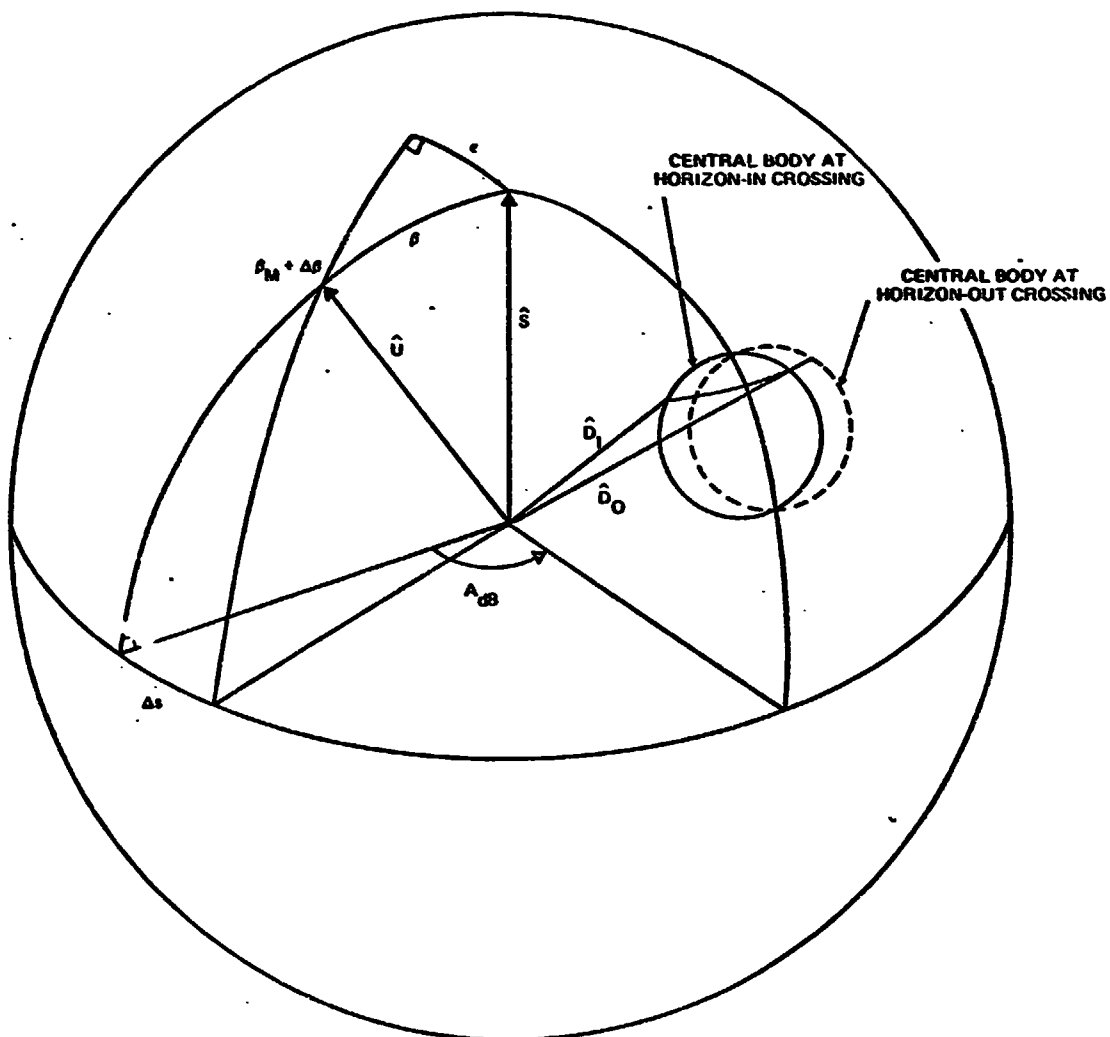


Figure 3-13. Geometry for Model 8--Sun to Earth  
Mid-Scan Dihedral Angle Model

ORIGINAL PAGE IS  
OF POOR QUALITY

The dihedral angle  $A_{d8}$  is shown in Figure 3-13. Its equation can be obtained by using the Model 5 result--Equation (3-51).

In fact

$$A_{d8} = 0.5 \left[ A_{d5} \text{ (in)} + A_{d5} \text{ (out)} \right]$$

and

$$y_c = 0.5 \left[ y_c \text{ (Model 5, in)} + y_c \text{ (Model 5, out)} \right]$$

$$A_{d8} = 0.5 \left[ \text{arc tan} \left\{ \frac{s \cdot [\hat{U} \times \hat{D}_I]}{\hat{U} \cdot \hat{D}_I - [\hat{D}_I \cdot \hat{S}][\hat{U} \cdot \hat{S}]} \right\} + \text{arc tan} \left\{ \frac{\hat{S} \cdot [\hat{U} \times \hat{D}_O]}{\hat{U} \cdot \hat{D}_O - [\hat{D}_O \cdot \hat{S}][\hat{U} \cdot \hat{S}]} \right\} \right] \quad (3-65)$$

where all vectors are resolved on frame GI.  $\hat{U}^{GI}$  is computed at  $t = t_s$ .

$\Delta s$  and  $\Delta H$  were defined previously (see Figure 3-10 and Equations (3-53) and (3-55)). For  $\Delta s$ ,

$$\Delta s = \text{arc sin} (\tan \epsilon \text{ ctn } \beta) \quad (3-66a)$$

where  $\beta$  is computed from

$$\beta = \text{arc cos} (\hat{U}^{GI} \cdot \hat{S}^{GI}) \quad (3-66b)$$

ORIGINAL PAGE IS  
OF POOR QUALITY

For  $\Delta H$ ,

$$\Delta H = \text{arc sin} [\tan \epsilon_H \text{ctn } \gamma] \quad (3-67a)$$

where  $\gamma$  is computed from

$$\gamma = \text{arc cos} [\cos \epsilon_H \cos (\gamma_s + \Delta\gamma)] \quad (3-67b)$$

In summary, Model 8 employs Equations (3-63) through (3-67). A check of the equations shows that Model 8 uses the following elements of  $\underline{X}$ :  $s_1$ ,  $s_2$ ,  $\epsilon_H$ ,  $\phi_H^O$ ,  $\phi_H^I$ ,  $\Delta\rho$ ,  $\omega$ ,  $\Delta\gamma$ ,  $\epsilon$ , and  $\Delta t$ .

ORIGINAL PAGE IS  
OF POOR QUALITY

### 3.7 COMPUTATION OF CENTRAL BODY ANGULAR RADIUS $\rho_c$

OABIAS uses the following equation to compute the angular radius  $\rho$  of the central body on the unit celestial sphere as seen from the satellite:

$$\rho = \rho_c + \Delta\rho \quad (3-68)$$

where  $\rho_c$  is computed deterministically using orbit information and  $\Delta\rho$  is a bias element which is included in the state vector  $\underline{X}$ .

OABIAS provides two methods for computing  $\rho_c$ . The first assumes that the central body is spherical; i. e., central body oblateness is omitted. Figure 3-14 shows the geometry for this case. For notational simplicity, the magnitudes of vectors will be referred to in this discussion as they are designated in Figure 3-14. By definition,  $\rho_c$  is the angle between the vector to the center of the central body  $-\vec{R}$  and the horizon sensor line-of-sight vector  $\vec{L}$  at a horizon crossing. At horizon crossings,  $\vec{L}$  is tangent to the central body surface. Hence, for a spherical central body,  $\vec{L}$  is perpendicular to the radius vector  $\vec{R}_e$  shown in the figure. By simple trigonometry,

$$\rho_c = \arcsin \left[ \frac{R_e + h}{R} \right] \quad (3-69)$$

where  $0 \text{ degree} \leq \rho_c \leq 90 \text{ degrees}$ ,  $R_e$  is the nominal radius of the central body, and  $h$  is a user-supplied correction.  $R$  is obtained from orbital data.

The second  $\rho_c$  computation method allows oblateness to be taken into account when the central body is the Earth. The mathematical model is an approximate one which uses Equation (3-69) with  $R_e$  redefined to be the geocentric radius

ORIGINAL PAGE 13  
 OF POOR QUALITY

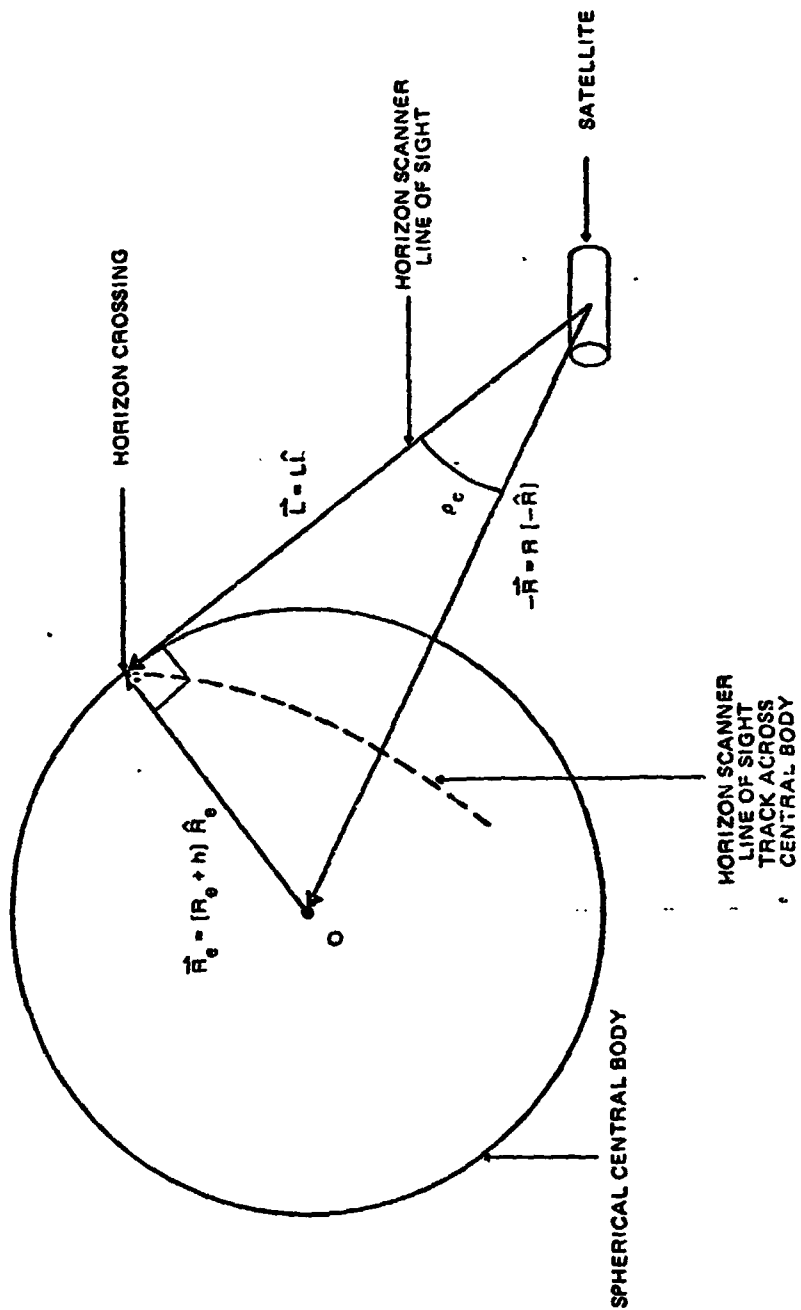


Figure 3-14.  $\rho_c$  Computation Geometry--Spherical Central Body

ORIGINAL PAGE IS  
OF POOR QUALITY

of Earth at the horizon crossing point.  $R_e$  is computed by the following equation:

$$R_e \text{ (kilometers)} = 6378.16 \left[ 1 - c_1 s^2 \lambda + c_2 s \lambda \right] + h \quad (3-70)$$

where  $\lambda$  is the geocentric latitude and  $c_1$  and  $c_2$  are constants which default to 0.0033528 and 0.0, respectively.  $c_2 s \lambda$  permits the user to include seasonal variations in the effective thickness of the atmosphere.

In order to compute  $R_e$  with the oblate Earth model, the location of the horizon crossing on the Earth's surface must be known. However, the computation of this location requires knowledge of the value of  $R_e$ . Because the equations of the model are highly nonlinear, an iterative procedure is needed. The main steps employed by OABIAS are summarized below utilizing the notation in Figure 3-14.

1. The latitude  $\lambda_0$  of the subsatellite point is computed as follows:

$$\lambda_0 = \arcsin \left[ -\hat{R}^{GI'} \cdot \hat{z}_{GI'} \right]$$

$-\hat{R}^{GI'}$  is obtained from orbital data, and because  $\hat{z}_{GI'}$  is the unit vector along the z-axis of frame  $GI'$ ,  $\hat{z}_{GI'} = [001]^T$ . It should be noted that if a 45-degree rotation has been made, the vectors must be retransformed to frame  $GI$ .  $\lambda_0$  serves as the initial estimate of the latitude of the horizon crossing point.

2.  $R_e$  is computed using Equation (3-70). The latitude  $\lambda$  obtained in step 1 is used in the first pass.
3.  $\rho_c$  is computed using Equation (3-69) with  $R_e$  from step 2.  $R$  is obtained from orbital data and  $h$  is supplied by the user.

ORIGINAL PAGE  
OF POOR QUALITY

4. The unit horizon crossing vector  $\hat{L}^{GI'}$  is computed in subroutine CONES using inputs  $-\hat{R}^{GI'}$  (from orbital data),  $\hat{S}^{GI'}$  and  $\gamma$  (from  $X$  and  $\gamma_s$ ), and  $\rho_c$  (from step 3). CONES returns two solutions corresponding to Earth-in and Earth-out crossings. The correct one is established with the aid of subroutine PHASE.
5.  $L$  is computed using  $L = R \cos \rho_c$ .
6. The Earth radius vector to the horizon crossing point  $\vec{R}_e^{GI'}$  is computed using

$$\vec{R}_e^{GI'} = \vec{R}^{GI'} + L \hat{L}^{GI'}$$

where  $\vec{R}^{GI'}$  is obtained from orbit data,  $L$  from the computations in step 5, and  $\hat{L}^{GI'}$  from step 4.

7.  $\vec{R}_e^{GI'}$  is now normalized to yield  $\hat{R}_e^{GI'}$ .
8. The latitude  $\lambda$  of the horizon crossing is computed using

$$\lambda = \arcsin \left[ -\hat{R}_e^{GI'} \cdot \hat{z}^{GI'} \right]$$

9. The program returns to step 2 and continues in a loop until the change in  $\rho_c$  computed in step 3 is less than 0.0001 radians or until the maximum number of iterations (10) is reached.

In system testing, it has been found that convergence usually occurs in one or two iterations.

### 3.8 COMPUTATION OF HORIZON CROSSING VECTOR $\hat{D}$

Models 4, 5, and 6 require that the following set of nonlinear algebraic equations be solved for  $\hat{D}^{GI}$ :

$$\hat{S}^{GI} \cdot \hat{D}^{GI} = \cos(\gamma_s + \Delta\gamma) \cos \epsilon_H \quad (3-71a)$$

$$\hat{R}^{GI} \cdot \hat{D}^{GI} = -\cos(\rho_c + \Delta\rho) \quad (3-71b)$$

$$\hat{D}^{GI} \cdot \hat{D}^{GI} = 1 \quad (3-71c)$$

The purpose of this section is to discuss the algorithm employed to solve this set. The variables in the above equations were defined in Figure 3-10. Super-script GI signifies that OABIAS uses GI coordinates for the calculation. Let the components of  $\hat{S}^{GI}$ ,  $\hat{D}^{GI}$  and  $\hat{R}^{GI}$  be designated by lower case letters. Then Equation (3-71) can be rearranged into the following form:

$$\begin{bmatrix} s_1 & r_2 \\ r_1 & r_2 \end{bmatrix} \begin{Bmatrix} d_1 \\ d_2 \end{Bmatrix} = \begin{Bmatrix} \cos(\gamma_s + \Delta\gamma) \cos \epsilon_H - s_3 d_3 \\ -\cos(\rho_c + \Delta\rho) - r_3 d_3 \end{Bmatrix} \quad (3-72a)$$

$$d_1^2 + d_2^2 + d_3^2 = 1 \quad (3-72b)$$

Assuming that the determinant (Det) of the  $2 \times 2$  coefficient matrix in Equation (3-72a) is not zero, Equation (3-72a) can be rearranged into the following form:

$$\begin{Bmatrix} d_1 \\ d_2 \end{Bmatrix} = \frac{1}{\text{Det}} \begin{bmatrix} r_2 & -s_2 \\ -r_1 & s_1 \end{bmatrix} \begin{Bmatrix} \cos(\gamma_s + \Delta\gamma) \cos \epsilon_H - s_3 d_3 \\ -\cos(\rho_c + \Delta\rho) - r_3 d_3 \end{Bmatrix} \quad (3-73)$$

$2 \times 2$                        $2 \times 1$

ORIGINAL PAGE IS  
OF POOR QUALITY

where

$$\text{Det} = s_1 r_2 - s_2 r_1 \quad (3-74)$$

The condition  $s_1 r_2 - s_2 r_1 = 0$  occurs when the two vectors formed by projecting  $\hat{S}$  and  $\hat{R}$  onto plane  $\hat{X} - \hat{Y}$  of frame GI are colinear. The problem can be circumvented (except in the unsolvable degenerate case of  $\hat{S} = \pm \hat{R}$ ) by permuting the subscripts of the  $\hat{S}^{GI}$ ,  $\hat{D}^{GI}$ , and  $\hat{R}^{GI}$  components.

Equation (3-74) can be put in the form

$$d_1 = p_1 d_3 + q_1 \quad (3-75a)$$

$$d_2 = p_2 d_3 + q_2 \quad (3-75b)$$

where

$$p_1 = \frac{1}{\text{Det}} [s_2 r_3 - s_3 r_2] \quad (3-75c)$$

$$p_2 = \frac{1}{\text{Det}} [s_3 r_1 - s_1 r_3] \quad (3-75d)$$

$$q_1 = \frac{1}{\text{Det}} [r_2 \cos(\gamma_s + \Delta\gamma) \cos \epsilon_H + s_2 \cos(\rho_c + \Delta\rho)] \quad (3-75e)$$

$$q_2 = \frac{-1}{\text{Det}} [r_1 \cos(\gamma_s + \Delta\gamma) \cos \epsilon_H + s_1 \cos(\rho_c + \Delta\rho)] \quad (3-75f)$$

Substituting Equations (3-75a) and (3-75b) into (3-72b) and rearranging yields

$$a_1 d_3^2 + 2 a_2 d_3 + a_3 = 0 \quad (3-76)$$

ORIGINAL PAGE IS  
OF POOR QUALITY

where

$$a_1 = 1 + p_1^2 + p_2^2 \quad (3-77a)$$

$$a_2 = p_1 q_1 + p_2 q_2 \quad (3-77b)$$

$$a_3 = q_1^2 + q_2^2 - 1 \quad (3-77c)$$

Solving Equation (3-76),

$$d_3 = -\frac{1}{a_1} \left[ -a_2 \pm \sqrt{a_2^2 - a_1 a_3} \right] \quad (3-78)$$

Equations (3-75), (3-77), and (3-78) constitute the basic algorithm for solving Equation (3-71) for the components  $d_1$ ,  $d_2$ , and  $d_3$  of  $\hat{D}^{GI}$ . However, the problem of resolving the sign ambiguity in Equation (3-78) still remains.

Geometric considerations show that one sign signifies a horizon-in crossing  $t_{HI}$  and the other, a horizon-out crossing  $t_{HO}$ . However, mere knowledge of whether a  $t_{HI}$  condition or a  $t_{HO}$  condition is being processed is not, by itself, sufficient to resolve the ambiguity. Therefore, OBIAS first computes the horizon crossing vector  $(\hat{D}_+^{GI})$  using the plus sign in Equation (3-78). The subroutine PHASE then computes the dihedral angle  $\nu_+$  from the  $\hat{D}_+ - \hat{S}$  plane to the  $\hat{D}_+ - [-\hat{R}]$  plane.  $\nu$  is shown for both the in-crossing and the out-crossing cases in Figure 3-15. The dihedral angle computed by PHASE is measured in the conventional right hand sense and will be in the range from 0 degree to 360 degrees. Since the angular radius of the Earth is always less than a right angle,  $\nu$  always lie in the range from 0 degree to 180 degrees for an out-crossing. For an in-crossing,  $\nu$  always will be in the range from 180 degrees to 360 degrees. Hence, the sign ambiguity in Equation (3-78) can

ORIGINAL PAGE IS  
OF POOR QUALITY

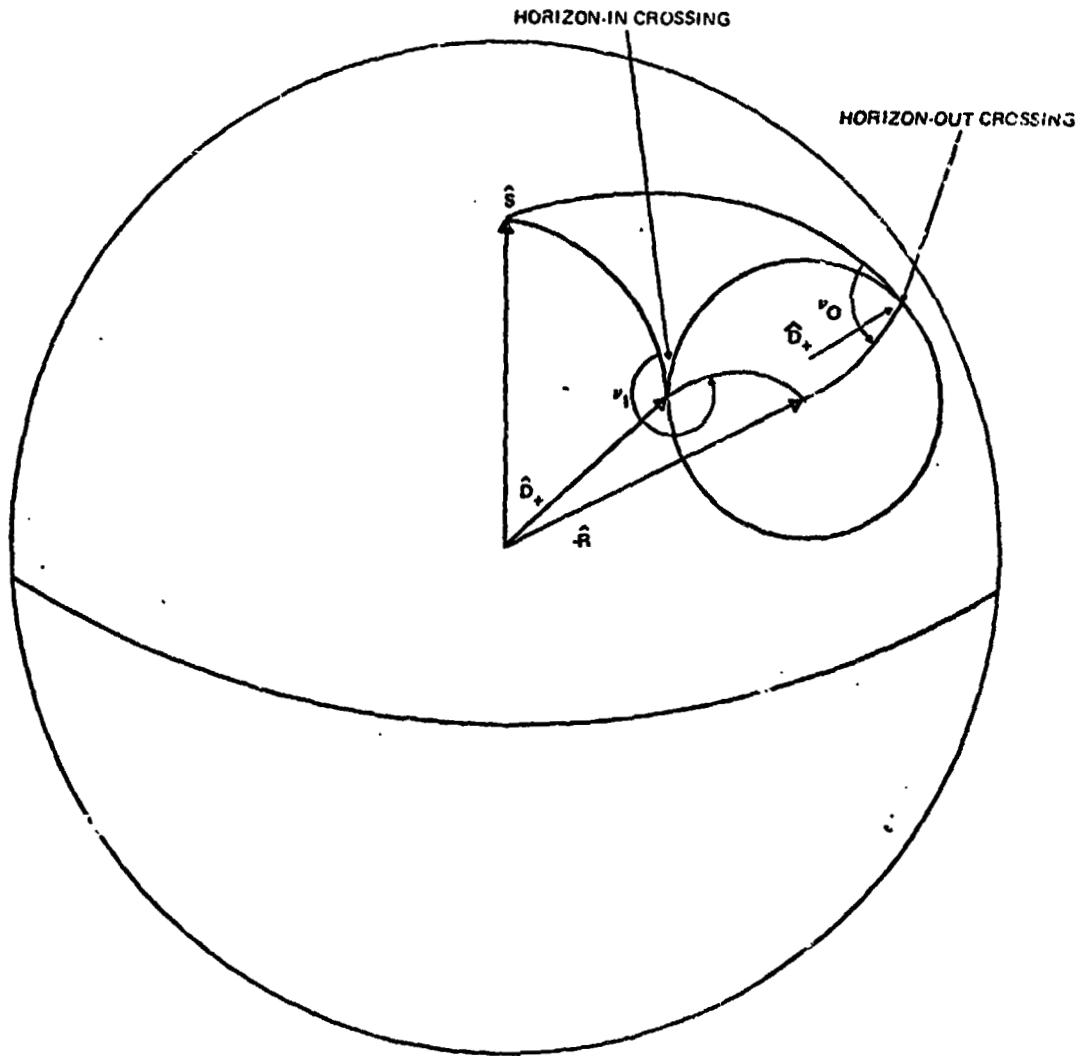


Figure 3-15. Resolution of Sign Ambiguity of  
Horizon Crossing Vector  $\hat{D}$

ORIGINAL PAGE IS  
OF POOR QUALITY

be resolved by checking whether  $\nu_+$  is within the correct range. The exact criteria is as follows:

<u><math>\nu_+</math> Value (degrees)</u>	<u>Horizon Crossing</u>	<u>Correct Sign</u>
$0 \leq \nu_+ \leq 180$	in	-
	out	+
$180 \leq \nu_+ \leq 360$	in	+
	out	-

A check of the  $\hat{D}$  computation equations shows that the following elements of  $\underline{X}$  are used:  $s_1$ ,  $s_2$ ,  $\Delta\gamma$ ,  $\epsilon_H$ , and  $\Delta\sigma$ . The element  $\Delta t$  of  $\underline{X}$  also appears implicitly through  $\hat{R}^{GI}$ .

### 3.9 WEIGHTING FACTORS OF THE OBSERVATION MODELS

Each time one of the eight observation models in OABIAS processes an observation  $j$ , the preliminary operations include the calculation of a weighting factor  $w_j$ . Each model has its own distinct equation for computing  $w_j$ .

These calculations use the following user-supplied inputs:

1.  $\sigma_\beta$ --The square root of the variance of the error in the Sun angle measurements (degrees)
2.  $\sigma_s$ --The square root of the variance of the error in the Sun sighting time measurements (seconds)
3.  $\sigma_H$ --The square root of the variance of the error in the horizon crossing time measurements (seconds)
4.  $\sigma_\gamma$ --The square root of the variance of the error in the RAE-B PAS angle (degrees)

The optimum technique for establishing the observation weighting factors  $w_j$  was discussed, in general terms, in Section 3.3.3. Ideally, each  $w_j$  should be the inverse of the variance of the error in the observation which is to be processed.<sup>1</sup> This conclusion assumes that the errors in the observations are statistically uncorrelated. The final result of Section 3.3.3 was Equation (3-11c).

With modification in notation to tailor it to the present discussion, this equation can be written as

---

<sup>1</sup>CSC reports on attitude estimation have been inconsistent in the use of the term "weighting factor" and the corresponding symbols  $W$  or  $w$ . The actual OABIAS coding uses the inverses of the weighting factors of the present discussion and designates them by  $W(\ )$ .

ORIGINAL PAGE IS  
OF POOR QUALITY

$$\begin{aligned} (1/w_j^*) = \sigma_{z_j}^2 &= \left( \frac{\partial z_j}{\partial \beta} \right)^2 \sigma_\beta^2 + \left( \frac{\partial z_j}{\partial t_s} \right)^2 \sigma_s^2 \\ &+ \left[ \left( \frac{\partial z_j}{\partial t_{HI}} \right)^2 + \left( \frac{\partial z_j}{\partial t_{HO}} \right)^2 \right] \sigma_H^2 + \left( \frac{\partial z_j}{\partial \gamma_s} \right)^2 \sigma_\gamma^2 \end{aligned} \quad (3-79)$$

where  $z_j$  signifies the residual  $(y_j - y_{cj})$  of observation  $j$  and  $w_j^*$  signifies the optimum weighting factor. The third term on the right side involves the assumption that the statistics of the error in the horizon crossing time measurements are identical for in-crossings and out-crossings.

The values of the partial derivatives in Equation (3-79) depend upon the model being processed. For example, with Model 1 (the Sun angle model) the basic measurement  $\beta$  enters  $z$  through  $y$ ;  $y = \beta$ . Hence,  $\partial z / \partial \beta = \partial y / \partial \beta = 1$  and the remaining partials are zero. With Model 8 (the Sun to Earth mid-scan dihedral angle model),  $y = 0.5 [t_{HI} + t_{HO}] - t_s$ . Hence,  $\partial z / \partial \beta = 0$ ,  $\partial z / \partial t_{HI} = \partial z / \partial t_{HO} = 0.5$ , and  $\partial z / \partial t_s = -1$ .

A modification to Equation (3-79) is convenient for those models (2, 3, and 4) in which the measurement-dependency enters the residual  $z_j$  via the rotation angle  $\phi$  in the  $y_c$  computation. For these three models, the following is adequate:

$$\frac{\partial z}{\partial t_{( )}} = - \frac{\partial y_c}{\partial t_{( )}} = - \omega \frac{\partial y_c}{\partial \psi_o}$$

where ( ) signifies  $s$ ,  $HI$ , or  $HO$ .

Then, Equation (3-79) becomes

$$\begin{aligned}
 (1/w_j^*) = & 0 \cdot \sigma_\beta^2 + 0 \cdot \sigma_\gamma^2 + \omega^2 \left( \frac{\partial y_c}{\partial \psi_o} \right)^2 \sigma_s^2 \\
 & + \omega^2 \left[ \left( \frac{\partial y_c}{\partial \psi_o} \right)^2_{\text{in-crossing}} + \left( \frac{\partial y_c}{\partial \psi_o} \right)^2_{\text{out-crossing}} \right] \sigma_{II}^2
 \end{aligned}
 \tag{3-80}$$

The equations for the partial derivatives  $\partial y_c / \partial \psi_o$  are given in Appendix A.

OBIAS has used two methods to compute the weighting factors; both are available in the current version (see Table 3-2). In principle, because Method 2 yields weighting factors which are in closer agreement with the theoretical ideal  $w^*$ , it should be superior to Method 1. This can be seen by a careful comparison of Table 3-2 with Equation (3-79) or, for Models 2, 3, and 4, Equation (3-80). Testing also has shown that Method 2 yields better results.

The question of resolution effects in the weighting factor computation now will be discussed. The conventional statistical filtering theory which was implicitly used in the preceding development assumes that the errors in the input measurements can be modeled statistically as white noise. With digital systems, the resolution error due to finite word length of the sensor or processing techniques is sometimes significant with respect to this type of noise; in some cases, may completely dominate it. On attitude determination systems, the resolution of digital Sun sensors, in particular, can be sufficiently great that difficult questions are raised on how to handle or weight the data. It is well known that errors due to resolution can be treated as white noise when the signal is sufficiently variable that it rarely stays in the same resolution cell on successive measurements. The near-constancy of the Sun angle seen by

ORIGINAL PAGE IS  
OF POOR QUALITY

Table 3-2. Weighting Factor Equation Used in OABIAS

Model	Observable	Weighting Factor ( $\omega$ ) Equation	
		Method I	Method II
1	$\beta$	$\left[ \left( \frac{\sigma_\rho}{57.296} \right)^2 \frac{1}{8} \right]^{-1}$	$\left[ \left( \frac{\sigma_f}{57.296} \right)^2 \right]^{-1}$
2	$\hat{U} \cdot \hat{N}$	$\left[ (\omega \sigma_s)^2 \right]^{-1}$	$\left[ \left( \omega \left\{ \frac{\partial y_c}{\partial \psi_o} \right\} \sigma_s \right)^2 \right]^{-1}$
3	$\cos \rho + \hat{R} \cdot \hat{L}$	$\left[ (\omega \sigma_H)^2 \right]^{-1}$	$\left[ \left( \omega \left\{ \frac{\partial y_c}{\partial \psi_o} \right\} \sigma_H \right)^2 \right]^{-1}$
4	$\hat{D} \cdot \hat{N}_H$	$\left[ (\omega \sigma_H)^2 \right]^{-1}$	$\left[ \left( \omega \left\{ \frac{\partial y_c}{\partial \psi_o} \right\} \sigma_H \right)^2 \right]^{-1}$
5	$t_H - t_s$	$\left[ (\sigma_s)^2 + (\sigma_H)^2 \right]^{-1}$	$\left[ (\sigma_s)^2 + (\sigma_H)^2 \right]^{-1}$
6	$t_{HO} - t_{HI}$	$\left[ (\sigma_H)^2 \right]^{-1}$	$\left[ 2 (\sigma_H)^2 \right]^{-1}$
7	$\gamma_s$	$\left[ \left( \frac{\sigma_\gamma}{57.296} \right)^2 \right]^{-1}$	$\left[ \left( \frac{\sigma_\gamma}{57.296} \right)^2 \right]^{-1}$
8	$0.5 (t_{HI} + t_{HO}) - t_s$	$\left[ (\sigma_s)^2 + (\sigma_H)^2 \right]^{-1}$	$\left[ (\sigma_s)^2 + .5 (\sigma_H)^2 \right]^{-1}$

NOTE 1: See Appendix A for the equations for the partial derivatives  $\partial y_c / \partial \psi_o$ .

NOTE 2: The terms within the brackets have the dimensions of variance.

**ORIGINAL PAGE IS  
OF POOR QUALITY**

spin stabilized satellites, however, makes this assumption difficult or impossible to justify in processing the data from the digital Sun sensor.

The question of how, in theory, the resolution phenomena can best be handled has not been addressed in this document. The equations in Table 3-2 assume that resolution is negligible and, therefore, that the errors in the Sun angle, Sun sighting times, and horizon crossing times can be modeled as white noises. The square roots of the variances of these noises are  $\sigma_\beta$ ,  $\sigma_s$ ,  $\sigma_H$ , and  $\sigma_\gamma$ . The single exception is  $\sigma_\rho$  in Method I which is modeled as the resolution cell width.

ORIGINAL PAGE IS  
OF POOR QUALITY

### 3.10 SUMMARY OF SECTION 3

The elements of the state vector  $\underline{X}$  used by OABIAS are as follows:

$x_1(s_1)$	component of spacecraft's unit spin vector ( $\hat{S}$ ) along the x-axis of frame GI
$x_2(s_2)$	component of $\hat{S}$ along the y-axis of frame GI
$x_3(\phi_0)$	initial phase angle of the spacecraft in its spin cycle
$x_4(\Delta\gamma)$	bias on horizon sensor mounting angle
$x_5(\phi_H^I)$	azimuth of the horizon sensor relative to the Sun sensor at horizon-in crossing
$x_6(\phi_H^O)$	azimuth of the horizon sensor relative to the Sun sensor at horizon-out crossing
$x_7(\Delta\rho)$	bias on the angular radius of the central body
$x_8(\Delta\beta)$	bias on the Sun angle measurement
$x_9(\omega)$	spin rate
$x_{10}(\epsilon)$	tilt of Sun sensor reference slit plane
$x_{11}(\epsilon_H)$	PAS horizon detector plane tilt (RAE-B)
$x_{12}(\Delta t)$	timing bias in spacecraft orbit data

A summary of each of the eight OABIAS observation models follows.

#### Model 1--Sun Angle Model

$$y = \beta_M$$

$$y_c = -\Delta\beta + \arccos \left( \frac{\hat{U}^{GI} \cdot \hat{S}^{GI}}{\cos \epsilon} \right)$$

where  $\beta_M$  = measured Sun angle

$\hat{U}$  = unit Sun vector

$\hat{S}$  = unit spin axis vector

GI = resolution on frame GI

Model 2--Sun Sighting Time Model

$$y = 0$$

$$y_c = \hat{U}^{GI} \cdot \hat{N}_S^{GI}$$

$$\hat{N}_S^{GI} = \begin{bmatrix} a_{21} & a_{31} \\ a_{22} & a_{32} \\ a_{23} & a_{33} \end{bmatrix} \begin{matrix} (\cos \epsilon) \\ (\sin \epsilon) \end{matrix}$$

where  $\hat{N}_S$  = unit vector perpendicular to Sun sensor reference slit plane

$a_{ij}$  = elements of transformation matrix A from frame GI to frame SC

Model 3--Nadir Vector Projection Model

$$y = 0$$

$$y_c = \cos(\rho_c + \Delta\rho) + \hat{R}^{GI} \cdot \hat{L}^{GI}$$

$$\hat{L}^{GI} = A^T B_H T_\gamma(\gamma)^T \hat{L}^H$$

$$\hat{L}^H = [001]^T$$

where  $\rho_c$  = computed angular radius of the central body

$\hat{R}$  = unit vector from central body toward spacecraft

$\hat{L}$  = unit vector along horizon detector line of sight

ORIGINAL PAGE IS  
OF POOR QUALITY

$B_{II}$  = transformation matrix from frame II (Figure 3-1) to frame SC

$$T_{y(y')}^T = \begin{bmatrix} \cos \gamma_s & 0 & \sin \gamma_s \\ 0 & 1 & 0 \\ -\sin \gamma_s & 0 & \cos \gamma_s \end{bmatrix}$$

$\gamma_s$  = nominal mounting angle of horizon detector relative to spin axis

Model 4--Horizon Crossing Time Model

$$y = 0$$

$$y_c = \hat{N}_H^{GI} \cdot \hat{D}^{GI}$$

$$\hat{N}_H^{GI} = A^T B_H \hat{N}_H^{H'}$$

$$\hat{N}_H^{H'} = [001]^T$$

where  $\hat{N}_H$  = unit vector perpendicular to PAS plane

$\hat{D}^{GI}$  = unit vector on central body perimeter at horizon crossing point

Model 5--Sun to Earth-In and Sun to Earth-Out Dihedral Angle Model

$$y = t_H - t_s$$

$$y_c = \frac{1}{\omega} \{A_{d5} - \Delta s + \Delta II - \phi_H + 2\pi n\}$$

$$A_{d5} = \arctan \left\{ \frac{\hat{S} \cdot [\hat{U} \times \hat{D}]}{\hat{U} \cdot \hat{D} - [\hat{U} \cdot \hat{S}][\hat{D} \cdot \hat{S}]} \right\}$$

$$\Delta s = \arcsin [\tan \epsilon \cot \beta]$$

$$\beta = \arccos [\hat{U} \cdot \hat{S}]$$

$$\Delta H = \arcsin [\tan \epsilon_{HI} \operatorname{ctn} \gamma]$$

$$\gamma = \arccos [\hat{S} \cdot \hat{D}]$$

where  $t_{HI}$  = measured horizon crossing time

$t_s$  = measured Sun crossing time

$A_{d5}$  = dihedral angle between spin axis/Sunline plane and spin axis/  
horizon vector plane (Frame GI resolution is used with all vectors)

$\Delta s$  = correction due to tilt of Sun sensor reference slit plane

$\Delta H$  = correction due to tilt of PAS horizon detector plane

NOTE:  $t_s$  and  $t_{HI}$  are measured by different sensors separated by dihedral  
angle  $\phi_H$ .

Model 6--Earth Width Model

$$y = t_{HO} - t_{HI}$$

$$y_c = \frac{1}{\omega} [A_{d6} - \phi_H^O + \phi_H^I + 2\pi n]$$

$$A_{d6} = \arctan \left[ \frac{\hat{S} \cdot (\hat{D}_I \times \hat{D}_O)}{\hat{D}_I \cdot \hat{D}_O - (\hat{S} \cdot \hat{D}_I)(\hat{S} \cdot \hat{D}_O)} \right]$$

where  $t_{HI}$  = measured horizon-in crossing time

$t_{HO}$  = measured horizon-out crossing time

$A_{d6}$  = dihedral angle between spin axis/horizon-in plane and spin axis/  
horizon-out plane (Frame GI resolution is used with all vectors)

$\hat{D}_I$  = horizon-in crossing unit vector

$\hat{D}_O$  = horizon-out crossing unit vector

Model 7--Small Target Model

$$y = \gamma_s$$

$$y_c = -\Delta\gamma + \arccos \left[ \frac{\hat{R}^{GI} \cdot \hat{S}^{GI}}{\cos \epsilon_H} \right]$$

where  $\gamma_s$  = measured PAS horizon detector angle

Model 8--Sun to Earth Mid-Scan Dihedral Angle Model

$$y = 0.5 [t_{HI} + t_{HO}] - t_s$$

$$y_c = \frac{1}{\omega} \left[ A_{d8} - 0.5 \{ \phi_H^O + \phi_H^I \} - \Delta s + \Delta H + n2\pi \right]$$

$$A_{d8} = 0.5 \left[ \arctan \left\{ \frac{\hat{S} \cdot [\hat{U} \times \hat{D}_I]}{\hat{U} \cdot \hat{D}_I - [\hat{D}_I \cdot \hat{S}][\hat{U} \cdot \hat{S}]} \right\} + \arctan \left\{ \frac{\hat{S} \cdot [\hat{U} \times \hat{D}_O]}{\hat{U} \cdot \hat{D}_O - [\hat{D}_O \cdot \hat{S}][\hat{U} \cdot \hat{S}]} \right\} \right]$$

$$\Delta s = \arcsin (\tan \epsilon \operatorname{ctn} \beta)$$

$$\beta = \arccos (\mathbf{U} \cdot \mathbf{S})$$

$$\Delta H = \arcsin (\tan \epsilon_H \operatorname{ctn} \gamma)$$

$$\gamma = \arccos (\cos \epsilon_H \cos (\gamma_s + \Delta\gamma))$$

where frame GI resolution is used with all vectors.

ORIGINAL PAGE IS  
OF POOR QUALITY

Models 2, 3, and 4 require the transformation matrix A whose components are:

$$A = \frac{1}{\sqrt{s_1^2 + s_2^2}} \begin{bmatrix} s_1 s_3 c\phi - s_2 s\phi & s_2 s_3 c\phi + s_1 s\phi & -\left[ \frac{2}{s_1 + s_2} \right] c\phi \\ -s_1 s_3 s\phi - s_2 c\phi & -s_2 s_3 s\phi + s_1 c\phi & \left[ \frac{2}{s_1 + s_2} \right] s\phi \\ s_1 \sqrt{\frac{2}{s_1 + s_2}} & s_2 \sqrt{\frac{2}{s_1 + s_2}} & s_3 \sqrt{\frac{2}{s_1 + s_2}} \end{bmatrix}$$

where  $s_3 = \pm \sqrt{1 - s_1^2 - s_2^2}$   
 $\phi = \phi_0 + \omega \{t - t_0\}$

and c and s signify cosine and sine, respectively.

The equation for the transformation matrix  $B_H$  shown in Models 3 and 4 is

$$B_H = \begin{bmatrix} c\Delta\gamma c\phi_H - s\Delta\gamma s\epsilon_H s\phi_H & -c\epsilon_H s\phi_H & s\Delta\gamma c\phi_H + c\Delta\gamma s\epsilon_H s\phi_H \\ c\Delta\gamma s\phi_H + s\Delta\gamma s\epsilon_H c\phi_H & c\epsilon_H c\phi_H & s\Delta\gamma s\phi_H - c\Delta\gamma s\epsilon_H c\phi_H \\ -s\Delta\gamma c\epsilon_H & s\epsilon_H & c\Delta\gamma c\epsilon_H \end{bmatrix}$$

$\hat{D}^{GI}$  (used for Models 4, 5, 6, and 8) is computed by solving the following set of equations:

$$\hat{S}^{GI} \cdot \hat{D}^{GI} = \cos(\gamma_s + \Delta\gamma) \cos \epsilon_H$$

$$\hat{R}^{GI} \cdot \hat{D}^{GI} = -\cos(\rho_c + \Delta\rho)$$

$$\hat{I} \cdot \hat{D}^{GI} = 1$$

The dependence of the observation models on the state vector components is shown in Table 1-1.

**ORIGINAL PAGE IS  
OF POOR QUALITY**

The equations of the basic recursive processing algorithm implemented in OABIAS are:

$$\underset{s \times 1}{\underline{K}_j} = \left[ \underset{j}{w}^{-1} + \underline{G}_{jR}^T \underset{j-1}{P} \underline{G}_{jR} \right]^{-1} \underset{j-1}{P} \underline{G}_{jR}$$

$$\underset{s \times s}{\underline{P}_j} = \begin{bmatrix} \underline{I} & -\underline{K}_j \underline{G}_{jR}^T \\ \underline{0} & \underline{G}_{jR} \end{bmatrix} \underset{j-1}{P}$$

$$\underset{s \times 1}{\hat{\underline{X}}_j} = \hat{\underline{X}}_{j-1} + \underline{K}_j \left\{ y_j - y_{cj}(\underline{X}_{jR}) - \underline{G}_{jR}^T \{ \hat{\underline{X}}_{j-1} - \underline{X}_{jR} \} \right\}$$

where  $\underline{G}_{jR}^T = \frac{\partial y_{cj}}{\partial \underline{X}}(\underline{X}_{jR})$

$\underline{X}_{jR}$  = reference vector used in processing observation  $j$ .

The equations for the weighting factors ( $w_{(1)}$  to  $w_{(8)}$ ) used in processing the eight observation models are in Table 3-2.

ORIGINAL PAGE IS  
OF POOR QUALITY

APPENDIX A - MODEL OBSERVATION  
PARTIAL DERIVATIVES

This appendix presents equations for the derivatives  $\partial y_c / \partial x_i$  which are used in the OABIAS observation models. Sections A.1 through A.8 present these equations for each of the eight models in numerical sequence. Section A.9 presents equations for the derivatives  $\partial A / \partial x_i$ ,  $\partial B / \partial x_i$ , and  $\partial \hat{D} / \partial x_i$  of matrices A and B and unit vector D which are used in the preceding eight sections.

In the interest of conciseness, the derivatives  $\partial y_c / \partial x_i$  which are zero are not shown explicitly; all others are.

Two equations for each derivative are included with Models 1, 2, 3, 4, and 7. The first equation in each case is in a form which is intended to provide maximum understanding of the geometrical factors (mainly the relationship between significant unit vectors) which influence the derivative's value. The second equation in each case is in a form which is analogous to that used in the OABIAS coding. Single equations which serve both functions are given for Models 5, 6, and 8. The second equations are not identical to the coding in all cases. In particular, the appendix employs a fuller use of rotation matrix notation with Models 3 and 4 than does the coding.

The main notation and notational techniques used in this appendix were defined previously in Section 3. Attention is called, in particular, to Figure 3-1 which shows the relationships between the various coordinate frames and to Table 3-1 which defines these coordinate frames and the significant unit vectors. Lower case letters ( $u_i$ ,  $s_i$ , etc.) are used to signify the components of unit vectors ( $\hat{U}$ ,  $\hat{S}$ , etc.) along the axes of Frame GI. The definitions of the 12 state vector elements  $x_\alpha$  and their alternate symbols are given in Section 3.10.

ORIGINAL PAGE IS  
OF POOR QUALITY

A.1 MODEL 1--SUN ANGLE MODEL

Subroutines: SANFUN

Observation Equations:

$$z = \beta_M - y_c$$

$$y_c = -\Delta\beta + \text{arc cos } \chi$$

where  $\chi = \hat{U} \cdot \hat{S} \sec \epsilon$

Partial Derivatives:

$$\frac{\partial y_c}{\partial x_1} = \frac{\partial y_c}{\partial s_1} = \frac{\hat{S} \cdot (\hat{e}_2 \times \hat{U})}{(\hat{S} \cdot \hat{e}_3) \sqrt{\cos^2 \epsilon - (\hat{U} \cdot \hat{S})^2}} = -\frac{\sec \epsilon}{\sqrt{1 - \chi^2}} \left[ u_1 - u_3 \frac{s_1}{s_3} \right]$$

$$\frac{\partial y_c}{\partial x_2} = \frac{\partial y_c}{\partial s_2} = \frac{-\hat{S} \cdot (\hat{e}_1 \times \hat{U})}{(\hat{S} \cdot \hat{e}_3) \sqrt{\cos^2 \epsilon - (\hat{U} \cdot \hat{S})^2}} = -\frac{\sec \epsilon}{\sqrt{1 - \chi^2}} \left[ u_2 - u_3 \frac{s_2}{s_3} \right]$$

$$\frac{\partial y_c}{\partial x_8} = \frac{\partial y_c}{\partial \Delta\beta} = -1$$

$$\frac{\partial y_c}{\partial x_{10}} = \frac{\partial y_c}{\partial \epsilon} = -\frac{\hat{U} \cdot \hat{S} \tan \epsilon}{\sqrt{\cos^2 \epsilon - (\hat{U} \cdot \hat{S})^2}} = -\frac{\chi \tan \epsilon}{\sqrt{1 - \chi^2}}$$

A.2 MODEL 2--SUN SIGHTING TIME MODEL

Subroutines: STMFUN, AMATRX, APARTS

Observation Equations:

$$z = -y_c$$

$$y_c = \hat{U} \cdot \hat{N}_S = \sum_{i=1}^3 u_i (a_{2i} \cos \epsilon + a_{3i} \sin \epsilon)$$

Partial Derivatives:

$$\frac{\partial y_c}{\partial x_1} = \frac{\partial y_c}{\partial s_1} = \hat{U} \cdot \frac{\partial \hat{N}_S}{\partial s_1} = \sum_{i=1}^3 u_i \left( \cos \epsilon \frac{\partial a_{2i}}{\partial s_1} + \sin \epsilon \frac{\partial a_{3i}}{\partial s_1} \right)$$

$$\frac{\partial y_c}{\partial x_2} = \frac{\partial y_c}{\partial s_2} = \hat{U} \cdot \frac{\partial \hat{N}_S}{\partial s_2} = \sum_{i=1}^3 u_i \left( \cos \epsilon \frac{\partial a_{2i}}{\partial s_2} + \sin \epsilon \frac{\partial a_{3i}}{\partial s_2} \right)$$

$$\frac{\partial y_c}{\partial x_3} = \frac{\partial y_c}{\partial \psi_0} = -\hat{U} \cdot \hat{e}'_1 \cos \epsilon = \sum_{i=1}^3 u_i \left( \cos \epsilon \frac{\partial a_{2i}}{\partial \psi_0} + \sin \epsilon \frac{\partial a_{3i}}{\partial \psi_0} \right)$$

$$\frac{\partial y_c}{\partial x_9} = \frac{\partial y_c}{\partial \omega} = -(t - t_0) \hat{U} \cdot \hat{e}'_1 \cos \epsilon = \sum_{i=1}^3 u_i \left( \cos \epsilon \frac{\partial a_{2i}}{\partial \omega} + \sin \epsilon \frac{\partial a_{3i}}{\partial \omega} \right)$$

$$\frac{\partial y_c}{\partial x_{10}} = \frac{\partial y_c}{\partial \epsilon} = \hat{U} \cdot (\cos \epsilon \hat{S} - \sin \epsilon \hat{C}'_2) = \sum_{i=1}^3 u_i (\cos \epsilon a_{3i} - \sin \epsilon a_{2i})$$

ORIGINAL PAGE IS  
OF POOR QUALITY

where  $\hat{e}'_1 = \hat{i} \cos \phi + \hat{j} \sin \phi$   
 $\hat{e}'_2 = -\hat{i} \sin \phi + \hat{j} \cos \phi$

NOTE:  $\partial \hat{N}_S / \partial s_\alpha$  (also  $\partial \hat{L} / \partial s_\alpha$  and  $\partial \hat{N}_{II} / \partial s_\alpha$  which appear in Sections A.3 and A.4) are the partial derivatives which would be detected by an observer whose orientation was invariant relative to Frame GI. These partials do not appear explicitly in the OBIAS coding. Algebraic expressions for them were not developed in the present study.

### A.3 MODEL 3--NADIR VECTOR PROJECTION MODEL

Subroutines: LRFUN, EPHEMV, VECROT, AMATRX, APARTS

Observation Equations:

$$z = -y_c$$

$$y_c = \cos \rho + \hat{R} \cdot \hat{L}$$

Partial Derivatives:

$$\frac{\partial y_c}{\partial x_1} = \frac{\partial y_c}{\partial s_1} = \hat{R} \cdot \frac{\partial \hat{L}}{\partial s_1} = \frac{1}{|\hat{R}|} \hat{R}^{GI, T} \frac{\partial A^T}{\partial s_1} \hat{L}^{SC}$$

$$\frac{\partial y_c}{\partial x_2} = \frac{\partial y_c}{\partial s_2} = \hat{R} \cdot \frac{\partial \hat{L}}{\partial s_2} = \frac{1}{|\hat{R}|} \hat{R}^{GI, T} \frac{\partial A^T}{\partial s_2} \hat{L}^{SC}$$

$$\frac{\partial y_c}{\partial x_3} = \frac{\partial y_c}{\partial \psi_0} = \hat{R} \cdot (\hat{S} \times \hat{L}) = \frac{1}{|\hat{R}|} \hat{R}^{GI, T} \frac{\partial A^T}{\partial \psi_0} \hat{L}^{SC}$$

$$\frac{\partial y_c}{\partial x_4} = \frac{\partial y_c}{\partial \Delta \gamma} = \hat{R} \cdot \hat{e}'_1 = \frac{1}{|\hat{R}|} \hat{R}^{GI, T} A^T \frac{\partial B}{\partial \Delta \gamma} \hat{L}^{H'}$$

ORIGIN PAGE 13  
OF POO. QUALITY

$$\frac{\partial y_c}{\partial x_5} = \frac{\partial y_c}{\partial \phi_H} = \hat{R} \cdot (\hat{S} \times \hat{L}_I) = \frac{1}{|\hat{R}|} \hat{R}^{GI, T} A^T \frac{\partial B_I}{\partial \phi_H} \hat{L}_I^{III'} \quad (\text{in-crossing})$$

$$= 0 \quad (\text{out-crossing})$$

$$\frac{\partial y_c}{\partial x_6} = \frac{\partial y_c}{\partial \phi_H} = 0 \quad (\text{in-crossing})$$

$$= \hat{R} \cdot (\hat{S} \times \hat{L}_O) = \frac{1}{|\hat{R}|} \hat{R}^{GI, T} A^T \frac{\partial B_O}{\partial \phi_H} \hat{L}_O^{HO'} \quad (\text{out-crossing})$$

$$\frac{\partial y_c}{\partial x_7} = \frac{\partial y_c}{\partial \Delta \rho} = -\sin \rho = -\cos \rho_c \sin \Delta \rho - \sin \rho_c \cos \Delta \rho$$

$$\frac{\partial y_c}{\partial x_9} = \frac{\partial y_c}{\partial \omega} = (t - t_o) \frac{\partial y_c}{\partial \psi_o} = \frac{1}{|\hat{R}|} \hat{R}^{GI, T} \frac{\partial A^T}{\partial \omega} \hat{L}^{SC}$$

$$\frac{\partial y_c}{\partial x_{11}} = \frac{\partial y_c}{\partial \epsilon_H} = -\hat{R} \cdot \hat{N}_H \cos(\Delta \gamma + \gamma_s) = \frac{1}{|\hat{R}|} \hat{R}^{GI, T} A^T \frac{\partial B}{\partial \epsilon_H} \hat{L}'$$

$$\frac{\partial y_c}{\partial x_{12}} = \frac{\partial y_c}{\partial \Delta t} = \hat{L} \cdot \frac{\partial \hat{R}}{\partial \Delta t} + \frac{\dot{R}}{|\hat{R}|} \frac{\partial \cos \rho}{\partial |\hat{R}|} = \hat{L} \cdot \frac{\partial \hat{R}}{\partial \Delta t} + \frac{\dot{R}}{|\hat{R}|} \tan \rho_c \sin \rho$$

where

$$\hat{L}^{SC} = B \hat{L}^{H'}$$

ORIGINAL PAGE IS  
OF POOR QUALITY

$$\hat{L}^{II'} = T_{\gamma_s}^{(y)} \hat{L}^H$$

$$\hat{L}^H = \begin{Bmatrix} 0 \\ 0 \\ 1 \end{Bmatrix}$$

$$\dot{R} = \frac{d}{dt} |\vec{R}|$$

$$\frac{\partial \hat{R}}{\partial \Delta t} = \frac{1}{|\vec{R}|} [\vec{V} - (\vec{V} \cdot \hat{R}) \hat{R}]$$

$$\rho = \rho_c + \Delta\rho$$

$$\sin \rho_c = (R_e + h) / |\vec{R}|$$

$$\cos \rho_c = \left( 1 - (R_e + h)^2 / |\vec{R}|^2 \right)^{0.5}$$

where  $R_e$  = Earth radius at horizon crossing

$h$  = effective height of atmosphere

NOTE: I signifies an in-crossing and O signifies an out-crossing; neither symbol is used with equations or variables which are applicable to both crossings.

A.4 MODEL 4--HORIZON CROSSING TIME MODEL

Subroutines: LNFUN, AMATRX, LPARTS, APARTS

Observation Equations:

$$z = -y_c$$

$$y_c = \hat{D} \cdot \hat{N}_H$$

Partial Derivatives:

$$\frac{\partial y_c}{\partial x_1} = \frac{\partial y_c}{\partial s_1} = \frac{\partial \hat{D}}{\partial s_1} \cdot \hat{N}_H + \frac{\partial \hat{N}_H}{\partial s_1} \cdot \hat{D} = \left( \frac{\partial \hat{D}}{\partial s_1} \right)^{GI} \cdot \hat{N}_H^{GI} + \hat{D}^{GI, T} \frac{\partial A^T}{\partial s_1} \hat{N}_H^{SC}$$

$$\frac{\partial y_c}{\partial x_2} = \frac{\partial y_c}{\partial s_2} = \frac{\partial \hat{D}}{\partial s_2} \cdot \hat{N}_H + \frac{\partial \hat{N}_H}{\partial s_2} \cdot \hat{D} = \left( \frac{\partial \hat{D}}{\partial s_2} \right)^{GI} \cdot \hat{N}_H^{GI} + \hat{D}^{GI, T} \frac{\partial A^T}{\partial s_2} \hat{N}_H^{SC}$$

$$\frac{\partial y_c}{\partial x_3} = \frac{\partial y_c}{\partial \psi_0} = \hat{S} \cdot (\hat{N}_H \times \hat{D}) = \hat{D}^{GI, T} \frac{\partial A^T}{\partial \psi_0} \hat{N}_H^{SC}$$

$$\frac{\partial y_c}{\partial x_4} = \frac{\partial y_c}{\partial \Delta\gamma} = \frac{\hat{R} \cdot (\hat{N}_H \times \hat{D}) \sin(\gamma_S + \Delta\gamma) \cos \epsilon_H}{\hat{R} \cdot (\hat{D} \times \hat{S})} = \left( \frac{\partial \hat{D}}{\partial \Delta\gamma} \right)^{GI} \cdot \hat{N}_H^{GI}$$

$$\frac{\partial y_c}{\partial x_5} = \frac{\partial y_c}{\partial \phi_{II}} = \hat{S} \cdot (\hat{N}_{III} \times \hat{D}) = \hat{D}^{GI, T} A^T \frac{\partial B_I}{\partial \phi_{II}} \hat{N}_{III}^{III} \text{ (in-crossing)}$$

$$= 0 \text{ (out-crossing)}$$

ORIGINAL PAGE IS  
OF POOR QUALITY

$$\frac{\partial y_c}{\partial x_6} = \frac{\partial y_c}{\partial \phi_H} = 0 \text{ (in-crossing)}$$

$$= \hat{S} \cdot (\hat{N}_{HO} \times \hat{D}) = \hat{D}^{GI, T} A^T \frac{\partial B_O}{\partial \phi_H} \hat{N}_{HO} \text{ (out-crossing)}$$

$$\frac{\partial y_c}{\partial x_7} = \frac{\partial y_c}{\partial \Delta \rho} = \frac{\hat{S} \cdot (\hat{N}_H \times \hat{D}) \sin \rho}{\hat{R} \cdot (\hat{D} \times \hat{S})} = \left( \frac{\partial \hat{D}}{\partial \Delta \rho} \right)^{GI} \cdot \hat{N}_H^{GI}$$

$$\frac{\partial y_c}{\partial x_9} = \frac{\partial y_c}{\partial \omega} = (t - t_o) \frac{\partial y_c}{\partial \psi_o} = \hat{D}^{GI, T} \frac{\partial A^T}{\partial \omega} \hat{N}_H^{SC}$$

$$\begin{aligned} \frac{\partial y_c}{\partial x_{11}} = \frac{\partial y_c}{\partial \epsilon_H} &= \frac{\hat{R} \cdot (\hat{N}_H \times \hat{D}) \cos(\gamma_S + \Delta\gamma) \sin \epsilon_H}{\hat{R} \cdot (\hat{D} \times \hat{S})} + \hat{D} \cdot \hat{e}_a \\ &= \left( \frac{\partial \hat{D}}{\partial \epsilon_H} \right)^{GI} \cdot \hat{N}_H^{GI} + \hat{D}^{GI, T} A^T \frac{\partial B}{\partial \epsilon_H} \hat{N}_H^H \end{aligned}$$

$$\frac{\partial y_c}{\partial x_{12}} = \frac{\partial y_c}{\partial \Delta t} = \frac{\hat{N}_H \cdot (\hat{S} \times \hat{D})}{\hat{R} \cdot (\hat{D} \times \hat{S})} \left[ \left( \hat{D} + \hat{R} \frac{\cos \Delta \rho}{\cos \rho_c} \right) \cdot \vec{V} \right] = \left( \frac{\partial \hat{D}}{\partial \Delta t} \right)^{GI} \cdot \hat{N}_H^{GI}$$

where  $\hat{N}_H^{GI} = A^T \hat{N}_H^{SC}$

$$\hat{N}_H^{SC} = B \hat{N}_H^H$$

$$\hat{N}_H^H = \begin{pmatrix} 0 \\ 1 \\ 0 \end{pmatrix}$$

$\hat{e}_a$  = defined in Figure 3-9

$\vec{V}$  = spacecraft velocity vector

ORIGINAL PAGE 13  
OF POOR QUALITY

NOTE: In the models in which  $\hat{D}$  appears, the derivatives are evaluated at the measured horizon crossing times. As a result, it would be possible to replace  $\hat{D}$  by  $\hat{L}$  in the  $\partial y_c / \partial x_i$  equations.  $\partial \hat{D} / \partial x_i$  however cannot be replaced by  $\partial \hat{L} / \partial x_i$ .

A.5 MODEL 5--SUN TO EARTH-IN AND SUN TO EARTH-OUT DIHEDRAL ANGLE MODEL

Subroutines: DIAFUN, LCOMP, LPARTS

Observation Equations:

$$z = (t_H - t_S) - y_c$$

$$y_c = \frac{1}{\omega} (A_{d5} - \Delta s + \Delta H - \phi_H)$$

$$A_{d5} = \arctan \left( \frac{\text{TOP}}{\text{BOT}} \right)$$

$$\text{TOP} = \hat{S} \cdot (\hat{U} \times \hat{D})$$

$$\text{BOT} = \hat{U} \cdot \hat{D} - (\hat{U} \cdot \hat{S})(\hat{D} \cdot \hat{S})^*$$

$$\Delta s = \arcsin [\tan \epsilon \operatorname{ctn} \beta]$$

$$\beta = \arccos (\hat{U} \cdot \hat{S}) = f(s_1, s_2)$$

$$\Delta H = \arcsin [\tan \epsilon_H \operatorname{ctn} \gamma]$$

$$\gamma = \arccos (\hat{D} \cdot \hat{S})^*$$

---

\* $\hat{D} \cdot \hat{S} = \cos \epsilon_H \cos (\gamma_S + \Delta \gamma) = f(\epsilon_H, \Delta \gamma)$

Partial Derivatives:

ORIGINAL PAGE IS  
OF POOR QUALITY

$$\frac{\partial y_c}{\partial x_1} = \frac{\partial y_c}{\partial s_1} = \frac{1}{\omega} \left( \frac{\partial A_{d5}}{\partial s_1} - \sec \Delta s \csc^3 \beta \tan \epsilon \hat{U} \cdot \frac{\partial \hat{S}}{\partial s_1} \right)$$

$$\frac{\partial y_c}{\partial x_2} = \frac{\partial y_c}{\partial s_2} = \frac{1}{\omega} \left( \frac{\partial A_{d5}}{\partial s_2} - \sec \Delta s \csc^3 \beta \tan \epsilon \hat{U} \cdot \frac{\partial \hat{S}}{\partial s_2} \right)$$

$$\frac{\partial y_c}{\partial x_4} = \frac{\partial y_c}{\partial \Delta \gamma} = \frac{1}{\omega} \left[ \frac{\partial A_{d5}}{\partial \Delta \gamma} - \sec \Delta H \csc^3 \gamma \sin \epsilon_H \sin (\gamma_S + \Delta \gamma) \right]$$

$$\frac{\partial y_c}{\partial x_5} = \frac{\partial y_c}{\partial \phi_H} = -\frac{1}{\omega} \text{ (in-crossing)}$$

$$= 0 \text{ (out-crossing)}$$

$$\frac{\partial y_c}{\partial x_6} = \frac{\partial y_c}{\partial \phi_H} = 0 \text{ (in-crossing)}$$

$$= -\frac{1}{\omega} \text{ (out-crossing)}$$

$$\frac{\partial y_c}{\partial x_7} = \frac{\partial y_c}{\partial \Delta \rho} = \frac{1}{\omega} \frac{\partial A_{d5}}{\partial \Delta \rho}$$

$$\frac{\partial y_c}{\partial x_9} = \frac{\partial y_c}{\partial \omega} = -\frac{y_c}{\omega}$$

ORIGINAL PAGE 19  
OF POOR QUALITY

$$\frac{\partial y_c}{\partial x_{10}} = \frac{\partial y_c}{\partial \epsilon} = -\frac{1}{\omega} \sec \Delta s \operatorname{ctn} \beta \sec^2 \epsilon$$

$$\frac{\partial y_c}{\partial x_{11}} = \frac{\partial y_c}{\partial \epsilon_H} = \frac{1}{\omega} \left\{ \frac{\partial A_{d5}}{\partial \epsilon_H} + \sec \Delta H \left[ \operatorname{ctn} \gamma \sec^2 \epsilon_H \right. \right. \\ \left. \left. - \tan \epsilon_H \operatorname{csc}^3 \gamma \sin \epsilon_H \cos (\gamma_S + \Delta \gamma) \right] \right\}$$

$$\frac{\partial y_c}{\partial x_{12}} = \frac{\partial y_c}{\partial \Delta t} = \frac{1}{\omega} \frac{\partial A_{d5}}{\partial \Delta t}$$

where

$$\frac{\partial A_{d5}}{\partial x_i} = \frac{1}{1 + \left(\frac{\text{TOP}}{\text{BOT}}\right)^2} \left( \frac{1}{\text{BOT}} \frac{\partial \text{TOP}}{\partial x_i} - \frac{\text{TOP}}{\text{BOT}^2} \frac{\partial \text{BOT}}{\partial x_i} \right)$$

$$\frac{\partial \text{TOP}}{\partial x_i} = (\hat{U} \times \hat{D}) \cdot \frac{\partial \hat{S}}{\partial x_i} + (\hat{S} \times \hat{U}) \cdot \frac{\partial \hat{D}}{\partial x_i}$$

$$\frac{\partial \text{BOT}}{\partial x_i} = \hat{U} \cdot \frac{\partial \hat{D}}{\partial x_i} - (\hat{D} \cdot \hat{S}) \left( \hat{U} \cdot \frac{\partial \hat{S}}{\partial x_i} \right) + (\hat{U} \cdot \hat{S}) \left( \sin (\gamma_S + \Delta \gamma) \cos \epsilon_H \frac{d\Delta \gamma}{dx_i} \right.$$

$$\left. + \cos (\gamma_S + \Delta \gamma) \sin \epsilon_H \frac{d\epsilon_H}{dx_i} \right)$$

ORIGINAL PAGE IS  
OF POOR QUALITY

and

$$\frac{\partial \hat{S}}{\partial x_i} = \frac{\hat{e}_2 \times \hat{S}}{\hat{S} \cdot \hat{e}_3} = \hat{e}_1 - \hat{e}_3 \frac{s_1}{s_3} \quad (i = 1)$$

$$= \frac{-\hat{e}_1 \times \hat{S}}{\hat{S} \cdot \hat{e}_3} = \hat{e}_2 - \hat{e}_3 \frac{s_2}{s_3} \quad (i = 2)$$

$$= \vec{0} \quad (i > 2)$$

$$\frac{d\Delta\gamma}{dx_i} = 1 \quad (i = 4)$$

$$= 0 \quad (i \neq 4)$$

$$\frac{d\epsilon_H}{dx_i} = 1 \quad (i = 11)$$

$$= 0 \quad (i \neq 11)$$

NOTE:  $\partial \hat{D} / \partial x_i \neq 0$  in any of the above expressions.

#### A.6 MODEL 6--EARTH WIDTH MODEL

Subroutines: DHFUN, LCOMP, LPARTS

Observation Equations:

$$z = (t_{HO} - t_{HI}) - y_c$$

$$y_c = \frac{1}{\omega} (A_{d6} + \phi_H^I - \phi_H^O)$$

ORIGINAL PAGE IS  
OF POOR QUALITY

$$A_{d6} = \arctan \left( \frac{\text{TOP}}{\text{BOT}} \right)$$

$$\text{TOP} = \hat{S} \cdot (\hat{D}_I \times \hat{D}_O)$$

$$\text{BOT} = \hat{D}_I \cdot \hat{D}_O - (\hat{S} \cdot \hat{D}_I)(\hat{S} \cdot \hat{D}_O) = \hat{D}_I \cdot \hat{D}_O - \cos^2 \epsilon_H \cos^2 (\gamma_s + \Delta\gamma)$$

Partial Derivatives:

$$\frac{\partial y_c}{\partial x_1} = \frac{\partial y_c}{\partial s_1} = \frac{1}{\omega} \frac{\partial A_{d6}}{\partial s_1}$$

$$\frac{\partial y_c}{\partial x_2} = \frac{\partial y_c}{\partial s_2} = \frac{1}{\omega} \frac{\partial A_{d6}}{\partial s_2}$$

$$\frac{\partial y_c}{\partial x_4} = \frac{\partial y_c}{\partial \Delta\gamma} = \frac{1}{\omega} \frac{\partial A_{d6}}{\partial \Delta\gamma}$$

$$\frac{\partial y_c}{\partial x_5} = \frac{\partial y_c}{\partial \phi_H^I} = \frac{1}{\omega} \text{ (in-crossing)}$$

$$= 0 \text{ (out-crossing)}$$

$$\frac{\partial y_c}{\partial x_6} = \frac{\partial y_c}{\partial \phi_H^O} = 0 \text{ (in-crossing)}$$

$$= -\frac{1}{\omega} \text{ (out-crossing)}$$

ORIGINAL PAGE IS  
OF POOR QUALITY

$$\frac{\partial y_c}{\partial x_7} = \frac{\partial y_c}{\partial \Delta \rho} = \frac{1}{\omega} \frac{\partial A_{d6}}{\partial \Delta \rho}$$

$$\frac{\partial y_c}{\partial x_9} = \frac{\partial y_c}{\partial \omega} = \frac{-y_c}{\omega}$$

$$\frac{\partial y_c}{\partial x_{11}} = \frac{\partial y_c}{\partial \epsilon_H} = \frac{1}{\omega} \frac{\partial A_{d6}}{\partial \epsilon_H}$$

$$\frac{\partial y_c}{\partial x_{12}} = \frac{\partial y_c}{\partial \Delta t} = \frac{1}{\omega} \frac{\partial A_{d6}}{\partial \Delta t}$$

where

$$\frac{\partial A_{d6}}{\partial x_i} = \frac{1}{1 - \left(\frac{TOP}{BOT}\right)^2} \left( \frac{1}{BOT} \frac{\partial TOP}{\partial x_i} - \frac{TOP}{BOT^2} \frac{\partial BOT}{\partial x_i} \right)$$

$$\frac{\partial TOP}{\partial x_i} = -(\hat{S} \times \hat{D}_O) \cdot \frac{\partial \hat{D}_I}{\partial x_i} + (\hat{S} \times \hat{D}_I) \cdot \frac{\partial \hat{D}_O}{\partial x_i} + (\hat{D}_I \times \hat{D}_O) \cdot \frac{\partial \hat{S}}{\partial x_i}$$

$$\begin{aligned} \frac{\partial BOT}{\partial x_i} = & \hat{D}_O \cdot \frac{\partial \hat{D}_I}{\partial x_i} + \hat{D}_I \cdot \frac{\partial \hat{D}_O}{\partial x_i} + 2 \cos \epsilon_H \sin \epsilon_H \cos^2 (\gamma_S + \Delta \gamma) \frac{d\epsilon_H}{dx_i} \\ & + 2 \cos^2 \epsilon_H \cos (\gamma_S + \Delta \gamma) \sin (\gamma_S + \Delta \gamma) \frac{d\Delta \gamma}{dx_i} \end{aligned}$$

ORIGINAL PAGE IS  
OF POOR QUALITY

and

$$\frac{d\Delta\gamma}{dx_1} = 1 \quad (i = 4)$$

$$= 0 \quad (i \neq 4)$$

$$\frac{d\epsilon_H}{dx_1} = 1 \quad (i = 11)$$

$$= 0 \quad (i \neq 11)$$

For  $\frac{\partial \hat{S}}{\partial x_1}$ , see Model 5.

#### A.7 MODEL 7--SMALL TARGET MODEL

Subroutines: SCBFUN, EPHEMV

Observation Equations:

$$z = \gamma_S - y_c$$

$$y_c = -\Delta\gamma + \arccos \sigma$$

where  $\sigma = -\hat{R} \cdot \hat{S} \sec \epsilon_H$

Partial Derivatives:

$$\frac{\partial y_c}{\partial x_1} = \frac{\partial y_c}{\partial s_1} \cdot \frac{-\hat{S} \cdot (\hat{e}_2 \times \hat{R})}{(\hat{S} \cdot \hat{e}_3) \sqrt{\cos^2 \epsilon_H - (\hat{R} \cdot \hat{S})^2}} = \frac{\sec \epsilon_H}{\sqrt{1 - \sigma^2}} \left[ r_1 - r_3 \frac{s_1}{s_3} \right]$$

ORIGINAL PAGE IS  
OF POOR QUALITY

$$\frac{\partial y_c}{\partial x_2} = \frac{\partial y_c}{\partial s_2} = \frac{\hat{S} \cdot (\hat{e}_1 \times \hat{R})}{(\hat{S} \cdot \hat{e}_3) \sqrt{\cos^2 \epsilon_H - (\hat{R} \cdot \hat{S})^2}} = \frac{\sec \epsilon_H}{\sqrt{1 - \sigma^2}} \left[ r_2 - r_3 \frac{s_2}{s_3} \right]$$

$$\frac{\partial y_c}{\partial x_4} = \frac{\partial y_c}{\partial \Delta \gamma} = \dots$$

$$\frac{\partial y_c}{\partial x_{11}} = \frac{\partial y_c}{\partial \epsilon_H} = \frac{\hat{R} \cdot \hat{S} \tan \epsilon_H}{\sqrt{\cos^2 \epsilon_H - (\hat{R} \cdot \hat{S})^2}} = \frac{-\sigma \tan \epsilon_H}{\sqrt{1 - \sigma^2}}$$

$$\frac{\partial y_c}{\partial x_{12}} = \frac{\partial y_c}{\partial \Delta t} = \frac{1}{\sqrt{\cos^2 \epsilon_H - (\hat{R} \cdot \hat{S})^2}} \hat{S} \cdot \frac{\partial \hat{R}}{\partial \Delta t} = \frac{\sec \epsilon_H}{\sqrt{1 - \sigma^2}} \hat{S}^{GI} \cdot \left( \frac{\partial \hat{R}}{\partial \Delta t} \right)^{GI}$$

For  $\frac{\partial \hat{R}}{\partial \Delta t}$ , see Section A.3.

NOTE: The mathematical similarity between Models 1 and 7 can be seen by comparing the above equations with those in Section A.1.

#### A.8 MODEL 8--SUN TO EARTH MID-SCAN DIHEDRAL ANGLE MODEL

Subroutines: DIAFUN, LCOMP, LPARTS

Observation Equations:

$$z = y - y_c$$

$$y = 0.5(t_{HI} + t_{HO}) \quad t_s$$

$$y_c = \frac{1}{\omega} \left( A_{ds} - \Delta s + \Delta H - 0.5 \left( \frac{I}{H} + \phi_H^O \right) \right)$$

ORIGINAL PAGE IS  
OF POOR QUALITY

$$A_{ds} = 0.5 \left[ \arctan \left( \frac{TOP_I}{BOT_I} \right) + \arctan \left( \frac{TOP_O}{BOT_O} \right) \right]$$

$$TOP_I = \hat{S} \cdot (\hat{U} \times \hat{D}_I)$$

$$BOT_I = \hat{U} \cdot \hat{D}_I - (\hat{U} \cdot \hat{S})(\hat{D}_I \cdot \hat{S})$$

$$TOP_O = \hat{S} \cdot (\hat{U} \times \hat{D}_O)$$

$$BOT_O = \hat{U} \cdot \hat{D}_O - (\hat{U} \cdot \hat{S})(\hat{D}_O \cdot \hat{S})$$

$$\Delta s = \arcsin (\tan \epsilon \operatorname{ctn} \beta)$$

$$\beta = \arccos (\hat{U} \cdot \hat{S}) = f(s_1, s_2)$$

$$\Delta H = \arcsin (\tan \epsilon_H \operatorname{ctn} \gamma)$$

$$\gamma = \arccos (\hat{D} \cdot \hat{S}) = \arccos (\cos \epsilon_H \cos (\gamma_S + \Delta \gamma)) = f(\epsilon_H, \Delta \gamma)$$

Partial Derivatives:

$$\frac{\partial y_c}{\partial x_1} = \frac{\partial y_c}{\partial s_1} = \frac{1}{\omega} \left( \frac{\partial A_{ds}}{\partial s_1} - \sec \Delta s \operatorname{csc}^3 \beta \tan \epsilon \hat{U} \cdot \frac{\partial \hat{S}}{\partial s_1} \right)$$

$$\frac{\partial y_c}{\partial x_2} = \frac{\partial y_c}{\partial s_2} = \frac{1}{\omega} \left( \frac{\partial A_{ds}}{\partial s_2} - \sec \Delta s \operatorname{csc}^3 \beta \tan \epsilon \hat{U} \cdot \frac{\partial \hat{S}}{\partial s_2} \right)$$

ORIGINAL PAGE IS  
OF POOR QUALITY

$$\frac{\partial y_c}{\partial x_4} = \frac{\partial y_c}{\partial \Delta \gamma} = -\frac{1}{\omega} \sec \Delta H \csc^3 \gamma \sin \epsilon_H \sin (\gamma_S + \Delta \gamma)$$

$$\frac{\partial y_c}{\partial x_5} = \frac{\partial y_c}{\partial \phi_H} = \frac{-0.5}{\omega}$$

$$\frac{\partial y_c}{\partial x_6} = \frac{\partial y_c}{\partial \phi_H} = \frac{-0.5}{\omega}$$

$$\frac{\partial y_c}{\partial x_9} = \frac{\partial y_c}{\partial \omega} = \frac{-y_c}{\omega}$$

$$\frac{\partial y_c}{\partial x_{10}} = \frac{\partial y_c}{\partial \epsilon} = -\frac{1}{\omega} \sec \Delta s \operatorname{ctn} \beta \sec^2 \epsilon$$

$$\frac{\partial y_c}{\partial x_{11}} = \frac{\partial y_c}{\partial \epsilon_H} = \frac{1}{\omega} \sec \Delta H \left( \operatorname{ctn} \gamma \sec^2 \epsilon_H - \tan \epsilon_H \csc^2 \gamma \sin \epsilon_H \cos (\gamma_S + \Delta \gamma) \right)$$

$$\frac{\partial y_c}{\partial x_{12}} = \frac{\partial y_c}{\partial \Delta t} = \frac{1}{\omega} \frac{\partial A_{d8}}{\partial \Delta t}$$

$$\frac{\partial A_{d8}}{\partial x_i} = 0.5 \left[ \frac{\partial}{\partial x_i} (A_{d5} \text{ (in)} + A_{d5} \text{ (out)}) \right]$$

where  $\partial A_{d5} / \partial x_i$  is defined in Section A.5.

## A.9 SUPPLEMENTARY PARTIAL DERIVATIVES

### A.9.1 Matrix A Partial Derivative

The equations for Matrix A were discussed and presented previously in Section 3.10. For the reader's convenience, they are repeated below.

$$\begin{aligned}
 A &= \begin{bmatrix} a_{11} & a_{12} & a_{13} \\ a_{21} & a_{22} & a_{23} \\ a_{31} & a_{32} & a_{33} \end{bmatrix} \\
 &= \frac{1}{\cos \delta} \begin{bmatrix} s_1 s_3 \cos \phi - s_2 \sin \phi & s_2 s_3 \cos \phi + s_1 \sin \phi & -\cos^2 \delta \cos \phi \\ -s_1 s_3 \sin \phi - s_2 \cos \phi & -s_2 s_3 \sin \phi + s_1 \cos \phi & \cos^2 \delta \sin \phi \\ s_1 \cos \delta & s_2 \cos \delta & s_3 \cos \delta \end{bmatrix}
 \end{aligned}$$

where  $\cos \delta = \sqrt{s_1^2 + s_2^2}$

ORIGINAL PAGE IS  
OF POOR QUALITY

The derivatives  $\partial A/\partial x_i$  can be obtained by direct differentiation. The results are as follows:

$$\frac{\partial A}{\partial x_1} = \frac{\partial A^*}{\partial s_1} = \frac{1}{\cos \delta} \begin{bmatrix} \cos \phi (s_3 - s_1^2/s_3) & \sin \phi & -s_1 \cos \phi \\ -s_1 a_{11}/\cos \delta & -\cos \phi (s_1 s_2/s_3) & \\ & -s_1 a_{12}/\cos \delta & \\ -\sin \phi (s_3 - s_1^2/s_3) & \cos \phi & s_1 \sin \phi \\ -s_1 a_{21}/\cos \delta & +\sin \phi (s_1 s_2/s_3) & \\ & -s_1 a_{22}/\cos \delta & \\ \cos \delta & 0 & -(s_1/s_3) \cos \delta \end{bmatrix}$$

$$\frac{\partial A}{\partial x_2} = \frac{\partial A^*}{\partial s_2} = \frac{1}{\cos \delta} \begin{bmatrix} -\sin \phi & \cos \phi (s_3 - s_2^2/s_3) & -s_2 \cos \phi \\ -\cos \phi (s_1 s_2/s_3) & -a_{12} s_2/\cos \delta & \\ -a_{11} s_2/\cos \delta & & \\ -\cos \phi & -\sin \phi (s_3 - s_2^2/s_3) & s_2 \sin \phi \\ +\sin \phi (s_1 s_2/s_3) & -a_{22} s_2/\cos \delta & \\ -a_{21} (s_2/\cos \delta) & & \\ 0 & \cos \delta & -(s_2/s_3) \cos \delta \end{bmatrix}$$

\*The use of the partial derivative symbol  $\partial$  here is a misnomer, because derivatives  $ds_3/ds_\alpha$ ,  $d \cos \delta/ds_\alpha$ , and  $d(\cos \delta)^{-1}/ds_\alpha$  ( $\alpha = 1, 2$ ) are included.

ORIGINAL PAGE IS  
OF POOR QUALITY

$$\frac{\partial A}{\partial x_3} = \frac{\partial A}{\partial \psi_0} = \begin{bmatrix} a_{21} & a_{22} & a_{23} \\ -a_{11} & -a_{12} & -a_{13} \\ 0 & 0 & 0 \end{bmatrix}$$

$$\frac{\partial A}{\partial x_9} = \frac{\partial A}{\partial \omega} = (t - t_0) \frac{\partial A}{\partial \psi_0}$$

### A.9.2 Matrix B Partial Derivatives

The equations for Matrix B are:

$$B = T_{\phi_H}^T T_{\epsilon_H}^T T_{\Delta\gamma}^T$$

where

$$T_{\phi_H}^T = \begin{bmatrix} \cos \phi_H & -\sin \phi_H & 0 \\ \sin \phi_H & \cos \phi_H & 0 \\ 0 & 0 & 1 \end{bmatrix}$$

$$T_{\epsilon_H}^T = \begin{bmatrix} 1 & 0 & 0 \\ 0 & \cos \epsilon_H & -\sin \epsilon_H \\ 0 & \sin \epsilon_H & \cos \epsilon_H \end{bmatrix}$$

$$T_{\Delta\gamma}^T = \begin{bmatrix} \cos \Delta\gamma & 0 & \sin \Delta\gamma \\ 0 & 1 & 0 \\ -\sin \Delta\gamma & 0 & \cos \Delta\gamma \end{bmatrix}$$

ORIGINAL PAGE IS  
OF POOR QUALITY

The partial derivatives of B can be obtained by direct differentiation; these are

$$\frac{\partial B}{\partial x_4} = \frac{\partial B}{\partial \Delta\gamma} = T_{\phi_H}^T T_{\epsilon_H}^T \begin{bmatrix} -\sin \Delta\gamma & 0 & \cos \Delta\gamma \\ 0 & 0 & 0 \\ -\cos \Delta\gamma & 0 & -\sin \Delta\gamma \end{bmatrix}$$

$$\frac{\partial B}{\partial x_5}, \frac{\partial B}{\partial x_6} = \frac{\partial B}{\partial \phi_H} = \begin{bmatrix} -\sin \phi_H & -\cos \phi_H & 0 \\ \cos \phi_H & -\sin \phi_H & 0 \\ 0 & 0 & 0 \end{bmatrix} T_{\phi_H}^T T_{\Delta\gamma}^T$$

$$\frac{\partial B}{\partial x_{11}} = \frac{\partial B}{\partial \epsilon_H} = T_{\phi_H}^T \begin{bmatrix} 0 & 0 & 0 \\ 0 & -\sin \epsilon_H & -\cos \epsilon_H \\ 0 & \cos \epsilon_H & -\sin \epsilon_H \end{bmatrix} T_{\Delta\gamma}^T$$

### A.9.3 $\hat{D}$ Partial Derivatives

The computation of  $\hat{D}$  in subroutine LCOMP was discussed in Section 3.8. The three fundamental equations used in the computation are repeated below.

$$\hat{S} \cdot \hat{D} = \cos(\gamma_S + \Delta\gamma) \cos \epsilon_H \quad (\text{A-1a})$$

$$\hat{R} \cdot \hat{D} = -\cos(\rho_c + \Delta\rho) \quad (\text{A-1b})$$

$$\hat{D} \cdot \hat{D} = 1 \quad (\text{A-1c})$$

The partial derivatives of  $\hat{D}$  with respect to the state vector elements  $x_i$  are computed in subroutine LPARTS. The derivation of the LPARTS algorithms

starts by differentiating Equation A-1 to obtain the following set of perturbation equations

$$\begin{aligned} \hat{S} \cdot d\hat{D} + \hat{D} \cdot d\hat{S} = & -\sin(\gamma_S + \Delta\gamma) \cos \epsilon_H d\Delta\gamma \\ & - \cos(\gamma_S + \Delta\gamma) \sin \epsilon_H d\epsilon_H \end{aligned} \quad (A-2a)$$

$$\begin{aligned} \hat{R} \cdot d\hat{D} + \hat{D} \cdot \frac{\partial \hat{R}}{\partial \Delta t} d\Delta t = & \sin(\rho_c + \Delta\rho) d\Delta\rho \\ & + \frac{\partial \cos(\rho_c + \Delta\rho)}{\partial R} \frac{\partial R}{\partial \Delta t} d\Delta t \end{aligned} \quad (A-2b)$$

$$\hat{D} \cdot d\hat{D} = 0 \quad (A-2c)$$

where  $d\hat{S}$  is constrained to be

$$d\hat{S} = \left( \hat{e}_1 - \hat{e}_3 \left( \frac{s_1}{s_3} \right) \right) ds_1 + \left( \hat{e}_2 - \hat{e}_3 \left( \frac{s_2}{s_3} \right) \right) ds_2 \quad (A-2d)$$

Equation (A-2) defines the perturbation  $d\hat{D}$  in  $\hat{D}$  which is produced by perturbations  $ds_1$ ,  $ds_2$ ,  $d\Delta\gamma$ ,  $d\Delta\rho$ ,  $d\epsilon_H$ , and  $d\Delta t$ .

The present discussion will use the simple symbol  $R$  to signify the magnitude of  $\vec{R}$ . As before,  $\dot{R}$  will signify the rate of change of  $R$ , and  $\vec{V}$  will signify the spacecraft's velocity vector.  $\partial \hat{R} / \partial \Delta t$  of Equation (A-2) is the velocity vector of  $\hat{R}$ ; later in the derivation, it will be specified by the following equation

$$\frac{\partial \hat{R}}{\partial \Delta t} = \frac{1}{R} \left[ \vec{V} - \dot{R} \hat{R} \right] \quad (A-3a)$$

ORIGINAL PAGE IS  
OF POOR QUALITY

where

$$\dot{R} = \frac{\partial R}{\partial \Delta t} = \vec{V} \cdot \hat{R} \quad (A-3b)$$

The second term on the right side of Equation (A-2b) is the change in  $\cos \rho$  due to the change  $dR$  in  $R$  which is produced, in non-circular orbits, by  $d\Delta t$ . The following equation for this term was developed with the aid of the equations for  $\sin \rho_c$  and  $\cos \rho_c$  listed in Section A.3.

$$\frac{\partial \cos (\rho_c + \Delta \rho)}{\partial R} \frac{\partial R}{\partial \Delta t} d\Delta t = \frac{\dot{R}}{R} \sin (\rho_c + \Delta \rho) \tan \rho_c d\Delta t \quad (A-4)$$

The problem now is to solve Equation (A-2) for  $d\hat{D}$ . As a tool for accomplishing this, the following  $3 \times 3$  matrix  $M$  will be introduced:

$$M = \begin{bmatrix} \hat{S}^T \\ \hat{R}^T \\ \hat{D}^T \end{bmatrix} \quad (A-5)$$

The left sides of Equations (A-2a) and (A-2b) do not necessarily imply that the vectors are resolved upon a coordinate frame. With the introduction of  $M$  into the development, however, it will become convenient (although not absolutely essential) to assume resolution upon a specified frame; namely, frame GI. For notational simplicity, however, the superscripts GI used elsewhere in the report to designate GI frame resolution will be omitted from the remainder of this discussion.

ORIGINAL PAGE IS  
OF POOR QUALITY

Arranging Equation (A-2) in a matrix format, introducing Equations (A-4) and (A-5), and solving for  $d\hat{D}$  now yields

$$d\hat{D} = M^{-1} \left\{ \begin{array}{l} -\hat{D} \cdot d\hat{S} - \sin(\gamma_S + \Delta\gamma) \cos \epsilon_H d\Delta\gamma - \cos(\gamma_S + \Delta\gamma) \sin \epsilon_H d\epsilon_{II} \\ \sin(\rho_c + \Delta\rho) d\Delta\rho - \hat{D} \cdot \frac{\partial \hat{R}}{\partial \Delta t} - \frac{\dot{R}}{R} \sin(\rho_c + \Delta\rho) \tan \rho_c d\Delta t \\ 0 \end{array} \right\} \quad (A-6)$$

Equation (A-6) is not meaningful when  $M$  is singular. The condition of singular  $M$  occurs if and only if the three vectors  $\hat{D}$ ,  $\hat{S}$ , and  $\hat{R}$  are in a common plane.

A general equation relating  $d\hat{D}$  to the state variable perturbations  $dx$  is as follows:

$$d\hat{D} = \sum_{i=1}^{12} \frac{\partial \hat{D}}{\partial x_i} dx_i \quad (A-7)$$

The desired equations for the partials  $\partial \hat{D} / \partial x_i$  now can be obtained by comparing Equation (A-6) with Equation (A-7). Equation (A-3) is employed where necessary. For this work, it is convenient to define the columns of  $M^{-1}$  explicitly; i.e.,

$$M^{-1} = [Q_1 \ Q_2 \ Q_3] \quad (A-8)$$

The resulting  $\partial D / \partial x_i$  equations are as follows:

$$\frac{\partial \hat{D}}{\partial x_1} = \frac{\partial \hat{D}}{\partial s_1} \left[ -Q_1 d_1 - d_3 \frac{s_1}{s_3} \right] \quad (A-9a)$$

$$\frac{\partial \hat{D}}{\partial x_2} = \frac{\partial \hat{D}}{\partial s_2} = -Q_1 \left[ d_2 - d_3 \frac{s_2}{s_3} \right] \quad (\text{A-9b})$$

$$\frac{\partial \hat{D}}{\partial x_4} = \frac{\partial \hat{D}}{\partial \Delta \gamma} = -Q_1 \sin (\gamma_S + \Delta \gamma) \cos \epsilon_H \quad (\text{A-9c})$$

$$\frac{\partial \hat{D}}{\partial x_7} = \frac{\partial \hat{D}}{\partial \Delta \rho} = Q_2 \sin (\rho_c + \Delta \rho) \quad (\text{A-9d})$$

$$\frac{\partial \hat{D}}{\partial x_{11}} = \frac{\partial \hat{D}}{\partial \epsilon_H} = -Q_1 \cos (\gamma_S + \Delta \gamma) \sin \epsilon_H \quad (\text{A-9e})$$

$$\frac{\partial \hat{D}}{\partial x_{12}} = \frac{\partial \hat{D}}{\partial \Delta t} = -Q_2 \left[ \hat{D} \cdot \frac{\partial \hat{R}}{\partial \Delta t} + \frac{\dot{R}}{R} \sin (\rho_c + \Delta \rho) \tan \rho_c \right] \quad (\text{A-9f})$$

Equations (A-9a) through (A-9f) are similar to those implemented in the OBIAS coding. An alternate form which better shows the geometric factors that influence the  $\partial \hat{D} / \partial x_i$  values, however, is possible. To derive these equations,  $M^{-1}$  is written in the following explicit form:

$$M^{-1} = (\det M)^{-1} \begin{bmatrix} \hat{R} \times \hat{D} & \hat{D} \times \hat{S} & \hat{S} \times \hat{R} \end{bmatrix} \quad (\text{A-10a})$$

where

$$\det M = \hat{D} \cdot (\hat{S} \times \hat{R}) = \hat{S} \cdot (\hat{R} \times \hat{D}) = \hat{R} \cdot (\hat{D} \times \hat{S}) \quad (\text{A-10b})$$

Equation (A-10) can be verified by premultiplying it by Equation (A-5) to produce the identity matrix.

**ORIGINAL PAGE IS  
OF POOR QUALITY**

The alternate form of the  $\partial \hat{D} / \partial x_i$  equations is obtained by substituting Equation (A-10) into (A-6) and proceeding as before. The  $\partial \hat{D} / \partial \Delta t$  equation can be simplified using Equation (A-2d) and (A-1b). The results are

$$\frac{\partial \hat{D}}{\partial x_1} = \frac{\partial \hat{D}}{\partial s_1} = \frac{\hat{D} \times \hat{R} \left( \hat{D} \cdot \frac{\partial \hat{S}}{\partial s_1} \right)}{\hat{R} \cdot (\hat{D} \times \hat{S})} \quad (\text{A-11a})$$

$$\frac{\partial \hat{D}}{\partial x_2} = \frac{\partial \hat{D}}{\partial s_2} = \frac{\hat{D} \times \hat{R} \left( \hat{D} \cdot \frac{\partial \hat{S}}{\partial s_2} \right)}{\hat{R} \cdot (\hat{D} \times \hat{S})} \quad (\text{A-11b})$$

$$\frac{\partial \hat{D}}{\partial x_4} = \frac{\partial \hat{D}}{\partial \Delta \gamma} = \frac{\hat{D} \times \hat{R} \sin(\gamma_S + \Delta \gamma) \cos \epsilon_H}{\hat{R} \cdot (\hat{D} \times \hat{S})} \quad (\text{A-11c})$$

$$\frac{\partial \hat{D}}{\partial x_7} = \frac{\partial \hat{D}}{\partial \Delta \rho} = \frac{\hat{D} \times \hat{S} \sin \rho}{\hat{R} \cdot (\hat{D} \times \hat{S})} \quad (\text{A-11d})$$

$$\frac{\partial \hat{D}}{\partial x_{11}} = \frac{\partial \hat{D}}{\partial \epsilon_H} = \frac{\hat{D} \times \hat{R} \cos(\gamma_S + \Delta \gamma) \sin \epsilon_H}{\hat{R} \cdot (\hat{D} \times \hat{S})} \quad (\text{A-11e})$$

$$\frac{\partial \hat{D}}{\partial x_{12}} = \frac{\partial \hat{D}}{\partial \Delta t} = \frac{\hat{S} \times \hat{D}}{\hat{R} \cdot (\hat{D} \times \hat{S})} \left[ \left( \hat{D} + \hat{R} \frac{\cos \Delta \rho}{\cos \rho_c} \right) \cdot \hat{V} \right] \quad (\text{A-11f})$$

where the  $\partial S / \partial s_i$  equations are given in Section A.5. Unlike Equation (A-9), the above equations can be regarded as vector equations per se, and not merely as equations for vector components along the GI frame axes.

APPENDIX B - DERIVATION OF RECURSIVE PROCESSING  
ALGORITHM USED IN OABIAS

B.1 INTRODUCTION

The purpose of this appendix is to derive the equations of the basic recursive processing algorithm used by OABIAS. The resulting equations are applicable to any system which uses subroutine RECURS (Reference 21) or RECUR1 now employed in OABIAS. A generalized least squares approach is taken in the derivation.

Section B.2 discusses the generalized least-squares loss function and then derives the batch processing differential corrector equations. This is a necessary preliminary step in the OABIAS equation derivation. Section B.3 presents the derivation of the nonrecursive least-squares algorithm. Section B.4 derives a preliminary set of recursive processing equations. These equations are essentially identical to the ones in Section B.3, except they are directly applicable to recursive processing. From the resulting equations in Section B.4, Section B.5 derives the basic algorithm used in OABIAS.

References 11, 20, and 22 through 24 provide the background for the derivation methods used in this appendix.

The main notational techniques used in the appendix are as follows. All symbols with an underbar, but no superscript T, are column vectors. Superscript T signifies the transpose of a column vector or of a matrix. Matrices are designated by uppercase symbols with no underbar. Lowercase symbols with no underbar are scalars. The derivative of a scalar with respect to a vector is considered to be a row vector. The dimensions of matrices and column vectors are indicated the first time they appear in equations. The

**ORIGINAL PAGE IS  
OF POOR QUALITY**

notation distinguishes between variables and algebraic expressions which are used to compute the values of these variables. For example, in the equation

$$\underline{Y}_c = \underline{Y}_c(\underline{M}, \underline{X}, t)$$

$\underline{Y}_c(\underline{M}, \underline{X}, t)$  is a known algebraic expression. The numerical values of the elements of  $\underline{Y}_c$  are computed by inserting values of  $\underline{M}$ ,  $\underline{X}$ , and  $t$  into it. Parentheses are used only in this manner.

## B.2 DISCUSSION OF THE LEAST-SQUARES LOSS FUNCTION

The purpose of the algorithms derived in this appendix is to compute optimal estimates of the state of a system using, as primary input, a sequence of observations performed on this system. The system state is assumed to be constant and is modeled as an  $s \times 1$  vector. The symbol  $\underline{X}$  will denote the unknown true state vector. A distinction will be made in the early stages of this discussion between "arbitrary" estimates of  $\underline{X}$ , which will be denoted by  $\hat{\underline{X}}$ , and the optimal estimate  $\hat{\underline{X}}^*$ . The symbol  $\hat{\underline{X}}_0$  signifies an a priori estimate of  $\underline{X}$ .

A generalized least-squares criteria will be used to develop the algorithms for computing  $\hat{\underline{X}}^*$ .  $\hat{\underline{X}}^*$ , by definition, is the  $\hat{\underline{X}}$  which minimizes the following loss function:

$$L_1 = 0.5 \underline{Z}_1^T \underline{W}_1 \underline{Z}_1 + 0.5 \left\{ \hat{\underline{X}}_1 - \hat{\underline{X}}_0 \right\}^T \underline{S}_0 \left\{ \hat{\underline{X}}_1 - \hat{\underline{X}}_0 \right\} \quad (\text{B-1a})$$

$p \times p$     $p \times 1$                        $s \times s$        $s \times 1$

where

$$\underline{Z}_1 = \underline{Y}_1 - \underline{Y}_{c1} = \underline{Z}_1(\hat{\underline{X}}_1, \underline{M}_1, t) \quad (\text{B-1b})$$

$p \times 1$     $p \times 1$                        $n \times 1$

and

$$\underline{Y}_1 = \underline{Y}_1(\underline{M}_1, t) \quad (B-1c)$$

$$\underline{Y}_{c1} = \underline{Y}_{c1}(\underline{M}_1, t, \hat{\underline{X}}_1) \quad (B-1d)$$

The 1 subscripts in the above equations signify that the estimate is to be obtained from a set of data designated as set 1. For notational simplicity, these 1 subscripts henceforth will be omitted until the development reaches the point where they can serve a useful purpose.

$\underline{Z}$  is the residual vector.  $\underline{Y}$  is called the real observation vector or just the observation vector.  $\underline{Y}_c$  is the model observation vector. It is important to distinguish between  $\underline{Y}$  and the measurement vector  $\underline{M}$ . The elements  $m_\alpha$  of  $\underline{M}$  are the basic scalar measurements generated by the onboard sensors and preliminary ground processing operations, and are the primary inputs to the composite attitude determination system. The elements  $y_i$  of  $\underline{Y}$  are the inputs to the estimation subsystem of the attitude determination system.

The elements  $y_{ci}$  of the model observation vector  $\underline{Y}_c$  are the predicted values of  $y_i$  using a mathematical model of the satellite and its sensor system. Under ideal conditions, each  $y_{ci}$  would be identical to its corresponding  $y_i$ . The residuals  $z_i$  between each  $y_i$  and  $y_{ci}$  provide an indication of the error in the estimate of  $\underline{X}$ .

In most estimation studies, a distinction is not made between  $\underline{Y}$  and  $\underline{M}$ . Also,  $\underline{Y}_c$  is not normally considered to be a function of  $\underline{M}$  as shown in Equation (B-1d). The OABIAS estimation system is unorthodox in several respects, however, and the purpose of the apparently general format of Equations (B-1b) through (B-1d) is to make the forthcoming derivation completely

ORIGINAL PAGE IS  
OF POOR QUALITY

applicable to OABIAS. The most unusual feature of OABIAS is that in several of the sensor models,  $y_i$  is known exactly and the M-dependency enters solely through  $y_{ci}$ .

The loss function  $l$  of Equation (B-1) is a blend of the new measurement data  $\underline{M}$  and the a priori state vector estimate  $\hat{\underline{x}}_0$ .  $W$  and  $S_0$  are weighting matrices whose function is to establish the relative weights to be assigned to the individual residuals  $z_i$  and to the state vector deviations  $(\hat{x}_\eta^* - \hat{x}_{0\eta})$ . The term "least squares" often is used to signify loss functions in which  $W$  is diagonal (sometimes with all diagonal elements identical) and/or  $S_0$  is zero. The present development will not make either of these restrictions in its early stages and, thus, can be considered to be a generalized least-squares approach.

$W$  and  $S_0$  are assumed to be symmetric. For  $l$  to be meaningful, both  $W$  and  $S_0$  must be nonnegative definite. The further restriction that  $W$  be positive definite usually is justified. A positive semidefinite  $W$  would imply measurement data to which no weight at all is to be attached. A positive semidefinite  $S_0$  is meaningful and acceptable, unless an  $\hat{\underline{x}}^*$  algorithm which requires its inverse is developed. A positive semidefinite  $S_0$  implies that the state vector contains components whose values are completely unknown a priori.

Estimation algorithm derivations which employ a least-squares approach sometimes assume a priori that  $W$  is the inverse of the covariance matrix  $R$  of the errors in the observations or residuals and that  $S_0$  is the inverse of the covariance matrix of the uncertainty in  $\hat{\underline{x}}_0$ . The present derivation, however, does not attach any necessary statistical significance to  $S_0$  and  $W$ . They are regarded only as weighting matrices and are subject only to the mathematical

ORIGINAL PAGE IS  
OF POOR QUALITY

restrictions noted in the above paragraph.  $W = R^{-1}$  and  $S_o = P_o^{-1}$  usually are considered, without verification, the optimal weighting conditions which make  $\hat{\underline{X}}^*$ , which satisfies the generalized least-squares criteria, truly the optimal estimate. However, such statistical restrictions on  $W$  and  $S_o$  are considered here to fall fundamentally outside of the basic least-squares mathematics.

In principle, a distinction should be made between the sensor event times  $t_s$ ,  $t_{HI}$ ,  $t_{HO}$  and the time variable  $t$  which is included in Equation (B-1).  $t$  is intended here to signify the time or times at which orbital or ephemeris data is evaluated to generate the Sun and central body reference information required by the estimation system. These times are not necessarily identical to the telemetered sensor event times. For OABIAS application, however, the point is not a significant one, because the program does use the telemetered sensor event times to generate the Sun and central body reference information. For this reason, the model observations  $y_{ci}$  of all the OABIAS models are functions, to at least some extent, of the elements  $t_s$ ,  $t_{HI}$ , or  $t_{HO}$  of  $\underline{M}$ . In the interest of notational simplicity, the  $t$ - and  $M$ -dependence will not be shown explicitly in the remaining equations of this appendix.

### B.3 DERIVATION OF THE NONRECURSIVE LEAST-SQUARES ALGORITHM

A necessary condition for  $\hat{\underline{X}}^*$  to be the estimate which minimizes the loss function  $\ell$  of Equation (B-1) is

$$\frac{\partial \ell}{\partial \hat{\underline{X}}} (\hat{\underline{X}}^*)^T = \underline{0}_{s \times 1} \quad (\text{B-2})$$

**ORIGINAL PAGE IS  
OF POOR QUALITY**

Differentiating Equation (B-1) with respect to  $\hat{\underline{X}}$ , setting  $\hat{\underline{X}}$  to  $\hat{\underline{X}}^*$ , and using Equation (B-2) yields

$$\frac{\partial \underline{Z}}{\partial \hat{\underline{X}}} (\hat{\underline{X}}^*)^T \underline{W} \underline{Z} (\hat{\underline{X}}^*) + \underset{s \times s}{S_0} \{ \hat{\underline{X}}^* - \hat{\underline{X}}_0 \} = \underset{s \times 1}{\underline{0}} \quad (B-3)$$

The problem now is to derive a method for solving Equation (B-3) for  $\hat{\underline{X}}^*$ . The usual Newton-Raphson procedure expands  $\underline{Z}(\hat{\underline{X}}^*)$  in a Taylor series about  $\hat{\underline{X}}_0$ . A slightly more general approach will be employed here, however, in order to obtain equations which can be used in the recursive estimator derivation. Instead, each element  $z_i$  of  $\underline{Z}$  will be expanded in a Taylor series about an arbitrary reference to be denoted as  $\underline{X}_{Ri}$ . The  $p$   $\underline{X}_{Ri}$ 's are not assumed to be identical to  $\hat{\underline{X}}_0$  nor to each other. They are assumed only to be sufficiently close to  $\hat{\underline{X}}^*$  to partially justify the forthcoming series truncation. The Taylor series result can be placed in the following form:

$$\underline{Z}(\hat{\underline{X}}^*) = \underset{p \times 1}{\underline{Y}} - \underset{p \times 1}{\underline{Y}_{cR}} + \underset{p \times 1}{\underline{B}_R} - \underset{p \times s}{\underline{G}_R} \cdot \underline{X}^* + \text{H.O.T.} (\hat{\underline{X}}^* - \hat{\underline{X}}_{Ri}) \quad (B-4a)$$

where

$$\underline{Y}_{cR}^T = \{ y_{c1}(\underline{X}_{R1}) \cdots y_{cp}(\underline{X}_{Rp}) \} \quad (B-4b)$$

$$\underline{G}_R = \begin{bmatrix} \underline{G}_{R1}^T \\ \vdots \\ \underline{G}_{Rp}^T \end{bmatrix} \quad (B-4c)$$

ORIGINAL PAGE IS  
OF POOR QUALITY

$$\underline{B}_R = \begin{pmatrix} \underline{G}_{R1}^T \cdot \underline{X}_{R1} \\ \vdots \\ \underline{G}_{Rp}^T \cdot \underline{X}_{Rp} \end{pmatrix} \quad (B-4d)$$

and

$$\underline{G}_{Ri} = \frac{\partial y_{ci}}{\partial \underline{\hat{X}}} (\underline{X}_{Ri})^T \quad (i = 1 \text{ to } p) \quad (B-4e)$$

$s \times 1$

The last expression on the right side of Equation (B-4a) signifies higher order terms in the series. In addition to Equation (B-4a), the Taylor series expansion of the partial derivative of  $\underline{Z}$  with respect to  $\underline{\hat{X}}^*$  is also needed. This can be obtained by differentiating Equation (B-4a).

$$\frac{\partial \underline{Z}}{\partial \underline{\hat{X}}} (\underline{\hat{X}}^*) = -\underline{G}_R + \text{H. O. T.} (\underline{\hat{X}}^* - \underline{X}_{Ri}) \quad (B-5)$$

$p \times s$

Substituting Equation (B-4) and (B-5) into (B-3), dropping the higher order terms (H. O. T.), and performing some minor algebraic manipulation yields

$$\begin{aligned} \left[ \underline{s}_0 + \underline{G}_{1R}^T \underline{W}_1 \underline{G}_{1R} \right] \left( \underline{\hat{X}}_1 - \underline{\hat{X}}_0 \right) &= \underline{G}_{1R}^T \underline{W}_1 \left( \underline{Y}_1 - \underline{Y}_{C1R} \right) \\ &+ \underline{B}_{1R} - \underline{G}_{1R} \underline{\hat{X}}_0 \end{aligned} \quad (B-6)$$

The previously noted 1 subscripts which signify that the estimate is obtained from data set number 1 have been inserted into Equation (B-6) for convenience in future references to the equation. Also, the optimal estimate will now be signified merely by  $\underline{\hat{X}}$  rather than by  $\underline{\hat{X}}^*$ . This simplification is being made

**ORIGINAL PAGE IS  
OF POOR QUALITY**

because the \* no longer serves a useful purpose. Also, it brings the current notation into closer agreement with that commonly used in Computer Sciences Corporation reports.

For the remainder of this section, the work can be restricted to the case where all reference vectors  $\underline{X}_{Ri}$  are identical;  $\underline{X}_{Ri} = \underline{X}_{1R}$  where  $i = 1$  to  $p$ . Equation (B-4) shows that  $\underline{B}_{1R}$  can be replaced by  $G_{1R} \underline{X}_{1R}$ .

Let  $Q_1$  be the  $s \times s$  coefficient matrix on the left side of Equation (B-6).

Equation (B-6) possesses a unique solution if, and only if,  $Q_1$  is nonsingular. Assuming that both  $S_0$  and  $G_{1R}^T W_1 G_{1R}$  are at least positive semidefinite, a sufficient condition for nonsingular  $Q_1$  is that one or both of the pair be positive definite. Positive definiteness of  $G_{1R}^T W_1 G_{1R}$  signifies that  $\underline{X}$  is observable from the set 1 observations alone. Nonsingularity of  $Q_1$  can be assured by choosing  $S_0$  to be positive definite.

In the nonsingular  $Q_1$  case, Equation (B-6) can be solved for  $\hat{\underline{X}}_1$ , and the result written as follows:

$$\hat{\underline{X}}_1 = \hat{\underline{X}}_0 + \underset{s \times p}{K_1} \left\{ \underset{p \times 1}{Y_1} - \underset{p \times 1}{Y_{c1R}} + \underset{p \times s}{G_{1R}} \left\{ \underset{s \times 1}{\underline{X}_{1R}} - \hat{\underline{X}}_0 \right\} \right\} \quad (B-7a)$$

where

$$\underset{s \times p}{K_1} = \underset{s \times s}{P_1} \underset{p \times s}{G_{1R}^T} \underset{p \times p}{W_1} \quad (B-7b)$$

$$\underset{s \times s}{P_1} = \underset{s \times s}{Q_1}^{-1} \quad (B-7c)$$

$$\underset{s \times s}{Q_1} = \underset{s \times s}{S_0} + \underset{p \times s}{G_{1R}^T} \underset{p \times p}{W_1} \underset{s \times p}{G_{1R}} \quad (B-7d)$$

At this point in the development, no special significance can be attached to  $Q_1$  and  $P_1$ ; they are merely convenient matrices for use in the equations.

Equation (B-7) constitutes a slightly generalized form of the usual nonrecursive least-squares algorithm. When employing this equation for batch processing, the reference vector  $\underline{x}_{1R}$  normally is set equal to the a priori estimate  $\hat{\underline{x}}_0$ . This enables the  $G_{1R}$  matrix on the right side of Equation (B-7a) to be discarded. It will be recalled, however, that when deriving Equation (B-7), it was necessary to truncate the higher order terms of Equations (B-4a) and (B-5). Thus, the  $\hat{\underline{x}}_1$  result of Equation (B-7a) will minimize the loss function  $\ell_1$  defined by Equation (B-1) only when  $\hat{\underline{x}}_1$  is sufficiently close to  $\underline{x}_{R1}$  (now  $\underline{x}_{1R} = \hat{\underline{x}}_0$ ) that the error due to discarding the higher order terms is negligibly small. An iterative processing operation, called differential correction, commonly is performed to overcome this difficulty. With this technique, data set 1 is passed through the processor several times. The state vector estimate obtained in any given pass becomes the a priori estimate for the following pass. In order to delineate the operation mathematically, let superscript  $\lambda$  denote the  $\lambda$ th pass through the processor. Equation (B-7) then can be converted to the following form:

$$\hat{\underline{x}}_1^\lambda = \hat{\underline{x}}_1^{\lambda-1} + \Delta \hat{\underline{x}}_1^\lambda \quad (\text{B-8a})$$

$$\Delta \hat{\underline{x}}_1^\lambda = K_1^\lambda \left\{ \underline{y}_1 - \underline{y}_{c1} \left( \hat{\underline{x}}_1^{\lambda-1} \right) \right\} \quad (\text{B-8b})$$

$$K_1^\lambda = P_1^\lambda G_1 \left( \hat{\underline{x}}_1^{\lambda-1} \right) W_1 \quad (\text{B-8c})$$

$$P_1^\lambda = \left[ Q_1^\lambda \right]^{-1} \quad (\text{B-8d})$$

$$Q_1^\lambda = S_0 + G_1 \left( \hat{\underline{x}}_1^{\lambda-1} \right)^T W_1 G_1 \left( \hat{\underline{x}}_1^{\lambda-1} \right) \quad (\text{B-8e})$$

ORIGINAL PAGE IS  
OF POOR QUALITY

and

$$\hat{\underline{X}}^{\infty} = \hat{\underline{X}}_0 \quad (\text{B-8f})$$

The process is said to have converged when the elements of  $\Delta \hat{\underline{X}}_1^\lambda$  become negligibly small. The iterative operations tend to degrade the meaning and usefulness of  $S_0$ . Equations (B-8a) through (B-8f) are equivalent to those used by GCONES, except GCONES does not include  $S_0$ .

#### B.4 DERIVATION OF A PRELIMINARY RECURSIVE LEAST-SQUARES ALGORITHM

The preliminary recursive least-squares algorithm derived in this section is not the algorithm used in OABIAS. However, it is a necessary by-product in the present derivation of the OABIAS equation and is of some significance in its own right.

Assume that data set 1 has been processed, iteratively or noniteratively, and that the final results  $\hat{\underline{X}}_1$  and  $P_1$  of  $Q_1$  have been saved. Let data set 2 now be received. Set 2 contains  $q$  scalar observations ( $q \geq 1$ ). Let the data set which is comprised of both sets 1 and 2 be denoted as set  $\Sigma$ . Set  $\Sigma$  contains  $r = p + q$  scalar observations where  $r \geq 2$ . The problem now is to obtain a new estimate  $\hat{\underline{X}}_2$  utilizing all the observations in set  $\Sigma$ ; the subscript 2 signifies that the estimate employs all data sets up to and including set 2. The batch processing approach to the problem would process the composite set  $\Sigma$  in the same way that set 1 was processed. With appropriate changes in subscripts, the equations developed in Section B.3 are applicable to this method. In essence, the method minimizes a loss function  $l_\Sigma$  defined by

$$l_\Sigma = 0.5 \sum_{\Sigma} Z^T \sum_{\Sigma} \frac{W}{r \times r} \frac{Z}{r \times 1} + 0.5 \begin{vmatrix} \hat{\underline{X}}_2 \\ \hat{\underline{X}}_0 \end{vmatrix}^T S_0 \begin{vmatrix} \hat{\underline{X}}_2 \\ \hat{\underline{X}}_0 \end{vmatrix} \quad (\text{B-9a})$$

where

$$\underline{Z}_{\Sigma}^T = \begin{Bmatrix} \underline{Z}_1^T & \underline{Z}_2^T \end{Bmatrix} \quad (\text{B-9b})$$

$$W_{\Sigma} = \begin{bmatrix} W_1 & W_{12} \\ W_{12}^T & W_2 \end{bmatrix} \quad (\text{B-9c})$$

The major drawback of this approach is that the resulting algorithm [Equation (B-7) or (B-8)] with appropriate changes in subscripts) includes vectors and matrices with dimensions equal to the total number of scalar observations  $r$  in set  $\Sigma$ . This increases the computation and storage requirements. If the approach is continued when additional data sets come in, these requirements will increase without bound.

The recursive processing approach to the problem uses only the new observations  $\underline{Y}_2$  and the results  $\hat{\underline{X}}_1$  and  $P_1$  or  $Q_1$  obtained from processing set 1. With these approaches  $\hat{\underline{X}}_2$  is the estimate which minimizes a loss function  $l_2$  defined by

$$l_2 = 0.5 \underline{Z}_2^T \begin{matrix} W_2 \\ q \times q \end{matrix} \underline{Z}_2 + 0.5 \begin{Bmatrix} \hat{\underline{X}}_2 - \hat{\underline{X}}_1 \end{Bmatrix}^T \begin{matrix} S_1 \\ s \times s \end{matrix} \begin{Bmatrix} \hat{\underline{X}}_2 - \hat{\underline{X}}_1 \end{Bmatrix} \quad (\text{B-10})$$

As will be shown later in this section, the recursive processing approach requires that  $W_{12} = 0$ . Comparison of Equation (B-10) with the loss function  $l_1$  of Equation (B-1) indicates that the batch processing equations developed in Section B.3 are applicable to this case with appropriate changes in subscripts and thus constitute a valid recursive processing algorithm. However, the problem of selecting  $S_1$  remains. Arbitrary selection of  $S_1$ , independent of  $S_0$ , is undesirable. A better approach is to establish  $S_1$  such that the

**ORIGINAL PAGE IS  
OF POOR QUALITY**

$\underline{X}_2$  computed by the recursive method is identical (at least under certain conditions) to the estimate obtained using the batch processing technique which minimizes  $\ell_{\Sigma}$ . An algorithm for computing  $S_1$  as a function of  $S_0$  is needed. The remainder of this section is devoted to this problem.

The derivation starts with Equation (B-6). Altering the 1 subscripts to make the equation applicable to set  $\Sigma$  yields

$$\begin{aligned} \left[ \begin{array}{c} S_0 + G_{\Sigma R}^T W_{\Sigma} G_{\Sigma R} \\ r \times s \end{array} \right] \begin{array}{c} | \underline{X}_2 - \underline{X}_0 | \\ r \times 1 \end{array} &= G_{\Sigma R}^T W_{\Sigma} \begin{array}{c} | \underline{Y}_{\Sigma} - \underline{Y}_{c\Sigma R} + \underline{B}_{\Sigma R} \\ r \times 1 \end{array} \\ &\quad - G_{\Sigma R} \hat{\underline{X}}_0 \end{aligned} \quad (B-11)$$

where

$$G_{\Sigma R}^T = \begin{bmatrix} G_{1R}^T & G_{2R}^T \end{bmatrix} \quad (B-12a)$$

$$\underline{Y}_{\Sigma}^T = \left\{ \underline{Y}_1^T \quad \underline{Y}_2^T \right\} \quad (B-12b)$$

$$\underline{Y}_{c\Sigma R}^T = \left\{ \underline{Y}_{c1R}^T \quad \underline{Y}_{c2R}^T \right\} \quad (B-12c)$$

$$\underline{B}_{\Sigma R}^T = \left\{ \underline{B}_{1R}^T \quad \underline{B}_{2R}^T \right\} \quad (B-12d)$$

$$W_{\Sigma} = \begin{bmatrix} W_1 & W_{12} \\ W_{12}^T & W_2 \end{bmatrix} \quad (B-12e)$$

ORIGINAL PAGE  
OF POOR QUALITY

For use below, let the corresponding set 1 equation (B-6) be rewritten in the following form:

$$\left[ S_o + G_{1R}^T W_1 G_{1R} \right] \hat{X}_1 = S_o \hat{X}_o + G_{1R}^T W_1 \left\{ Y_1 - Y_{c1R} + B_{1R} \right\} \quad (B-13)$$

Equation (B-11) now is written in its full form by inserting Equation (B-12).

$$\left[ S_o + \begin{bmatrix} G_{1R}^T & G_{2R}^T \end{bmatrix} \begin{bmatrix} W_1 & W_{12} \\ W_{1w}^T & W_2 \end{bmatrix} \begin{bmatrix} G_{1R} \\ G_{2R} \end{bmatrix} \right] \left\{ \hat{X}_2 - \hat{X}_o \right\} = \begin{bmatrix} G_{1R}^T & G_{2R}^T \end{bmatrix} \begin{bmatrix} W_1 & W_{12} \\ W_{12}^T & W_2 \end{bmatrix} \left\{ \begin{array}{l} \left\{ Y_1 - Y_{c1R} + B_{1R} \right\} - \begin{bmatrix} G_{1R} \\ G_{2R} \end{bmatrix} \hat{X}_o \\ \left\{ Y_2 - Y_{c2R} + B_{2R} \right\} \end{array} \right\} \quad (B-14)$$

Performing the matrix multiplications in Equation (B-14), canceling identical  $\hat{X}_o$  terms where possible, and rearranging the result slightly yields

$$\begin{aligned} & \left[ S_o + G_{1R}^T W_1 G_{1R} + G_{2R}^T W_2 G_{2R} + G_{1R}^T W_{12} G_{2R} + G_{2R}^T W_{12}^T G_{1R} \right] \hat{X}_2 \\ & = \left[ S_o \hat{X}_o + G_{1R}^T W_1 \left\{ Y_1 - Y_{c1R} + B_{1R} \right\} \right] + \left[ G_{2R}^T W_{12}^T \left\{ Y_1 - Y_{c1R} + B_{1R} \right\} \right] \quad (B-15) \\ & + \left[ G_{1R}^T W_{12} \left\{ Y_2 - Y_{c2R} + B_{2R} \right\} \right] + \left[ G_{2R}^T W_2 \left\{ Y_2 - Y_{c2R} + B_{2R} \right\} \right] \end{aligned}$$

Development of a recursive algorithm requires elimination of terms involving  $\hat{X}_o$ ,  $Y_1$ ,  $Y_{c1R}$ , and  $B_{1R}$  from Equation (B-15). The terms within the first set of brackets on the right side thus are unacceptable. These, however, are identical to the right side of Equation (B-13) and hence can be replaced by the left side of (B-13). The remaining unacceptable terms in Equation (B-15) are those inside the second set of brackets on the right side. These involve the coupling matrix  $W_{12}$ . To obtain the desired recursive processing algorithm,  $W_{12}$  must be restricted to zero.

**ORIGINAL PAGE IS  
OF POOR QUALITY**

A restriction that all reference vectors  $\underline{X}_{2Ri}$  in set 2 are identical ( $\underline{X}_{2Ri} = \underline{X}_{2R}$ , where  $i = 1$  to  $q$ ) now is acceptable. This enables  $\underline{B}_{2R}$  to be replaced by  $G_{2R} \underline{X}_{2R}$ . The concept of nonidentical reference vectors was a mathematical tool used to avoid the restriction that the same Taylor series expansion reference vector be employed for both set 1 and set 2. The tool now has served its purpose in the derivation and is no longer necessary.

The desired recursive processing algorithm is obtained by implementing the above-noted operations into Equation (B-15) and performing a few minor additional algebraic manipulations. The result is

$$\hat{\underline{X}}_2 = \hat{\underline{X}}_1 + \underset{s \times q}{K_2} \left\{ \underset{q \times s}{\underline{Y}_2 - \underline{Y}_{c2R} + G_{2R} \left\{ \underline{X}_{2R} - \hat{\underline{X}}_1 \right\}} \right\} \quad (\text{B-16a})$$

$$K_2 = \underset{s \times s}{P_2} G_{2R}^T W_2 \quad (\text{B-16b})$$

$$P_2 = Q_2^{-1} \quad (\text{B-16c})$$

$$Q_2 = \underset{s \times s}{Q_1} + G_{2R}^T W_2 G_{2R} \quad (\text{B-16d})$$

where

$$Q_1 = S_0 + G_{1R}^T W_1 G_{1R} \quad (\text{B-17})$$

Equations (B-7) and (B-16) constitute a valid method for processing data sets 1 and 2 sequentially. They can, in fact, be generalized immediately for sequential processing of an arbitrary number of data sets. Before doing this, however, it is desirable to answer the previous question concerning the correct weighting factor  $S_1$  for Equation (B-10). It should be evident that

ORIGINAL PAGE 13  
OF POOR QUALITY

direct use of Equation (B-10) to derive an optimal estimate  $\hat{X}_2$  with  $\hat{X}_1$  and  $S_1$  as the a priori inputs would yield results identical to Equation (B-7) obtained from the  $k_1$  equation, except the 1 and 0 subscripts would be replaced by 2 and 1, respectively. Equation (B-7d) would now be

$$Q_2 = S_1 + G_{2R}^T W_2 G_{2R} \quad (B-18)$$

The results obtained from Equation (B-10) should be identical to those of Equations (B-16) and (B-17). Comparing Equation (B-18) with Equations (B-16d) and (B-17), it is concluded that

$$S_1 = Q_1 = S_0 + G_{1R}^T W_1 G_{1R} \quad (B-19)$$

Equation (B-19) is the desired equation for updating  $S_0$  to obtain  $S_1$ . It is evident that this result can be extended to yield  $S_2 = Q_2$ ,  $S_3 = Q_3$ , etc.

Because the variables  $Q$  can be replaced by  $S$ , their use has become superfluous. Also, superscripts 2 and 1 of Equation (B-16) can be replaced by more general ones  $j$  and  $j - 1$ . Therefore, the final recursive processing equations of this section are

$$\hat{X}_j = \hat{X}_{j-1} + K_j \left\{ Y_j - Y_{cjR} + G_{jR} \left[ X_{jR} - \hat{X}_{j-1} \right] \right\} \quad (B-20a)$$

$$K_j = P_j G_{jR}^T W_j \quad (B-20b)$$

$$P_j = S_j^{-1} \quad (B-20c)$$

$$S_j = S_{j-1} + G_{jR}^T W_j G_{jR} \quad (B-20d)$$

ORIGINAL PAGE IS  
OF POOR QUALITY

B.5 DERIVATION OF THE RECURSIVE LEAST-SQUARES ALGORITHM USED  
IN OABIAS

Equation (B-20) or the equivalent usually is considered to constitute a poor recursive processing algorithm because the inversion of an  $s \times s$  matrix is required at each step. They are not used in OABIAS and hence constitute only an intermediate result in the present development.

In deriving the OAPLAS algorithm, Equations (B-20c) and (B-20d) first are combined into

$$P_j = \left[ P_{j-1}^{-1} + G_{jR}^T W_j G_{jR} \right]^{-1} \quad (B-21)$$

Equation (B-20) now is manipulated using the following matrix identity

$$\left[ A^{-1} + BC \right]^{-1} = A - \hat{A}B \left[ I + CAB \right]^{-1} CA \quad (B-22)$$

with  $A = P_{j-1}$   
 $B = G_{jR}^T$   
 $C = W_j G_{jR}$

The result is

$$P_j = P_{j-1} - P_{j-1} G_{jR}^T \left\{ \left[ I + W_j G_{jR} P_{j-1} G_{jR}^T \right]^{-1} W_j \right\} G_{jR} P_{j-1} \quad (B-23)$$

ORIGINAL PAGE IS  
OF POOR QUALITY

Now assume that  $W_j$  is nonsingular and manipulate the term within the brackets using the matrix identity

$$D^{-1} W = [W^{-1} D]^{-1} \quad (B-24)$$

The result is

$$P_j = P_{j-1} - P_{j-1} G_{jR} \left[ W_j^{-1} + G_{jR} P_{j-1} G_{jR}^T \right]^{-1} G_{jR} P_{j-1} \quad (B-25)$$

Equation (B-25) now is substituted into Equation (B-20b) to give

$$\begin{aligned} K_j &= P_{j-1} \left\{ 1 - G_{jR}^T \left[ W_j^{-1} + G_{jR} P_{j-1} G_{jR}^T \right]^{-1} G_{jR} P_{j-1} \right\} G_{jR}^T W_j \\ &= P_{j-1} G_{jR}^T \left\{ 1 - \left[ W_j^{-1} + G_{jR} P_{j-1} G_{jR}^T \right]^{-1} G_{jR} P_{j-1} G_{jR}^T \right\} W_j \\ &= P_{j-1} G_{jR}^T \left[ W_j^{-1} + G_{jR} P_{j-1} G_{jR}^T \right]^{-1} \end{aligned} \quad (B-26)$$

To finish the derivation, Equation (B-26) is substituted into Equation (B-25) to simplify the equation for  $P_j$ . The final equations for the new processing algorithm are

$$\hat{X}_j = \hat{X}_{j-1} + K_j \left\{ Y_j - Y_{cJR} + G_{jR} \left[ X_{jR} - \hat{X}_{j-1} \right] \right\} \quad (B-27a)$$

$$K_j = P_{j-1} G_{jR}^T \left[ W_j^{-1} + G_{jR} P_{j-1} G_{jR}^T \right]^{-1} \quad (B-27b)$$

$$P_j = [I - K_j G_{jR}] P_{j-1} \quad (B-27c)$$

**ORIGINAL PAGE IS  
OF POOR QUALITY**

Assuming that  $W_j$  is passed to the recursive processor, a processor which employs Equation (B-27) must invert two  $p_j \times p_j$  matrices in each processing step  $j$ , where  $p_j$  is the number of scalar observations on set  $j$ . Only one  $p_j \times p_j$  matrix inversion is needed if the processor is given  $W_j^{-1}$ . However, the observations can be processed one at a time in applications where all off-diagonal elements  $W_{\mu\nu}$ , where  $\mu \neq \nu$ , of the weighting matrix  $W_{\Sigma}$  can be made zero. This method avoids matrix inversions and minimizes computer storage requirements. Assuming the observations to be processed one at a time enables Equation (B-27) to be converted into the following form

$$y_{cjR} = y_{cj} (X_{jR}) \quad (B-28a)$$

$$G_{jR} = w_j (X_{jR}) \quad (B-28b)$$

$s \times 1$

$$K_j = \left[ w_j^{-1} + G_{jR}^T P_{j-1} G_{jR} \right]^{-1} P_{j-1} G_{jR} \quad (B-28c)$$

$s \times 1$

$$P_j = \begin{bmatrix} I & -K_j G_{jR}^T \\ s \times s & \end{bmatrix} P_{j-1} \quad (B-28d)$$

$$\Delta \hat{X}_j = K_j \left\{ y_j - y_{cjR} - G_{jR}^T \left( \hat{X}_{j-1} - X_{jR} \right) \right\} \quad (B-28e)$$

$$\hat{X}_j = \hat{X}_{j-1} + \Delta \hat{X}_j \quad (B-28f)$$

Unlike the other equations of this appendix, Equations (B-28a) through (B-28f) have been arranged into a possible sequence for utilization in a computer routine. These equations are the end result of this appendix and are the basic recursive estimation equations used in OABIAS except for implement modifications discussed in Section 3.4.

GLOSSARY

The symbols most commonly used in this document are listed below. References are provided to figures or equations in which symbols are defined whenever such figures or equations occur. The most common superscripts, subscripts, and overhead symbols are listed at the end of the glossary.

<u>Symbol</u>	<u>Definition</u>
$A$	A 3 x 3 matrix which transforms vectors from frame GI resolution to frame SC resolution (reference Figure 3-1)
$A_d$	A dihedral angle
$A_{d5}$	The Model 5 dihedral angle (reference Figure 3-10)
$A_{d6}$	The Model 6 dihedral angle (reference Figure 3-11)
$A_{d8}$	The Model 8 dihedral angle (reference Figure 3-13)
$A_{\mu\nu}$	The elements of $A$
$B$	A symbol used to indicate either $B_I$ or $B_O$ in equations that are applicable to both
$B_I$	A 3 x 3 matrix which transforms vectors from frame HI' resolution to frame SC resolution (reference Figure 3-1)
$B_O$	A 3 x 3 matrix which transforms vectors from frame HO' resolution to frame SC resolution (reference Figure 3-1)
$B_R$	Defined in Equation (B-4d)
$BOT$	The denominators in the equations for $\tan A_{d5}$ , $\tan A_{d6}$ , or $\tan A_{d8}$
$b_{\mu\nu}$	The elements of $B$

**ORIGINAL PAGE IS  
OF POOR QUALITY**

Symbol	Definition
$c$	Cosine
$\hat{D}$	A symbol used to indicate either $\hat{D}_I$ or $\hat{D}_O$ in equations that are applicable to both (reference Figure 3-9)
$\hat{D}_I$	The unit vector directed from the spacecraft toward the horizon-in crossing point on the central body surface
$\hat{D}_O$	The unit vector directed from the spacecraft toward the horizon-out crossing point on the central body surface
Det	The determinant of the $2 \times 2$ matrix in Equation (3-72a)
Det M	The determinant of M
$d_1, d_2, d_3$	The components of $\hat{D}$ along the axes of frame GI
$d\underline{M}$	The vector of the errors in a set of measurements $\underline{M}$
$dm_\alpha$	The error in element $m_\alpha$ of $\underline{M}$
$d\underline{Y}$	The vector of the errors in a set of observations $\underline{Y}$
$dy_j$	The error in element $y_j$ of $\underline{Y}$
E	The angle generated by Sun sensor misalignment $\epsilon$ (reference Figure 3-10); also, expectation operator
$\hat{e}$	A symbol used to signify a unit vector along an axis of a reference coordinate frame
$\hat{e}_a$	See Figure 3-9
$\hat{e}_{S1}, \hat{e}_{S2}, \hat{e}_{S3}$	The unit vectors along the axes of frame SS
$\hat{e}_1, \hat{e}_2, \hat{e}_3$	The unit vectors along the axes of frame GI
$\hat{e}'_1, \hat{e}'_2, \hat{e}'_3$	The unit vectors along the axes of frame SC
$\hat{e}''_{I1}, \hat{e}''_{I2}, \hat{e}''_{I3}$	The unit vectors along the axes of frame HI
$\hat{e}''_{O1}, \hat{e}''_{O2}, \hat{e}''_{O3}$	The unit vectors along the axes of frame HO

ORIGINAL PAGE IS  
OF POOR QUALITY

<u>Symbol</u>	<u>Definition</u>
FOV	Field of view
G	The partial derivative matrix of computed observation vector $\underline{Y}_c$ with respect to state vector $\underline{X}$
$\underline{G}_j$	The partial derivative vector of computed observation $y_{cj}$ with respect to state vector $\underline{X}$ ; the jth column of $G^T$
GI'	The geocentric inertial frame (usually the true-of-date frame); $x_{GI}$ directed toward the vernal equinox of epoch, $z_{GI}$ directed toward the celestial north pole of epoch
GI	The geocentric inertial frame used internally in OBIAS
$g_\eta$	The partial derivative of computed observation $y_c$ with respect to $x_\eta$ ; the $\eta$ th element of $\underline{G}$
H	The partial derivative matrix of observation vector $\underline{Y}$ with respect to measurement vector $\underline{M}$
HI	The horizon detector line-of-sight frame for in-crossings $z_{HI}$ along $\hat{L}_I$ (reference Figures 3-1 and 3-5)
HI'	The horizon detector alignment frame for in-crossings (reference Figure 3-1)
HO	The horizon detector line-of-sight frame for out-crossings; $z_{HO}$ along $\hat{L}_O$ (reference Figure 3-1)
HO'	The horizon detector alignment frame for out-crossings (reference Figure 3-1)
H. O. T.	Higher order terms
h	The effective height of the atmosphere (reference Figure 3-14)
$\underline{h}_j$	The jth column of $\underline{H}^T$
$h_{j\alpha}$	The $\alpha$ th element of $\underline{h}_j$
I	Identity matrix

Symbol	Definition
$\hat{i}, \hat{j}, \hat{k}$	The unit vectors along the axes of frame SC
$K, K_j$	The gain matrix of an estimation algorithm
$\underline{K}_j$	The gain vector of the estimation algorithm used in OABIAS
$\vec{L}$	The vector from the spacecraft to the horizon crossing point (reference Figure 3-14)
$L$	The magnitude of $\vec{L}$
$\hat{L}$	The unit vector directed along $\vec{L}$
$l$	The least-squares loss function [reference Equation (B-1a)]
$l_{1GI}, l_{2GI}, l_{3GI}$	The components of $L$ along the axes of frame GI
$l_{1SC}, l_{2SC}, l_{3SC}$	The components of $L$ along the axes of frame SC
$M$	A matrix whose three rows are the components of the three vectors $\hat{S}$ , $\hat{R}$ , and $\hat{D}$ , respectively, along the axes of frame GI
$\underline{M}$	A vector composed of a set of scalar measurements
$\underline{M}_j$	A subvector of $\underline{M}$
$\underline{m}$	A vector composed of the four measurements $\beta_M$ , $t_s$ , $t_{III}$ , and $t_{HO}$ provided in a single telemetry frame
$m_\alpha$	An element of $\underline{M}$
$m_{j\alpha}$	An element of $\underline{M}_j$
$\hat{N}_{III}, \hat{N}_{HO}$	The unit vectors along the $y$ axes of frames HI and HO (reference Figure 3-9)
$\hat{N}_s, \hat{N}_S$	The unit vector along the $y$ axis of frame SS (reference Figure 3-1)

**ORIGINAL PAGE IS  
OF POOR QUALITY**

Symbol	Definition
$n_{H1GI}, n_{H2GI}, n_{H3GI}$	The components of $\hat{N}_H$ along the axes of frame GI
$n_{H1SC}, n_{H2SC}, n_{H3SC}$	The components of $\hat{N}_H$ along the axes of frame SC
$n_1, n_2, n_3$	The components of $\hat{N}_S$ along the axes of frame GI
$P$	A matrix generated in the estimation computations; usually considered to be the estimated covariance matrix of the error in $\hat{X}$
$P_0$	The a priori $P$ matrix
$p_1, p_2$	Defined in Equations (3-75c and 3-75d)
$Q$	The inverse $P^{-1}$ of the estimated covariance matrix $P$ of a state vector estimate $\hat{X}$
$Q_1, Q_2, Q_3$	The columns of the inverse $M^{-1}$ of the $3 \times 3$ matrix $M$
$q_1, q_2$	Defined in Equations (3-75e) and (3-75f)
$\vec{R}$	The vector from the spacecraft to the center of the central body
$R,  \vec{R} $	The magnitude of $\vec{R}$
$\hat{R}$	The unit vector oriented in the direction of $\vec{R}$
$R_e$	Radius of the Earth (reference Figure 3-14)
$\vec{R}_e$	The vector from the center of the central body to the effective horizon crossing point (reference Figure 3-14)
$\hat{R}_e$	The unit vector in the direction of $\vec{R}_e$ (reference Figure 3-14)
$R_M$	The covariance matrix of a set of measurements $\underline{M}$

ORIGINAL PAGE IS  
OF POOR QUALITY

Symbol	Definition
$R_Y$	The covariance matrix of a set of observations $\underline{Y}$
$R_{M_j}$	The $j$ th element on the diagonal of $R_M$
$R_1, R_2, R_3$	The components of $\vec{R}$ along the axes of frame GI
$r_1, r_2, r_3$	The components of $\hat{R}$ along the axes of frame GI
$\hat{S}$	The unit vector along the spacecraft spin axis
$S_0$	The weighting matrix in least-squares loss function $\ell_1$ [reference Equation (B-1a)]
$S_1$	The weighting matrix in least-squares loss function $\ell_2$ [reference Equation (B-10)]
SC	The spacecraft-fixed reference frame; $z_{SC}$ along $\hat{S}$ (reference Figure 3-1)
SI	The inertial frame with $z_{SI}$ along $\hat{S}$ (reference Fig- ure 3-1)
SS, ss	The Sun sensor-fixed reference frame (reference Fig- ure 3-1)
s	Sine
$s_1, s_2, s_3$	The components of $\hat{S}$ along the axes of frame GI; $s_1$ and $s_2$ are elements $x_1$ and $x_2$ of $\underline{X}$
$T_\alpha(x_i)$	A 3 x 3 matrix which transforms vector components from the axes of an initial frame, a, to those of a new frame, b, where frame b is generated by rotating frame a about one of its axes ( $x_i = x_a, y_a, \text{ or } z_a$ ) through an angle $\alpha$
TOP	The numerators in the equations for $\tan A_{d5}, \tan A_{d6},$ $\tan A_{d7}$
	Time

ORIGINAL PAGE IS  
OF POOR QUALITY

Symbol	Definition
$t_H$	The time at which a horizon crossing, in or out, is encountered
$t_{HI}$	The time at which a horizon-in crossing is encountered
$t_{HO}$	The time at which a horizon-out crossing is encountered
$t_j$	The time at which an observation $j$ was obtained
$t_o$	The initial or reference time
$t_s$	The time at which a Sun sighting is encountered
$\hat{U}$	The unit vector along the Sunline (reference Figure 3-4)
$u_1, u_2, u_3$	The components of $\hat{U}$ along the axes of frame GI
$u'_1, u'_2, u'_3$	The components of $\hat{U}$ along the axes of frame GI'
$\vec{V}$	The velocity vector of the spacecraft center of mass
$v_j$	The error in observation $j$
$W$	The observation weighting factor matrix
$w_j$	The weighting factor for observation $j$
$w_j^*$	The optimum value of $w_j$ [reference Equation (3-11)]
$\underline{X}$	The true state vector
$\hat{\underline{X}}$	The estimate of $\underline{X}$
$\hat{\underline{X}}^*$	The optimal estimate of $\underline{X}$
$\underline{X}_R$	The reference value of $\underline{X}$
$\underline{X}_S$	The subvector of $\underline{X}$ composed of the Sun sensor bias parameters
$\hat{\underline{X}}_o$	The a priori estimate of $\underline{X}$

Symbol	Definition
$\underline{Y}$	A vector of "real" observations computed algebraically from a vector $\underline{M}$ of measurements
$\underline{Y}_c$	A vector of "computed" observations obtained using a mathematical model and an estimate of the system's state vector $\underline{X}$
$y_j$	The jth element of $\underline{Y}$
$y_{cj}$	The jth element of $\underline{Y}_c$
$\underline{Z}$	The vector of residuals; $\underline{Z} = \underline{Y} - \underline{Y}_c$
$z_j$	The jth element of $\underline{Z}$
$\alpha$	The right ascension angle of $\hat{S}$ relative to frame GI
$\alpha'$	The right ascension angle of $\hat{S}$ relative to frame GI'
$\beta$	The angle between $\hat{S}$ and $\hat{U}$ (reference Figure 3-4)
$\beta_M$	The angle measured by the Sun sensor; ideally identical to $\beta$ (reference Figure 3-4)
$\gamma$	The angle between $\hat{L}$ and $\hat{S}$ (reference Figure 2-3)
$\gamma_s, \gamma_S$	The angle of horizon detector line-of-sight vector $\hat{L}$ relative to the detector's reference axis $\hat{z}_{H'}$ ; ideally identical to $\gamma$ (reference Figure 2-3)
$\Delta H$	The perturbation in dihedral angle $A_d$ due to horizon detector misalignment angle $\epsilon_H$ (reference Figure 3-10)
$\Delta s$	The perturbation in dihedral angle $A_d$ due to Sun sensor misalignment angle $\epsilon$ (reference Figure 3-10)
$\Delta t$	A time bias in the location of the spacecraft in its orbit; element $x_{12}$ of $\underline{X}$
$\Delta X_j$	The correction to state vector estimate $\underline{X}_{j-1}$ or to reference state vector $\underline{X}_R$ generated by processing observation j [reference Equations (3-3) or (3-12)]

ORIGINAL PAGE IS  
OF POOR QUALITY

Symbol	Definition
$\Delta\beta$	The bias in Sun angle measurement; element $x_8$ of $\underline{X}$ (reference Figure 3-4)
$\Delta\gamma$	The horizon detector alignment error; element $x_4$ of $\underline{X}$ (reference Figure 2-3)
$\Delta\rho$	A bias in the effective angular radius $\rho$ of the central body; element $x_7$ of $\underline{X}$
$\Delta\phi_H^I$	The bias on horizon detector azimuth angle $\phi_H$ at horizon-in crossings
$\Delta\phi_H^O$	The bias on horizon detector azimuth angle $\phi_H$ at horizon-out crossings
$\delta$	The declination angle of $\hat{S}$ relative to frame GI
$\delta'$	The declination angle of $\hat{S}$ relative to frame GI'
$\delta'_0$	The a priori value of $\delta'$
$\epsilon$	The alignment error of the Sun sensor; element $x_{10}$ of $\underline{X}$ (reference Figure 3-4)
$\epsilon_H$	The alignment error of the horizon detector; element $x_{11}$ of $\underline{X}$ (reference Figure 2-3)
$\zeta$	The angle between horizon crossing vector $\hat{D}$ and horizon detector reference axis $\hat{N}_H$ (reference Figure 3-9)
$\eta$	The Sun sensor FOV value (reference Figure 2-1)
$\Lambda$	$90-\epsilon$ (reference Figure 3-10)
$\lambda$	The latitude of the horizon crossing location on the central body surface
$\lambda_0$	The geocentric latitude of the spacecraft; initial estimate of $\lambda$
$\nu$	The angle between $\hat{S}-\hat{D}$ plane and $\hat{D}-\hat{R}$ plane (reference Figure 3-15)

**ORIGINAL PAGE IS  
OF POOR QUALITY**

<u>Symbol</u>	<u>Definition</u>
$\xi_m$	The elevation mounting angle of the Sun sensor relative to the plane perpendicular to the spacecraft's spin axis (reference Figure 2-1)
$\xi_s$	The elevation angle of the Sun relative to the Sun sensor (reference Figure 2-1)
$\rho$	The angular radius of the central body at the horizon crossing point as seen from the spacecraft (reference Figure 3-8)
$\rho_c$	The computed value of $\rho$
$\sigma$	$-\hat{R} \cdot \hat{S}$ secant $\epsilon_H$
$\sigma_H^2$	The variance of the error in the horizon crossing time measurements
$\sigma_{m_j\alpha}^2$	The variance of the error in measurement $m_{j\alpha}$
$\sigma_s^2$	The variance of the error in the Sun sighting time measurements
$\sigma_{y_j}^2$	The variance of the error in an observation $y_j$
$\sigma_\beta^2$	The variance of the error in the Sun angle $\beta_M$ measurements
$\sigma_\gamma^2$	The variance of the error in the measurements of the panoramic horizon scanner angle $\gamma_s$
$\tau$	The instantaneous angle between $\hat{U}$ and the Sun sensor axis $y_{SS}$ (reference Figure 3-4)
$\phi$	The instantaneous rotation angle of the spacecraft in its spin cycle (reference Figure 3-3)
$\phi_{II}$	The azimuth alignment angle between the Sun sensor and the horizon detector
$\phi_{HNOM}$	The nominal value of $\phi_{II}$

**ORIGINAL PAGE IS  
OF POOR QUALITY**

<u>Symbol</u>	<u>Definition</u>
$\phi_H^I$	The effective value of $\phi_H$ at horizon-in crossings; element $x_5$ of $\underline{X}$ (reference Figure 3-5)
$\phi_H^O$	The effective value of $\phi_H$ at horizon-out crossings; element $x_6$ of $\underline{X}$
$\chi$	$\hat{U} \cdot \hat{S}$ secant $\epsilon$
$\psi_0$	The rotation angle of the spacecraft in its spin cycle at reference time $t_0$ ; element $x_3$ of $\underline{X}$
$\omega$	The spacecraft's angular rate about its center of mass; element $x_9$ of $\underline{X}$

<u>Superscript</u>	<u>Definition</u>
GI, GI', etc.	Signifies components of vectors along the axes of coordinate frames GI, GI', etc.
I	Signifies a parameter associated with a horizon-in crossing of the horizon detector
O	Signifies a parameter associated with a horizon-out crossing of the horizon detector
T	Signifies the transpose of a matrix or of a column vector
$\lambda$	Signifies a parameter associated with the $\lambda$ th iteration in an iterative processing operation
*	Signifies an optimal quantity or estimate

<u>Subscript</u>	<u>Definition</u>
C, c	Signifies computed
f	Signifies final
GI, GI', etc.	Used with $x, y, z$ , or $1, 2, 3$ to signify the axes of the indicated coordinate frame

<u>Subscript</u>	<u>Definition</u>
I, HI	Signifies a parameter associated with a horizon-in crossing
H	Signifies a parameter associated with a horizon crossing; usually used with symbols that are applicable to both horizon-in and horizon-out crossings
j	Usually signifies a parameter associated with the processing of observation data set $\underline{Y}_j$ or scalar observation $y_j$
M, m	Signifies measured
O, HO	Signifies a parameter associated with a horizon-out crossing
o	Signifies an a priori or initial value
R	Signifies a parameter computed using $\underline{X} = \underline{X}_R$
1	Signifies a parameter associated with data set 1 in Appendix B
2	Signifies a parameter associated with data set 2 in Appendix B
$\Sigma$	Signifies the combination of data sets 1 and 2 and parameters associated with this set in Appendix B
+	Signifies a parameter computed using the plus sign in Equation (3-78)

<u>Overhead Symbols</u>	<u>Definition</u>
$\rightarrow$	Signifies a Cartesian vector of arbitrary length
$\hat{\phantom{x}}$	Signifies a Cartesian vector of unit length; also, signifies a computed or estimated variable

# PRELIMINARY DRAFT

ORIGINAL PAGE IS  
OF POOR QUALITY

## REFERENCES

1. Computer Sciences Corporation, 5035-22300-05TR, Evaluation of Filtering Methods for Optical Aspect and Horizon Sensor Data, W. Pettus, G. Fang, and Dr. S. Kikkawa, June 1972
2. --, 9101-09700-01TN, Preliminary Design of the Optical Aspect Bias Determination System (OABIAS), Dr. M. Plett and A. Dennis, July 1972
3. --, 5035-19700-01TR, Definitive Orbit Determination System Module Performance and Design Descriptions, F. DeCain, et al., March 1972
4. NASA Goddard Space Flight Center, Goddard Trajectory Determination System (GTDS) User's Guide, February 1974
5. National Aeronautics and Space Administration, Technical Report 32-1181, JPL Development Ephemeris Number 19, C. J. Devine, November 1967
6. NASA Goddard Space Flight Center, X-552-73-20, Generation and Use of the Goddard Trajectory Determination System SLP Ephemeris Files, M. G. Armstrong and I. B. Tamaszewski, January 1973
7. Computer Sciences Corporation, 9101-13300-02TR, Optical Aspect Data Prediction (ODAP) Program, System Description and Operating Guide, Version 2.0, M. Joseph and M. A. Shear, October 1972
8. --, 9101-13300-03TR, Optical Aspect Attitude Determination System (OASYS), System Description and Operating Guide, Version 2.0, M. Joseph and M. A. Shear, October 1972
9. --, Horizon Sensor Behavior of the Atmosphere Explorer-C Spacecraft, CSC/TM-75/6004, J. R. Wertz, et al., April 1975
10. --, 3000-06000-03TR, GRECRS and GRPIOT Package Descriptions and User's Manual, Dr. M. Plett, et al., August 1973
11. W. Denham and S. Pines, "Sequential Estimation When Measurement Function Nonlinearity Is Comparable to Measurement Error," AIAA Journal, June 1966, vol. 4, no. 6, pp. 1071-1076
12. Computer Sciences Corporation, 9101-06900-05TN, Multi-Satellite Attitude Determination System (MSAD) Executive System Structure, M. Cumill, et al., October 1972

# PRELIMINARY DRAFT

ORIGINAL PAGE #  
OF POOR QUALITY

13. --, 5035-2900-01TM, Multi-Satellite Attitude Determination (MSAD) Executive System, Preliminary User's Guide, D. Jahn, et al., March 1973
14. --, 3000-25800-03TR, MSAD/AE-C System Description, M. Grelland, A. Dydley (in preparation)
15. --, 3000-05300-02TR, RAE-B Attitude Support System Description and Operating Guide, Dr. R. Williams, et al., June 1974
16. International Business Machines Corporation, Federal Systems Division, Multi-Applications Subroutines, Volume I, Contract NAS 5-10022, August 1968
17. Computer Sciences Corporation, 9101-07000-01TR, Star Data Analysis Program (SDAP) System Description and Operating Guide, M. Shear, July 1972
18. --, 5035-22300-03TR, Optical Aspect Simulator (MAINSIM) System Description and Operating Guide, M. A. Shear, October 1971
19. --, 5035-22300-04TR, System Description and Operating Guide for the Orbit, Sun, and Attitude Geometry Program (OSAG), M. A. Shear, January 1972
20. P. Swerling, "Modern State Estimation Methods From the Viewpoint of the Method of Least Squares," IEEE Transactions on Automatic Control, December 1971, vol. AC-16, no. 6, pp. 707-719
21. Computer Sciences Corporation, 9101-16600-01TM, Recurs Subroutine Description and Operating Guide, S. E. Chevront, December 1972
22. A. H. Jazwinski, Stochastic Processes and Filtering Theory. New York: Academic Press, 1970
23. V. O. Mowery, "Least Square Recursive Differential Correction Estimation on Nonlinear Problems," IEEE Transactions on Automatic Control, October 1965, vol. 10, no. 5, pp. 399-407
24. S. L. Fagin, "Recursive Linear Regression Theory, Optimal Filtering Theory, and Error Analysis of Optimal System," IEEE National Convention, 1964, part 1, pp. 216-240

C-3